2367

2367

THE PHYSICS OF DEBRIS FLOWS

Richard M. Iverson

Reprinted from
REVIEWS OF GEOPHYSICS
Volume 35 Number 3 August 1997

THE PHYSICS OF DEBRIS FLOWS

Richard M. Iverson
Cascades Volcano Observatory
U.S. Geological Survey
Vancouver, Washington

Abstract. Recent advances in theory and experimentation motivate a thorough reassessment of the physics of debris flows. Analyses of flows of dry, granular solids and solid-fluid mixtures provide a foundation for a comprehensive debris flow theory, and experiments provide data that reveal the strengths and limitations of theoretical models. Both debris flow materials and dry granular materials can sustain shear stresses while remaining static; both can deform in a slow, tranquil mode characterized by enduring, frictional grain contacts; and both can flow in a more rapid, agitated mode characterized by brief, inelastic grain collisions. In debris flows, however, pore fluid that is highly viscous and nearly incompressible, composed of water with suspended silt and clay, can strongly mediate intergranular friction and collisions. Grain friction, grain collisions, and viscous fluid flow may transfer significant momentum simultaneously. Both the vibrational kinetic energy of solid grains (measured by a quantity termed the granular temperature) and the pressure of the intervening pore fluid facilitate motion of grains past one another, thereby enhancing debris flow mobility. Granular temperature arises from conversion of flow translational energy to grain vibrational energy, a process that depends on shear rates, grain properties, boundary conditions, and the ambient fluid viscosity and pressure. Pore fluid pressures that exceed static equilibrium pressures result from local or global debris contraction. Like larger, natural debris flows, experimental debris flows of ~10 m^3 of poorly sorted, water-saturated sediment invariably move as an unsteady surge or series of surges. Measurements at the base of experimental flows show that coarse-grained surge fronts have little or no pore fluid pressure. In contrast, finer-grained, thoroughly saturated debris behind surge fronts is nearly liquefied by high pore pressure, which persists owing to the great compressibility and moderate permeability of the debris. Realistic models of debris flows therefore require equations that simulate inertial motion of surges in which high-resistance fronts dominated by solid forces impede the motion of low-resistance tails more strongly influenced by fluid forces. Furthermore, because debris flows characteristically originate as nearly rigid sediment masses, transform at least partly to liquefied flows, and then transform again to nearly rigid deposits, acceptable models must simulate an evolution of material behavior without invoking preternatural changes in material properties. A simple model that satisfies most of these criteria uses depth-averaged equations of motion patterned after those of the Savage-Hutter theory for gravity-driven flow of dry granular masses but generalized to include the effects of viscous pore fluid with varying pressure. These equations can describe a spectrum of debris flow behaviors intermediate between those of wet rock avalanches and sediment-laden water floods. With appropriate pore pressure distributions the equations yield numerical solutions that successfully predict unsteady, nonuniform motion of experimental debris flows.

1. INTRODUCTION

Debris flows occur when masses of poorly sorted sediment, agitated and saturated with water, surge down slopes in response to gravitational attraction. Both solid and fluid forces vitally influence the motion, distinguishing debris flows from related phenomena such as rock avalanches and sediment-laden water floods. Whereas solid grain forces dominate the physics of avalanches, and fluid forces dominate the physics of floods, solid and fluid forces must act in concert to produce a debris flow. Other criteria for defining debris flows emphasize sediment concentrations, grain size distributions, flow front speeds, shear strengths, and shear rates [e.g., *Beverage and Culbertson*, 1964; *Varnes*, 1978; *Pierson and Costa*, 1987], but the necessity of interacting solid and fluid forces makes a broader, more mechanistic distinction. By this rationale, many events identified as debris slides, debris torrents, debris floods, mudflows, mudslides, mudspates, hyperconcentrated flows, and lahars may be regarded as debris flows [cf. *Johnson*, 1984]. The diverse nomenclature reflects the diverse origins, compositions, and appearances of debris flows, from quiescently streaming, sand-rich slurries to tumultuous surges of boulders and mud.

Interaction of solid and fluid forces not only distinguishes debris flows physically but also gives them unique destructive power. Like avalanches of solids, debris flows can occur with little warning as a consequence of slope failure in continental and seafloor en-

Published in 1997 by the American Geophysical Union.

Reviews of Geophysics, 35, 3 / *August 1997*
pages 245–296
Paper number 97RG00426

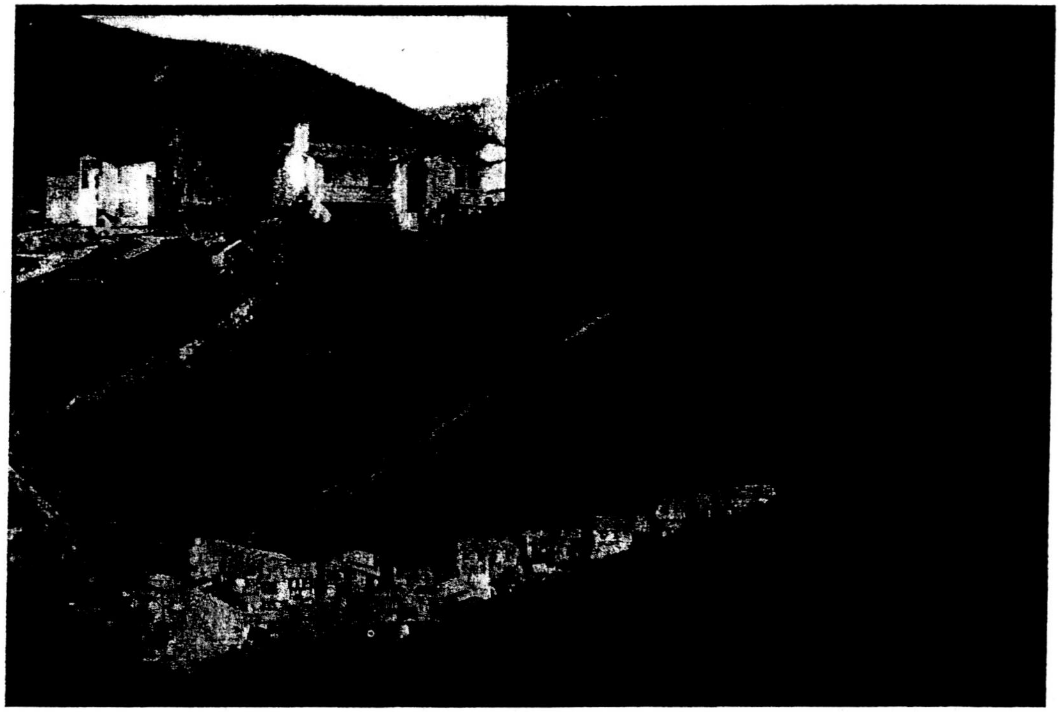

Figure 1. Digitally enhanced photographs of the path of the 2300 m^3 Oddstad debris flow, which occurred January 4, 1982, in Pacifica, California. The flow destroyed two homes and killed three people. The source area slopes 26°. The flow path slopes 21° on average and extends 170 m downslope. Deposits at the base of the flow path have been removed [*Schlemon et al.*, 1987; *Wieczorek et al.*, 1988; *Howard et al.*, 1988]. (Modified from *USGS* [1995], courtesy of S. Ellen and R. Mark.)

vironments, and they can exert great impulsive loads on objects they encounter. Like water floods, debris flows are fluid enough to travel long distances in channels with modest slopes and to inundate vast areas. Large debris flows can exceed 10^9 m^3 in volume and release more than 10^{16} J of potential energy, but even commonplace flows of $\sim 10^3$ m^3 can denude vegetation, clog drainageways, damage structures, and endanger humans (Figure 1).

The capricious timing and magnitude of debris flows hamper collection of detailed data. Scientific understanding has thus been gleaned mostly from qualitative field observations and highly idealized, first-generation experiments and models. However, a new generation of experiments and models has begun to yield improved insight by simulating debris flows' key common attributes. For example, all debris flows involve gravity-driven motion of a finite but possibly changing mass of poorly sorted, water-saturated sediment that deforms irreversibly and maintains a free surface. Flow is unsteady and nonuniform, and is seldom sustained for more than 10^4 s. Peak flow speeds can surpass 10 m/s and are characteristically so great that bulk inertial forces are important. Total sediment concentrations differ little from those of static, unconsolidated sediment masses and typically exceed 50% by volume. Indeed, most debris flows mobilize from static, nearly rigid masses of sediment, laden with water and poised on slopes. When mass movement occurs, the sediment-water mixtures transform to a flowing, liquid-like state, but eventually they transform back to nearly rigid deposits. New models and measurements that clarify the physical basis of debris flow behavior from mobilization to deposition are the focus of this paper.

Including this introduction, the paper has 10 sections. Section 2 describes the net energetics of debris flow motion, the variability of debris flow mass, and the challenges these phenomena pose for researchers. In section 3 a compilation of key observations, data, and concepts summarizes qualitatively the factors that control debris flows' mass, momentum, and energy content. In section 4, scaling analyses assist identification and classification of debris flow behavior on the basis of dimensionless parameters that distinguish dominant modes of momentum transport in solid-fluid mixtures. In section 5 a retrospective of traditional, one-phase models for momentum transport in debris flows explains why such models are incompatible with current understanding. In section 6, mass, momentum, and energy conservation equations for two-phase debris-flow mixtures establish a theoretical framework that highlights the variable composition of debris flows and the importance of solid-fluid interactions. In section 7 a relatively complete analysis of an idealized debris-flow mixture moving steadily along a rough bed helps clarify the complicated interplay between local solid and fluid motion, boundary forces, and mechanisms of energy dissipation and momentum transport. In section 8 a less complete analysis of unsteady debris flow motion focuses on persistence of nonequilibrium fluid pressures that differ with proximity to debris flow surge fronts. In section 9, numerical calculations using a simplified, depth-averaged routing model that emphasizes the effects of Coulomb grain friction mediated by persistent nonequilibrium fluid pressures indicate that the model can predict the velocities and depths of experimental debris flows. Section 10 summarizes the strengths and limitations of current understanding and suggests priorities for future research. Appendices A–C provide some key mathematical details omitted in previous sections, and a complete summary of mathematical notation follows in a separate notation section.

Because this paper emphasizes physical aspects of debris flow motion, it includes only incidental coverage of important topics such as debris flow habitats, frequencies, magnitudes, triggering mechanisms, hazard assessments, engineering countermeasures, morphology and sedimentology of debris flow deposits, and the relationship between debris flows and other mass movements. Several previous reviews and compilations, such as those by *Takahashi* [1981, 1991, 1994], *Innes* [1983], *Costa* [1984], *Johnson* [1984], *Costa and Wieczorek* [1987], *Hooke* [1987], *Pierson* [1995], and *Iverson et al.* [1997] treat these subjects more completely. In addition, videotape recordings [*Costa and Williams*, 1984; *Sabo Publicity Center*, 1988] reveal many qualitative attributes of debris flows, and summaries by *Iverson and Denlinger* [1987], *Miyamoto and Egashira* [1993], *Savage* [1993], and *Hutter et al.* [1996] introduce some of the quantitative concepts elaborated here.

2. BULK ENERGETICS AND RUNOUT EFFICIENCY

The energetics of debris flows differ dramatically from those of a homogeneous solid or fluid. The interactions, and not merely the additive effects of the solid and fluid constituents, are important. A simple thought experiment helps illustrate this phenomenon:

Consider first a very unrealistic but simple model of a debris flow. A mass of identical, dense, frictionless elastic spheres flows down a bumpy, rigid incline and onto a horizontal runout surface, all within a vacuum. The spheres jostle and collide as they accelerate downslope, but no energy dissipation occurs, and the flow runs out forever. Then fill the spaces between the spheres with a viscous fluid less dense than the spheres (e.g., liquid water), and repeat the experiment. Owing to viscous shearing, the mixture loses energy as it moves downslope, and runout remains finite. The fluid retards the motion. Next, replace the elastic spheres with rough, inelastic sediment grains, and repeat the two experiments. In the vacuum the collection of grains runs out a finite distance and stops owing to energy dissipation caused by grain contact friction and inelastic collisions. What is the outcome of the experiment when the interstices between the sediment grains are filled with viscous fluid? A logical possibility, suggested by the behavior of elastic spheres, is that the viscous fluid will increase dissipation and reduce runout. However, experience with water-saturated debris flows shows that the presence of viscous fluid increases runout even though the fluid dissipates energy. Interactions of viscous fluid with dissipative solid grains of widely varying sizes produce this behavior and merit emphasis in efforts to understand debris flow motion.

As the preceding thought experiment implies, debris flow motion involves a cascade of energy that begins with incipient slope movement and ends with deposition. As a debris flow moves downslope, its energy degrades to higher entropy states and undergoes the following conversions:

bulk gravitational potential energy

$\rightarrow$ bulk translational kinetic energy

$\rightleftharpoons$ grain vibrational kinetic energy

$+$ fluid pressure energy $\rightarrow$ heat

Here right pointing arrows denote conversions that are irreversible, except in special circumstances, whereas the two-way arrow denotes a conversion that apparently involves significant positive feedback. The details of this energy cascade encompass virtually all the important issues of debris flow physics. Before pursuing these details, however, it is worthwhile to consider debris flow energetics from a broader perspective.

The net efficiency of debris flows, and of kindred phenomena such as rock and snow avalanches, describes conversion of gravitational potential energy to the work done during debris flow translation. The more efficiently this conversion occurs, the less vigorously energy degrades to irrecoverable forms such as heat, and the farther the flow runs out before stopping. Net efficiency can be evaluated by integrating an equation that describes motion of the debris flow center of mass as a function of time. Alternatively, as was recognized originally by *Heim* [1932] for rock avalanches, the outcome of the integration can be obtained without specifying an equation of motion by equating the total potential energy lost during motion, MgH, to the total energy degraded to irrecoverable forms by resisting forces, MgR, that work through the distance L to make the debris flow stop:

$$MgH = MgRL \tag{1}$$

Here M is the debris flow mass, g is the magnitude of gravitational acceleration, and R is a dimensionless net resistance coefficient, which incorporates the effects of internal forces but which depends also on external forces that act at the bed to convert gravitational potential to horizontal translation. The coordinates H and L de-

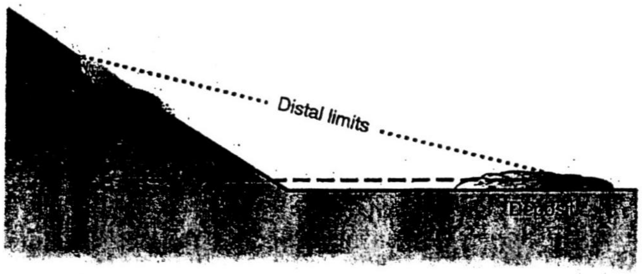

Figure 2. Schematic cross section defining H and L for debris flow paths. Strictly, H and L are defined by lines that connect the source area center of mass and the deposit center of mass. In practice, H and L are commonly estimated from the distal limits of the source area and deposit.

scribe displacement of the debris flow center of mass during motion: H is the vertical elevation of the debris flow source above the deposit, and L is the horizontal distance from source to deposit (Figure 2).

Even though all debris flow energy ultimately degrades to heat, thermodynamic data provide few constraints for evaluating R in (1). The equation shows that a debris flow's total energy dissipation per unit mass is given by gH, which implies about 10 J/kg of heat production per meter of flow descent. Even without heat loss, this 10 J/kg suffices to raise the temperature of a typical debris flow mixture only about 0.005°C. Consequently, debris flow temperature measurements in open, outdoor environments, with unrestricted heat exchange and ambient temperatures that vary widely, yield little resolution of energy dissipation due to flow resistance. Instead, debris flow physics conventionally emphasizes the purely mechanical behavior of an isothermal system, and this paper follows that convention.

The mechanical phenomena that govern R must be quantified in detail to understand and predict debris flow motion, but evaluation of net efficiency from the aftermath of a debris flow is far simpler. Dividing each side of (1) by $MgHR$ yields

$$1/R = L/H \tag{2}$$

which shows that the net efficiency, defined as $1/R$, increases as the runout distance L increases for a fixed descent height, H. Thus net efficiency may be determined from surveys of debris flow source areas and deposits that yield the value of L/H.

Rigorous evaluations of L/H from debris flows' center-of-mass displacements have been rare, but field mapping of debris flow paths and detailed measurements on experimental debris flows demonstrate three important points [cf. *Vallance and Scott*, 1997]: (1) L/H of water-saturated debris flows exceeds that of drier sediment flows with comparable masses, (2) Large debris flows appear to have greater efficiency than small flows, and (3) L/H depends on runout path geometry and boundary conditions that determine, for example, the extent of erosion, sedimentation, and flow channelization. Table 1 summarizes typical L/H values inferred from the distal limits of debris flow source areas and deposits. The tabulated L/H values can be compared in only the broadest sense because the data were collected on debris flows with diverse origins and flow path geometries by investigators with diverse objectives. Nonetheless, the data of Table 1 indicate that L/H increases roughly in proportion to the logarithm of volume for debris flows with volumes greater than about 10^5 m^3 but that L/H remains fixed at ~2–4 for smaller flows. Data for dry rock avalanches exhibit similar trends but indicate that dry avalanches typically have only about half the efficiency (L/H) of debris flows of comparable volume [cf. *Scheidegger*, 1973; *Hsu*, 1975; *Davies*, 1982; *Li*, 1983; *Siebert*, 1984; *Hayashi and Self*, 1992; *Pierson*, 1995]. These empirical trends are noteworthy, but case-by-case variations in debris-flow behavior make runout prediction on the basis of only L/H rather questionable.

Rigorous evaluation of L/H from center-of-mass displacements under controlled initial and boundary conditions has been possible at the U.S. Geological Survey (USGS) debris flow flume (Figure 3) [*Iverson and LaHusen*, 1993]. Experiments in which about 10 m^3 of a water-saturated, poorly sorted, sand-gravel debris flow mixture is suddenly released from a gate at the head of the flume yield $L/H \sim 2$ for unconfined runout but $L/H > 2$ for channelized runout (Figure 4). These values surpass the L/H for runout of similar sand-gravel masses not saturated with water [*Major*, 1996]. When the sand-gravel mix is replaced by well-sorted gravel, however, the influence of water on the outcome of experiments changes: dry gravel produces $L/H > 2$, but water-saturated gravel produces $L/H < 2$. Thus water enhances the mobility of poorly sorted debris flow sediments in a manner not manifested by mixtures of well-sorted gravel and water, and experiments with water-gravel mixtures provide a poor surrogate for experiments with realistic debris-flow materials.

Effects of water-sediment interactions pose challenging problems that consume much of the remainder of this paper, but effects of debris flow mass are even more enigmatic. According to equations (1) and (2), debris flow mass should not affect runout efficiency, but the data of Table 1 contradict this inference. The cause of this contradiction is difficult to resolve because debris flows and avalanches can change their mass and composition while in motion and can spread longitudinally to change their mass distribution [cf. *Davies*, 1982]. Some debris flows grow severalfold in mass owing to bed and bank erosion [*Pierson et al.*, 1990] and others decline substantially in solids concentration as a result of mixing with stream water [*Pierson and Scott*, 1985]. Changes in debris flow mass or composition have been identified somewhat interchangeably by the terms "bulking" (increase of mass or solids concentration) and "debulking" (decrease of mass or solids concentration), but more precise terminology is desirable because changes in de-

TABLE 1. Estimated Values of Total Flow Volume, Runout Distance *L*, Descent Height *H*, and Efficiency *L/H* of Various Debris Flows

Flow Location	*Date*	*Reference*	*Flow Volume, m^3*	*L, m*	*H, m*	*L/H*	*Origin*
Mount Rainier, Osceola mudflow	circa 5700 B.P.	*Vallance and Scott* [1997]	$\sim 10^9$	120,000	4,800	25	landslide and downstream erosion
Nevados Huascaran, Peru	May 31, 1970	*Plafker and Ericksen* [1978]	$\sim 10^8$	120,000	6,000	20	landslide
Nevado del Ruiz, Colombia, Río Guali	Nov. 13, 1985	*Pierson et al.* [1990]	$\sim 10^7$	103,000	5,190	20	pyroclasts melting snow
Mount St. Helens, South Fork Toutle	May 18, 1980	*Fairchild and Wigmosta* [1983]	$\sim 10^7$	44,000	2,350	19	wet pyroclastic surge
Mount St. Helens, Muddy River	May 18, 1980	*Pierson* [1985]	$\sim 10^7$	31,000	2,150	14	wet pyroclastic surge
Wrightwood, Calif., Heath Canyon	May 7, 1941	*Sharp and Nobles* [1953]	$\sim 10^6$	24,140	1,524	16	landslide
Three Sisters, Oreg., Separation Creek	1933	J. E. O'Connor et al. (manuscript in preparation, 1997)	$\sim 10^6$	6,000	700	9	glacier breakout flood
Mount Thomas, NZ, Bullock Creek	April 1978	*Pierson* [1980]	$\sim 10^5$	3,500	600	6	landslide
Wrightwood, Calif., Heath Canyon	May 1969	*Morton and Campbell* [1974]	$\sim 10^5$	2,700	680	4	landslide
Santa Cruz, Calif., Whitehouse Creek	Jan. 4, 1982	*Wieczorek et al.* [1988]	$\sim 10^5$	600	200	3	landslide
Pacifica, Calif., Oddstad site	Jan. 4, 1982	*Howard et al.* [1988]	$\sim 10^3$	190	88	2	landslide
USGS debris flow flume	Sept. 25, 1992	*Iverson and LaHusen* [1993]	$\sim 10^1$	78	41	2	artificial release from flume gate

Most data are for flows that were observed during motion or within hours of deposition. With the exception of the Osceola mudflow, all flows apparently maintained a relatively constant mass (within a factor of 2) from initiation to deposition. The Osceola is included in the tabulation because it is the largest well-documented debris flow in the terrestrial geologic record.

bris-flow mass, independent of changes in composition, might influence efficiency.

Attempts to use elementary energy balances to predict effects of mass change on debris flow efficiency encounter difficulties, which can be traced to assumptions implicit in equation (1) and in similarly simple momentum balances [cf. *Cannon and Savage*, 1988; *Hungr*, 1990; *Erlichson*, 1991]. It might seem from (1), for example, that loss of mass during motion should increase efficiency because the potential energy initially available to power the motion, MgH, stays fixed, while the work done by resisting forces apparently declines as the flow mass declines. The problem with this logic lies in the assumption that R remains constant or decreases as the flow mass declines. This assumption would be correct if R depended only on internal forces, but R depends also on the external forces that cause the flow mass to decline. Loss of debris flow mass requires that work be done on the flow by the banks and bed to decelerate and deposit the lost mass. This work adds to the work that would be done over the same path length in the absence of deposition. The critical question is whether the additional work is less than the energy savings accrued by leaving mass behind. Universal answers to this question are perhaps unattainable. The same is true for the question of whether mass gain will increase bulk mobility and runout. In each case, mass change depends on work done during momentum exchange with the bed and banks, which may differ greatly in different localities. Despite the lack of clear resolution, recognition of the fundamental effects of external forces on debris flow efficiency is essential, for otherwise it may be tempting to attribute differences in runout solely to differences in flow composition and rheology. Section 7 delves more deeply into the mechanical effects of external forces.

3. MASS, MOMENTUM, AND ENERGY CONTENT: DESCRIPTION AND DATA

An empirical picture of debris flow physics can be drawn from a combination of real-time field observations and measurements [e.g., *Okuda et al.*, 1980; *Li and Yuan*, 1983; *Johnson*, 1984; *Pierson*, 1980, 1986], detailed observations and measurements during controlled field and laboratory experiments [e.g., *Takahashi*, 1991; *Khegai et al.*, 1992; *Iverson and LaHusen*, 1989, 1993], and analyses of debris flow paths and deposits [e.g., *Fink et al.*, 1981; *Pierson*, 1985, 1995; *Whipple and Dunne*, 1992; *Major*, 1996]. Furthermore, videotape compilations of debris flow recordings provide many qualitative insights [*Costa and Williams*, 1984; *Sabo Publicity Center*, 1988]. Relatively little detailed information is available for subaqueous debris flows, but most aspects of their behavior (other than their tendency to hydroplane, entrain sur-

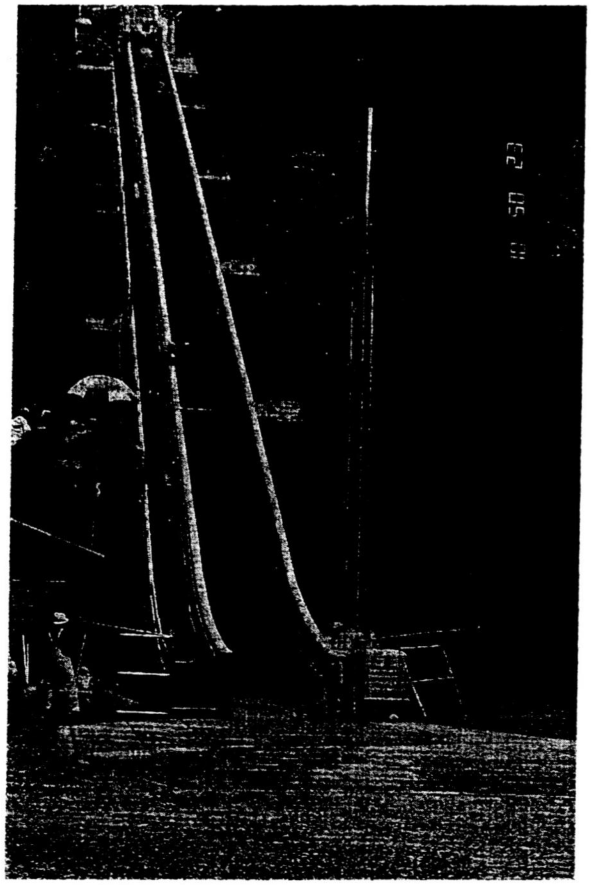

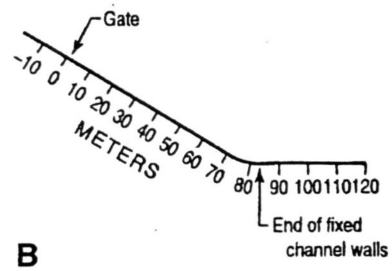

Figure 3. U.S. Geological Survey (USGS) debris flow flume [*Iverson et al.*, 1992]. (a) Photograph of an experiment in progress, May 6, 1993. (b) Schematic vertical cross-sectional profile.

rounding water, and transform to dilute density currents) appear similar to those of their subaerial counterparts [*Prior and Coleman*, 1984; *Weirich*, 1989; *Mohrig et al.*, 1995; *Hampton et al.*, 1996]. This summary focuses on the subaerial case and particularly on inferences drawn from detailed experimental data.

3.1. Material Properties

Some properties of debris flow materials can be measured readily and accurately in a static state, whereas other properties depend on the character of debris motion. The most readily measured static property is the grain size distribution. Abundant grain size data demonstrate that individual debris flows can contain grains that range from clay size to boulder size. However, many published grain size distributions are biased because they ignore the presence of cobbles and boulders that are difficult to sample [*Major and Voight*, 1986]. Nonetheless, it is clear that sand, gravel, and larger grains compose most of the mass of debris flows and that silt and clay-sized grains commonly constitute less than 10% of the mass [e.g., *Daido*, 1971; *Costa*, 1984; *Takahashi*, 1991; *Pierson*, 1995; *Major*, 1997]. Grain size data reveal the oversimplification of debris flow models that assume a single grain size or a preponderance of fine-grained sediment [e.g., *Coussot and Proust*, 1996], and they reinforce the notion that a diversity of grain sizes may be critical to debris flow behavior. Beyond this, grain size data by themselves add little to the understanding of debris flow physics. Such understanding requires data on debris properties that are rigorously measurable only during motion.

Few acceptable techniques exist to measure properties of flowing debris, even simple properties such as bulk density. Grossly invasive techniques such as plunging buckets or sensors into debris flows conspicuously change the state of the debris, and the inconsistent, noisy, dirty character of debris flows has discouraged attempts to use noninvasive techniques such as ultrasonic, X ray, laser sheet, or magnetic resonance imaging that are useful for probing simpler solid-fluid mixtures [*Lee et al.*, 1974; *Malekzadeh*, 1993; *Kytomaa and Atkinson*, 1993; *Abbott et al.*, 1993]. The most concerted efforts to determine properties of flowing debris have relied either on real-time measurements at the boundaries of debris flows in artificial channels or on postdepositional measurements on desiccated debris flow sediment samples reconstituted by adding water [*Takahashi*, 1991]. Precise real-time measurements have been possible only with experimental flows that contain sediments no coarser than gravel [e.g., *Iverson et al.*, 1992]; measurements on reconstituted samples have generally excluded sediment coarser than gravel and have also involved uncertainties about appropriate water contents and deformation styles [e.g., *Phillips and Davies*, 1991; *Major and Pierson*, 1992].

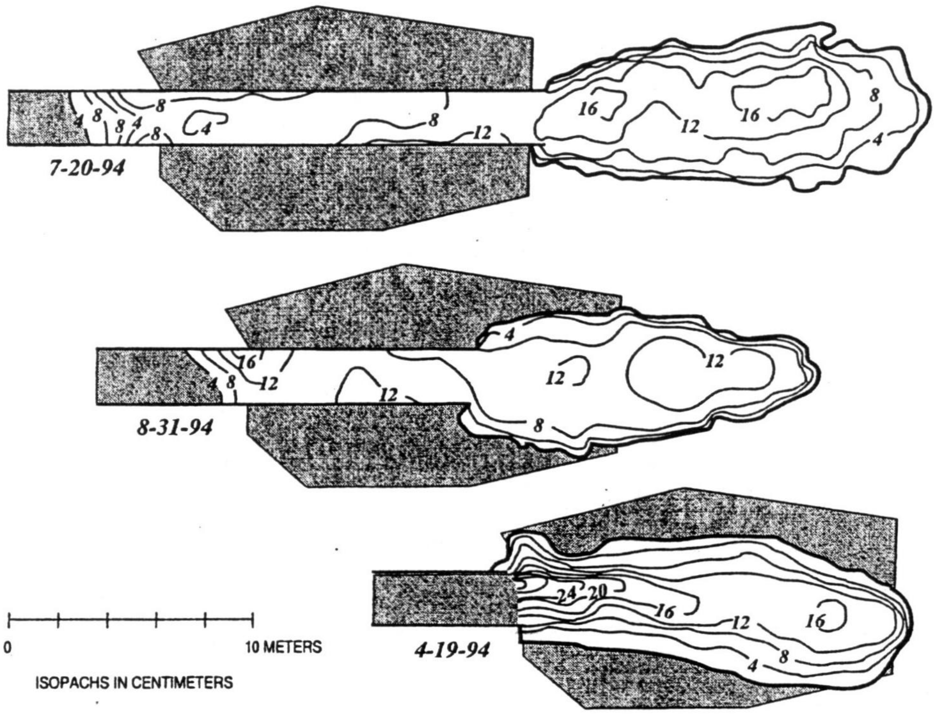

Figure 4. Isopach maps of deposits that formed at the base of the USGS debris flow flume during three experiments in which nearly identical volumes (~10 m^3) of water-saturated sand and gravel were released from the gate at the flume head. In each map the shaded area denotes the position of a nearly horizontal concrete pad adjacent to the flume base. Differences in positioning of deposits, which indicate differences in flow runout, are attributable to different distances of flow confinement by rigid channel walls [after *Major*, 1996].

Graphs of flow depth and total basal normal stress recorded simultaneously at fixed cross sections have been used to estimate the average bulk density ρ of experimental debris flows in the USGS debris flow flume (Figure 5). Measured basal fluid pressures vary somewhat asynchronously with the basal total normal stress (as they do in larger natural debris flows [e.g., *Takahashi*, 1991]), and bulk density estimates based on the fluid pressure alone may be inaccurate. Further complicating the picture, debris flows invariably move as one or more pulses or surges, and steady, uniform flow seldom, if ever, occurs. The relationship between flow depth, basal fluid pressure, and basal normal stress changes markedly as surges pass (Figure 5) [cf. *Takahashi*, 1991]. Only for brief intervals when flow is nearly steady and uniform (implying negligible velocity normal to the bed) can the average bulk density be estimated with confidence from the measured basal normal stress σ and a simple static force balance, $\sigma = \rho g h \cos \theta$, where θ is the bed slope and h is the flow depth measured normal to the bed. Employing this force balance and data from Figure 5 for an interval when nearly steady flow occurred (between 18.1 and 18.3 seconds) yields the density estimate ρ = 2100 kg/m^3. Similarly computed estimates for additional flume debris flows range from 1400 to 2400 kg/m^3, whereas mean bulk densities of samples excavated from fresh deposits of the same flows range only from 2100 to 2400 kg/m^3 (Table 2). Bulk densities of natural debris flows inferred from deposits seldom range outside 1800 to 2300 kg/m^3 [cf. *Costa*, 1984; *Pierson*, 1985; *Major and Voight*, 1986]. The data of Table 2 imply that deposit densities provide crudely accurate estimates of debris flow densities but that relatively low density (dilute) debris flows may produce deposits that yield deceptively high estimates of flow density. The data also indicate that the volume fraction of solid grains in debris flows typically ranges from about 0.5 to 0.8, although more dilute flows are possible. The wide variety of grain sizes and shapes in debris flows allows them to attain densities that substantially surpass those of random packings of identical spheres [*Rodine and Johnson*, 1976], which have solid volume fractions no greater than 0.635 [*Onada and Liniger*, 1990]. The ability of debris flow solids to exhibit dense, interlocked packings as well as loose, high-porosity packings has significant ramifications for mixture behavior [*Rogers et al.*, 1994].

Rheometric investigations of debris flow mixtures reconstituted by adding water to samples of debris flow deposits have demonstrated that mixture behavior varies markedly with subtle variations in solid volume fraction (concentration), shear rate (an approximate surrogate for kinetic energy content), and grain size distribution (particularly the silt and clay content, which strongly influences solid-fluid interactions) [*O'Brien and Julien*, 1988; *Phillips and Davies*, 1991; *Major and Pierson*, 1992; *Coussot and Piau*, 1995]. Such behavior evokes strong

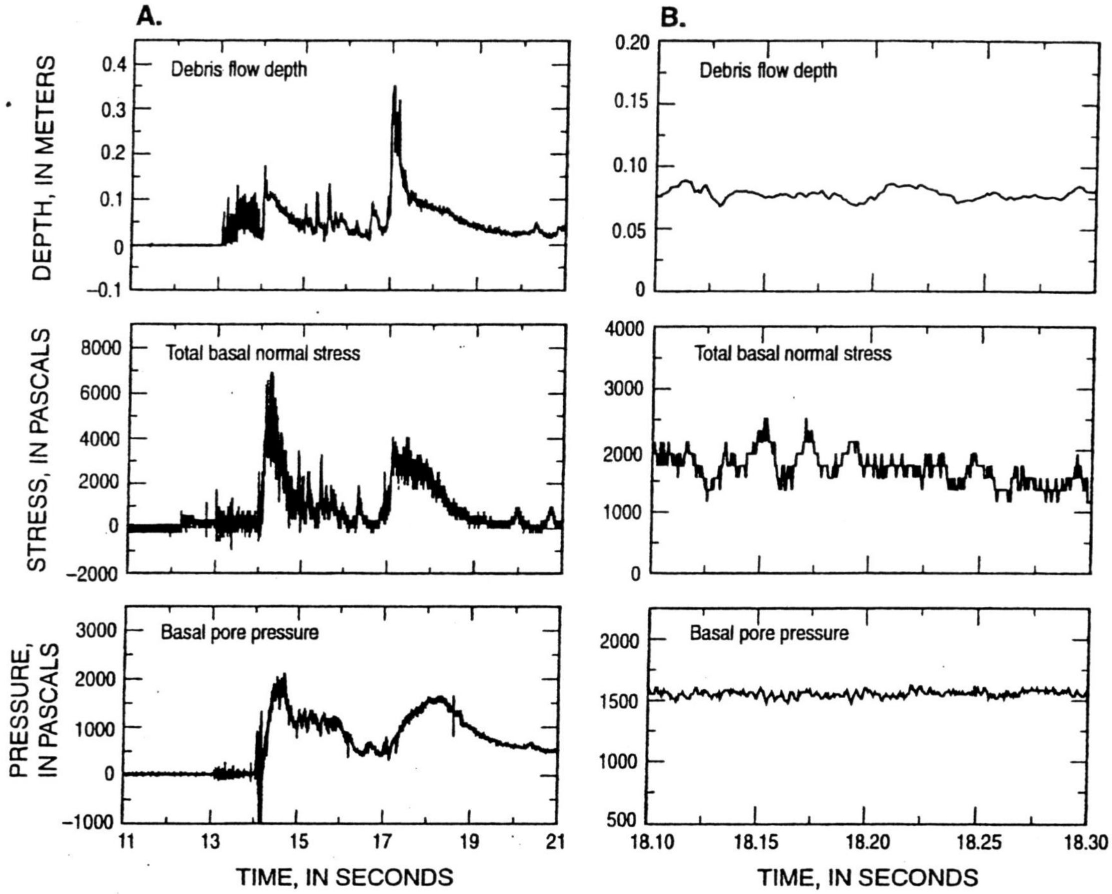

Figure 5. Representative measurements of flow depth, basal total normal stress, and basal fluid pressure made at a cross section 67 m downslope from the head gate at the USGS debris flow flume. Data are for a debris flow of 9 m^3 of water-saturated loamy sand and gravel released August 31, 1994. The flume gate opened at $t = 6.577$ s. All data were sampled at 2000 Hz. Depth measurements were made with a laser triangulation system. Total stresses were measured with a load cell attached to a 500-cm^2 steel plate mounted flush with the flume bed and roughened to match the texture of the surrounding concrete. Pore pressures were measured with a transducer mounted flush with the flume bed. The transducer diaphragm was isolated from debris flow sediment by a number 230 mesh wire screen, and the transducer port was prefilled with water to retard entry of fine sediment particles. (a) Data for the entire event duration. (b) Details of the same data for a 0.2-s interval when flow was nearly steady.

analogies between debris flow mixtures and better understood mixtures such as ideal, dense gases [cf. *Campbell*, 1990]. In dense gases the concentrations of distinct molecular species, their kinetic energies (temperature), and their interaction forces determine bulk mixture properties such as density, flow resistance, and the propensity for changes of state. Similarly, the bulk properties of debris flow mixtures depend fundamentally on the concentrations, kinetic energies, and interactions of distinct solid and fluid constituents [cf. *Johnson*, 1984, pp. 289–290]. Therefore the following description eschews the traditional practice of assuming that debris flow solids and fluids are inextricably joined to form a single-phase material; instead it emphasizes the distinct properties and interactions of debris flows' solid and fluid constituents.

The salient mechanical properties of a solid grain are its mass density ρ_s, characteristic diameter δ (defined as the diameter of a sphere of identical volume), friction coefficient $\tan \phi_g$ (where ϕ_g is the angle of sliding friction, which depends on grain shape and roughness), and restitution coefficient e (which varies from 1 for perfectly elastic grains to 0 for perfectly inelastic) [*Spiegel*, 1967, p. 195]. The granular solids as a whole occupy a fraction υ_s of the total mixture volume and have a distribution of δ that characteristically spans many orders of magnitude. The fluid component of the mixture is characterized by its mass density ρ_f (assumed less than ρ_s), effective viscosity μ, and volume fraction υ_f. At mean normal stresses typical in debris flows (<100 kPa), the solid and fluid constituents are effectively incompressible, and variations in υ_s/υ_f greatly exceed those in ρ_s/ρ_f. Two additional properties link the behavior of the solid and fluid: the volume fractions obey $\upsilon_s + \upsilon_f = 1$ (thus the mixture density obeys $\rho = \rho_s\upsilon_s + \rho_f\upsilon_f$), and a parameter such as the hydraulic permeability k charac-

TABLE 2. Comparison of Bulk Densities of Experimental Debris Flows and Their Deposits

Experiment Date	*Material*	*Mean Flow Depth h, m*	*Laser Measurement Time Interval, s*	*Mean Bed Stress on 500-cm² Plate, Pa*	*Mean Bulk Density From Bed Stress, kg/m³*	*Dried Bulk Densities of Deposit Samples, kg/m³*	*Calculated Mean Saturated Density of Deposit, kg/m³*
April 19, 1994	sand-gravel mix	0.05	17.0–17.2	1000	2400	1870	2200
						1930	
April 21, 1994	sand-gravel mix	0.06	18.0–18.2	1200	2400	1940	2200
						1850	
						1830	
						1930	
May 25, 1994	loam-gravel mix	0.05	16.0–16.5	600	1400	1630	2100
			24.0–24.5			1770	
Aug. 31, 1994	loam-gravel mix	0.08	18.1–18.3	1400	2100	2050	2200
						1910	
						1680	
						1770	
April 26, 1995	sand-gravel mix	0.07	9.6–9.8	1400	2400	1920	2400
						2260	
						2050	
						2460	

Bulk densities were determined on the basis of (1) simultaneous measurements of flow depth and bed normal stress during intervals of nearly steady flow and (2) average values of deposit densities sampled by the excavation method, as described by *Blake* [1965].

terizes the resistance to relative motion of solids and fluid [*Iverson and LaHusen*, 1989]. Table 3 summarizes the definitions and typical values of these properties, and Figure 6 shows that key properties (e.g., fluid volume fraction and permeability) can be strongly related.

Definition of distinct solid and fluid properties prompts two difficult questions: (1) What effectively constitutes the fluid fraction, when a debris flow may contain solids of any size, including colloidal and clay particles carried in solution and suspension? (2) If the fluid fraction includes fine solid particles, can it be characterized by the simple properties ρ_f and μ?

Criteria for distinguishing the effective fluid and solid fractions in debris flows can be developed on the basis of time and length scales. *Rodine and Johnson* [1976], for example, used a length scale approach and suggested that all grains with $\delta < \delta'$ effectively act like fluid as they exert forces on a grain with diameter δ'. This applies for any arbitrary δ' and results in distinctions between solid and fluid constituents purely relative to the choice of δ'. However, an absolute distinction between solid and fluid constituents is necessary for application of formal mixture theories [*Atkin and Craine*, 1976] and can be deduced if time as well as length scales are considered.

If the duration t_D of a debris flow is long in comparison with the timescale for settling of a grain of diameter δ in static, pure water with viscosity μ_w, the grain must be considered part of the solid fraction. Such a grain requires either sustained interactions with other grains or fluid turbulence to keep it suspended in the debris flow mixture (Figure 7). On the other hand, if a grain can remain suspended for times that exceed t_D as a result of only the viscous resistance of water, the grain may act as part of the fluid. Timescales for debris flow durations range from about 10 s for small but significant events (e.g., Figure 1) to 10^4 s for the largest. The timescale for grain settling can be estimated by dividing the characteristic settling distance or half thickness, $h/2$, of a debris flow by the grain settling velocity v_{set} estimated from Stokes' law or a more general equation that accounts for grain inertia [*Vanoni*, 1975]. Thus if $h/(2t_D v_{set}) < 1$, the debris flow duration is large compared with the timescale for settling. The half thickness of debris flows ranges from about 0.01 m for small flows to 10 m for large ones. Thus $h/2t_D \sim 0.001$ m/s, which implies $v_{set} < 0.001$ m/s for grains to act as part of the fluid. Settling velocities of 0.001 m/s or less in water require grains with diameters less than about 0.05 mm [*Vanoni*,

TABLE 3. Typical Values of Basic Physical Properties of Debris Flow Mixtures

Property and Unit	*Symbol*	*Typical Values*
Solid Grain Properties		
Mass density, kg/m³	ρ_s	2500–3000
Mean diameter, m	δ	10^{-5}–10
Friction angle, deg	ϕ_g	25–45
Restitution coefficient	e	0.1–0.5
Pore Fluid Properties		
Mass density, kg/m³	ρ_f	1000–1200
Viscosity, Pa s	μ	0.001–0.1
Mixture Properties		
Solid volume fraction	v_s	0.4–0.8
Fluid volume fraction	v_f	0.2–0.6
Hydraulic permeability, m²	k	10^{-13}–10^{-9}
Hydraulic conductivity, m/s	K	10^{-7}–10^{-2}
Compressive stiffness, Pa	E	10^3–10^5
Friction angle, deg	ϕ	25–45

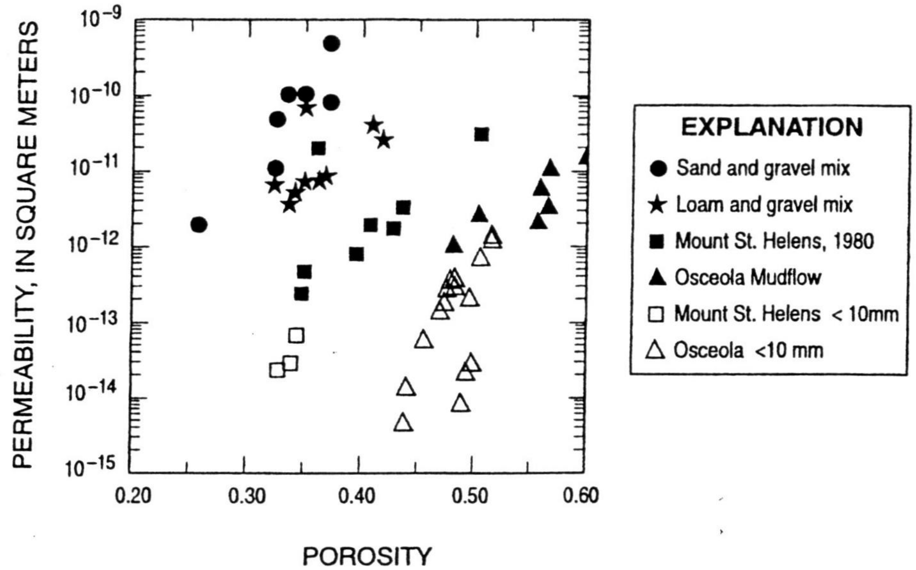

Figure 6. Hydraulic permeabilities of representative debris-flow materials as a function of porosity (fluid volume fraction) υ_f. Tests with sediments sieved to remove grains >32 mm (solid symbols) were conducted in a compaction permeameter, and the volume fractions depicted for each material represent the full range achievable in the device under very low (~2 kPa) effective stress. Tests at lower volume fractions (open symbols) were conducted under compression in a triaxial cell using only the sediment fraction <10 mm [*Major*, 1996]. Each material exhibits an approximately exponential dependence of permeability on volume fraction, i.e., $k = k_0 \exp(a\upsilon_f)$ where k_0 and a are constants. Grain size distributions of all materials are given by *Major* [1996].

1975, p. 25]. This critical grain size corresponds quite well with the silt-sand boundary of 0.0625 mm, and it also falls in the range where settling is characterized by grain Reynolds numbers ($N_{\mathrm{Rey}} = \delta\rho_f v_{\mathrm{set}}/\mu_w$) much less than 1, so that viscous forces dominate grain motion. By this rationale a useful but inexact guideline states that grains larger than silt size compose the debris flow solids, whereas grains in the silt-clay fines fraction act as part of the fluid. Analyses of fluids that drained from deposits of four debris flows at the USGS debris flow flume provide empirical support for this guideline: the sediment mass in each debris flow included only 1–6% grains finer than sand, but more than 94% of the sediment mass in each sample of the effluent fluid consisted of grains finer than sand (Table 4) [*Major*, 1996].

Incorporation of fine grains influences the mass density of debris flow fluid, ρ_f, defined as

$$\rho_f = \rho_s \upsilon_{\mathrm{fines}} + \rho_w(1 - \upsilon_{\mathrm{fines}}) \tag{3}$$

where $\upsilon_{\mathrm{fines}}$ is the volume fraction of fluid occupied by fine (i.e., silt and clay) grains, ρ_w is the mass density of pure water, and ρ_s is the mass density of fine grains (for simplicity assumed equal to that of the coarser sediment). Direct measurements of ρ_f of effluent fluids in flume experiments yield values that range from 1030 to 1110 kg/m^3 (Table 4). Where direct measurements are impossible, estimates of ρ_f can be made from (3) and the dry bulk densities and grain size distributions of debris flow deposits. These estimates exploit the fact that the dry bulk density of undisturbed deposit samples is given by $\rho_{\mathrm{dry}} = \rho_s \upsilon_{\mathrm{fines}}(1 - \upsilon_s) + \rho_s \upsilon_s$, which can be manipulated to yield a simple expression for $\upsilon_{\mathrm{fines}}$:

$$\upsilon_{\mathrm{fines}} = \frac{(\rho_{\mathrm{dry}}/\rho_s) - \upsilon_s}{1 - \upsilon_s} = \frac{\alpha\upsilon_s}{1 - \upsilon_s} = \frac{\alpha}{(\rho_s/\rho_{\mathrm{dry}})(1 + \alpha) - 1} \tag{4}$$

Here $\alpha = \rho_s \upsilon_{\mathrm{fines}}(1 - \upsilon_s)/\rho_s \upsilon_s$ is the mass of fine grains divided by the mass of coarser clasts in disaggregated, dried sediment samples; equivalently, $(100\alpha)/(1 + \alpha)$ is the mass percentage of fines in such samples. Estimates of $\upsilon_{\mathrm{fines}}$ from (4) and ρ_f from (3) are inexact because (4) assumes that the sampled portion of the deposit loses no fines during drainage. By judiciously sampling where drainage has been minimal, the estimation error can be

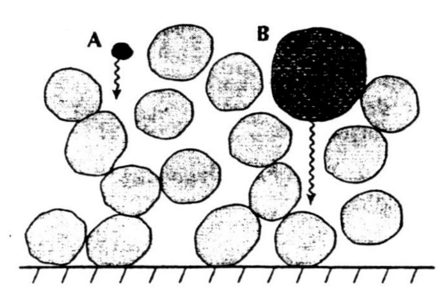

Figure 7. Schematic diagram illustrating the distinction between a small grain that remains suspended exclusively by viscous forces and thus can act as part of the fluid (grain A) and a large grain that requires interaction with other grains to remain suspended (grain B).

TABLE 4. Densities ρ_f and Volumetric Sediment Concentrations $\upsilon_{sediment}$ of the Fluid Fraction in Four Experimental Debris Flows at the USGS Debris Flow Flume

		Measured From Effluent Fluid Samples			Calculated From Deposit Samples*	
Experiment Date	Material	ρ_f, kg/m³	$\upsilon_{sediment}$	Sediments Consisting of Fines, wt%	υ_{fines}	ρ_f, kg/m³
April 19, 1994	sand-gravel mix	1030	0.02	100	0.02–0.05	1030–1080
April 21, 1994	sand-gravel mix	1040	0.025	99.7	0.02–0.05	1030–1080
June 21, 1994†	sand-gravel mix	1160	0.095	94.2	0.02–0.05	1030–1080
July 20, 1994	sand-gravel-loam mix	1110	0.064	94.6	0.07–0.12	1120–1200

Measured densities are those of fluid that drained from debris flow deposits within the first few minutes following deposition. Calculated densities are obtained from equations (3) and (4) and the grain size distribution and dried bulk density of deposit sediment samples obtained several hours after deposition. All calculations assume $\rho_s = \rho_{fines} = 2650$ kg/m^3 and $\rho_w = 1000$ kg/m^3; also assumed is the value $\rho_{dry} = 1900$ kg/m^3, which is the mean of deposit dried bulk densities inferred from tens of measurements.

*Calculations for deposits employ the range of α values inferred from numerous grain size analyses of deposits: 0.01–0.02 for the sand-gravel mix and 0.03–0.06 for the sand-gravel-loam mix.

†Some of the June 21, 1994, fluid leaked from the sample jar during transit, and the resulting fluid loss may be responsible for the relatively large $\upsilon_{sediment}$ and ρ_f values measured thereafter.

minimized. Comparison of direct measurements of ρ_f with estimates calculated from deposit properties and equations (3) and (4) shows that estimation errors of about 10% are common (Table 4).

The presence of fine grains in the pore fluid also influences the effective fluid viscosity. The influence is complex and has been the object of systematic research dating at least to *Einstein* [1906], who deduced the well-known equation $\mu/\mu_w = 1 + 2.5\upsilon_{fines}$, in which μ is the effective viscosity of the fine-grain suspension and μ_w is the viscosity of the fluid alone. Einstein's equation applies to dilute suspensions of chemically inert spheres that satisfy $\upsilon_{fines} < \sim 0.1$ and $N_{Rey} \ll 1$, conditions that are roughly met by the fluids in the experimental debris flows characterized in Table 4. Some natural debris flows have higher concentrations of fines, however [*Major and Pierson*, 1992], so treatments more general than Einstein's are necessary. Although numerous investigators [e.g., *Frankel and Acrivos*, 1967] have deduced equations to predict the effective viscosity of concentrated suspensions of fine spheres, other investigations have explained why no such equation can be expected to work well for the full range of υ_{fines} and all conceivable flow fields [*Batchelor and Green*, 1972; *Acrivos*, 1993]. For the special case of gravity-driven settling, in which buoyancy and drag dominate solid-fluid interaction forces, an empirical formula developed by *Thomas* [1965] predicts the viscosity of suspensions with diverse concentrations relatively well [*Poletto and Joseph*, 1995]. This formula reduces to Einstein's equation in the low-concentration limit and has the form

$$\mu/\mu_w = 1 + 2.5\upsilon_{fines} + 10.05\upsilon_{fines}^2 + 0.00273 \exp(16.6\upsilon_{fines}) \quad (5)$$

Among the shortcomings of this and similar formulas is the neglect of shear rate effects that are especially pronounced if $\upsilon_{fines} > 0.4$, if grain geometries deviate greatly from spheres, or if physicochemical influences of Van der Waals or electrostatic forces between clay and colloidal particles are significant [*Coussot*, 1995]. Nonetheless, an expression such as (5), which predicts increased effective Newtonian viscosity as a consequence of increased fines concentration in the fluid fraction, provides a useful guideline. Viscometric tests of suspensions of only the fines fraction from debris flow sediments provide empirical support for such a guideline but also reveal complications that remain incompletely resolved [*O'Brien and Julien*, 1988; *Major and Pierson*, 1992; *Coussot and Piau*, 1994].

3.2. Debris Flow Mobilization

Successful models of debris flows must describe the mechanics of mobilization as well as those of subsequent flow and deposition. Although debris flows can originate by various means, as when pyroclastic flows entrain and melt snow and ice [*Pierson et al.*, 1990] or when abrupt floods of water undermine and incorporate ample sediment (J. E. O'Connor et al., manuscript in preparation, 1997) origination from slope failures predominates. Hence mobilization is defined here as the process by which a debris flow develops from an initially static, apparently rigid mass of water-laden soil, sediment, or rock. Mobilization requires failure of the mass, sufficient water to saturate the mass, and sufficient conversion of gravitational potential energy to internal kinetic energy to change the style of motion from sliding on a localized failure surface to more widespread deformation that can be recognized as flow. These three requirements may be satisfied almost simultaneously, and the mechanics of mobilization are understood moderately well [*Ellen and Fleming*, 1987; *Anderson and Sitar*, 1995]. *Iverson et al.* [1997] discuss the mechanics of mobilization in detail, whereas the following discussion summarizes only some rudiments.

Debris flows can result from individual slope failures or from numerous small failures that coalesce downstream. In exceptional cases, failure can occur almost grain by grain, as it might during sapping erosion or

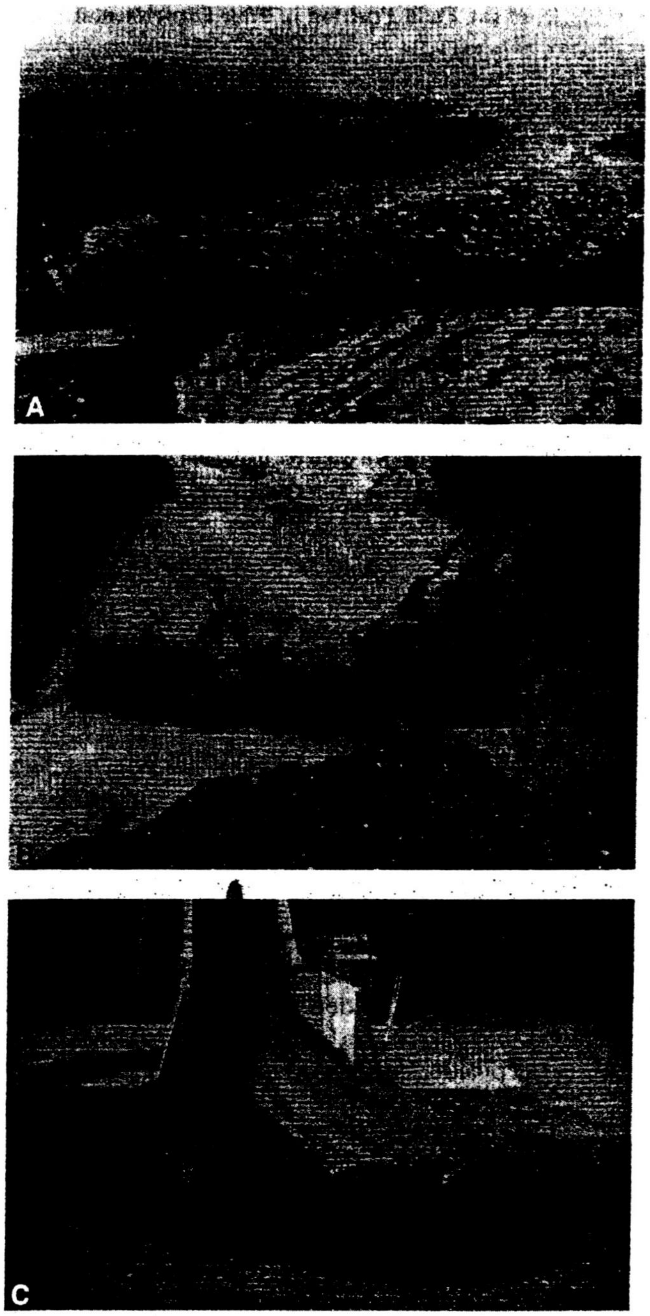

Figure 8. Photographs of advancing fronts of debris flow surges. (a) Nojiri River, Kagoshima, Japan, September 10, 1987. Flow is about 20 m wide and 2–3 m deep. (photo courtesy Japan Ministry of Construction.) (b) Jiang Jia Ravine, Yunnan, China, June 24, 1990. Flow is about 12 m wide and 2–3 m deep (photo courtesy K. M. Scott.) (c) USGS debris flow flume, July 20, 1994. Flow is about 4 m wide and 0.2 m deep.

sediment impact by a water jet [*Johnson*, 1984]. Failure on all scales, from single grains to great landslides, is resisted primarily by strength due to grain contact friction [*Mitchell*, 1978]. Cohesive strength due to soil cementation or electrostatic attraction of clay particles may be important in some circumstances, however. Results from experimental soil and rock mechanics and analyses of failed slopes indicate that the well-known Coulomb criterion adequately describes the state of stress on surfaces where frictional failure occurs [e.g., *Lambe and Whitman*, 1979]. In its simplest form, the Coulomb criterion may be expressed as

$$|\tau| = (\sigma - p) \tan \phi + c \tag{6}$$

Here τ is the average shear or driving stress on the failure surface, and the resisting strength depends on the average effective normal stress $(\sigma - p)$, bulk friction angle ϕ, and cohesion c on the same surface. The bulk friction angle depends on the friction angle of individual grains, ϕ_g, and also on the packing geometry of the assemblage of grains along the failure surface. During failure, cohesive bonds are gradually broken, so that $c \approx 0$ obtains in failed zones of even clay-rich soils [*Skempton*, 1964, 1985]. Thus as failure proceeds, ϕ and the effective stress, here defined simplistically as the difference of the total compressive normal stress σ and pore fluid pressure p [cf. *Passman and McTigue*, 1986], determine the resistance to motion. The value of ϕ might change somewhat as grains rearrange during failure [cf. *Hungr and Morgenstern*, 1984; *Hanes and Inman*, 1985], but changes in effective stress due to stress field rotation and pore pressure change are generally more significant [*Sassa*, 1985; *Anderson and Sitar*, 1995].

In some debris flows the water necessary to saturate the mass comes from postfailure mixing with streams or other surface water, but in most debris flows, all water necessary for mobilization exists in the mass when failure occurs. Indeed, many debris flows are triggered by changes in pore pressure distributions that result from infiltration of rain or snowmelt water that precipitates slope failure [e.g., *Sharp and Nobles*, 1953; *Sitar et al.*, 1992]. To aid mobilization in these circumstances, the debris may contract as failure proceeds [*Ellen and Fleming*, 1987]. Contraction produces transient excess pore pressures that help weaken the mass and enhance the transformation from localized failure to generalized flow [*Bishop*, 1973; *Iverson and Major*, 1986; *Eckersley*, 1990; *Iverson et al.*, 1997]. Contraction during failure has traditionally been regarded as atypical of natural debris because only very loosely packed soils exhibit contractive behavior during standard laboratory compression tests [cf. *Casagrande*, 1976; *Sassa*, 1984; *Anderson and Sitar*, 1995]. However, recent experimentation has shown that even dense soils may undergo volumetric contraction during failure that occurs in an extensional mode [*Vaid and Thomas*, 1995]. Extensional (active Rankine state) failure does indeed occur during mobilization of experimental debris flows [*Iverson et al.*, 1997], and contraction of water-saturated debris during extensional slope failure might thus explain the apparent enigma of debris flows that mobilize from hillslope debris that is relatively dense [cf. *Ellen and Fleming*, 1987].

Transformation from localized failure to generalized flow might occur without debris contraction if sufficient energy is available to agitate the failing mass. This type of transformation can occur in dry granular materials as well as debris flows [*Jaeger and Nagel*, 1992; *Zhang and Campbell*, 1992]. For example, a landslide that becomes agitated and disaggregated as it tumbles down a steep slope can transform into a debris flow if it contains or acquires sufficient water for saturation. Some of the largest and most devastating debris flows originate in this manner [e.g., *Plafker and Ericksen*, 1978; *Scott et al.*, 1995].

3.3. Debris Flow Motion

Following mobilization, debris flows appear to move like churning masses of wet concrete. The largest flows can transport boulders 10 m or more in diameter. However, large-scale experimental debris flows (Figure 3) that contain clasts no larger than 5 cm in diameter exhibit the same qualitative features as larger natural flows. These experimental flows yield the most detailed, quantitative data (e.g., Figure 5) and provide the best evidence for much of the behavior summarized here.

Virtually all debris flows move downslope as one or more unsteady and nonuniform surges. Commonly, an abrupt bore forms the head of the flow, followed by a gradually tapering body and thin, more watery tail [e.g., *Pierson*, 1986; *Takahashi*, 1991] (Figure 8). When multiple surges occur in individual debris flows, each exhibits a conspicuous head and tail [*Jahns*, 1949; *Sharp and Nobles*, 1953; *Pierson*, 1980; *Davies*, 1988, 1990]. Graphs of flow depth or discharge versus time illustrate the generally irregular character of these surges (Figure 9) [*Takahashi*, 1991; *Khegai et al.*, 1992; *Ohsumi Works Office*, 1995]. Observations during experiments at the USGS debris flow flume show that surges can arise

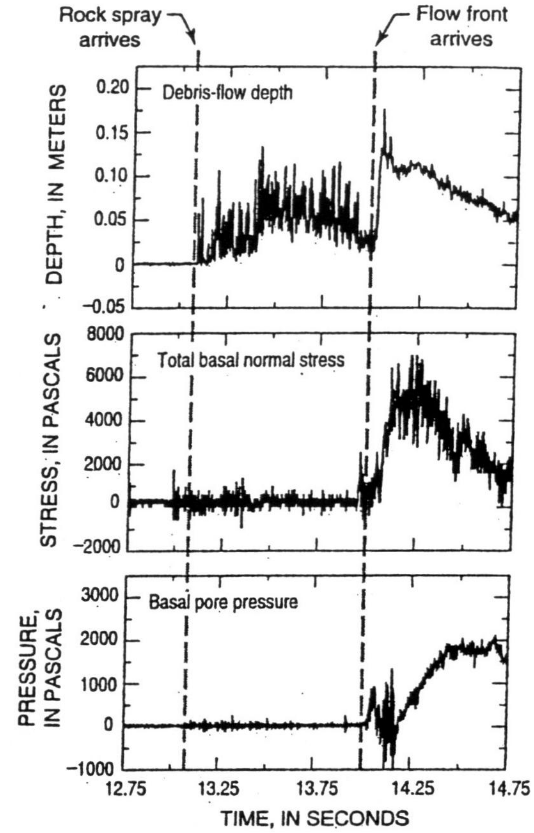

Figure 10. Data from Figure 5a plotted on an expanded time base to show details during arrival of the debris flow front. Note that a spray of tumbling rocks precedes the arrival of the flow front, which occurs at $t \approx 14$ s. Pore pressures do not rise appreciably until the deepest part of the flow front passes the measurement cross section.

spontaneously, without extraneous perturbations of the flow. The resulting low-amplitude surface waves resemble roll waves that form in open channel flows of water on steep slopes [e.g., *Henderson*, 1966]. In experimental debris flows, larger waves tend to overtake and cannibalize smaller waves, as may be anticipated from kinematic wave theory [*Lighthill and Whitham*, 1955]. Consequent coalescence of wave fronts can produce a sequence of large-amplitude surges, which may themselves become unstable. Although other processes, such as transient damming or episodic slope failures, might also generate surges [*Jahns*, 1949], intrinsic flow instability and wave coalescence suffice.

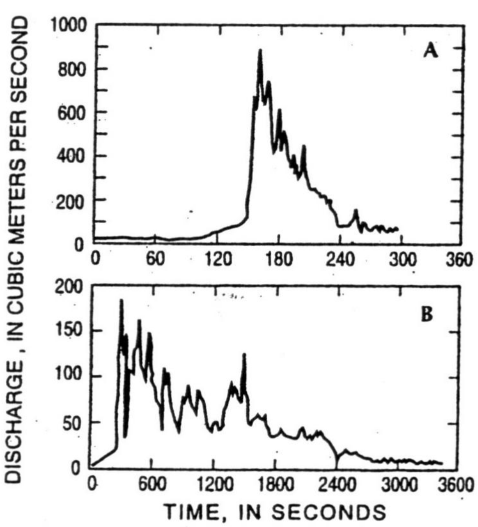

Figure 9. Measurements of debris flow discharge, which illustrate multiple surges within a flow event. (a) Data from Name River, Japan. (Redrafted from *Takahashi* [1991]; copyright A. A. Balkema). (b) Data from Chemolgan River, Kazakhstan [*Khegai et al.*, 1992].

Heads of debris flow surges have several distinctive attributes [*Takahashi*, 1991]. Pore fluid pressures measured at the base of surge heads are close to zero, whereas fluid pressures in the flow body behind the head commonly approach or even exceed those necessary to balance the total normal stress and liquefy the sediment mass (Figure 10). Surge heads generally carry the greatest concentration of large sediment clasts and incidental items, such as downed trees, mangled bridges, or distressed automobiles. The heads appear to remain relatively dry and to restrain downslope flow of the more fluid, water-saturated debris that follows. Pore fluid does not escape visibly by draining through surge heads in moving debris flows, even though the permeability of heads may be great owing to the concentration of large clasts.

Large clasts accumulate at surge heads by two means: they can be incorporated and retained there if the flow acquires the clasts in transit, or they can migrate to the head by preferential transport. Migration and retention of large clasts appear to result chiefly from kinetic sieving similar to that described by *Middleton* [1970]. In kinetic sieving, selective entrainment or transport of large clasts occurs because gravity and boundary drag do not suffice to force the clasts through small voids that open and close as the agitated debris deforms. As small grains translocate through voids, large grains accumulate as a residue near the flow surface and snout. Both physical and numerical experiments demonstrate the efficacy of kinetic sieving in dry granular materials [*Bridgwater et al.*, 1978; *Rosato et al.*, 1987; *Savage*, 1987; *Vallance*, 1994], whereas little experimental or theoretical evidence supports an alternative, dispersive stress mechanism proposed by *Bagnold* [1954] [*Iverson and Denlinger*, 1987; *Vallance*, 1994]. Nonetheless, grain size segregation mechanisms in debris flows may be complicated and may involve more than one process [*Suwa*, 1988].

Agitation of flowing debris influences not only kinetic sieving but also the bulk density of the debris (Table 2) and the ability of grains to move past one another. Improved understanding of the influence of agitation on the mobility of flowing granular materials has constituted a major advance of the last 2 decades [e.g., *Savage*, 1984; *Campbell*, 1990; *Jaeger and Nagel*, 1992]. The role of agitation can be characterized by defining instantaneous grain velocities $\mathbf{v}_s$ as the sum of mean $\bar{\mathbf{v}}_s$ and fluctuating $\mathbf{v}_s'$ components. The intensity of fluctuations and degree of agitation is then measured by a mechanical quantity that has come to be known, following *Ogawa* [1978], as the granular temperature T. The granular temperature may be interpreted as twice the fluctuation kinetic energy per unit mass of granular solids and defined as

$$\mathrm{T} = \langle \mathbf{v}_s'^2 \rangle = \langle (\mathbf{v}_s - \bar{\mathbf{v}}_s)^2 \rangle \tag{7}$$

where angle brackets denote an appropriate average such as the ensemble average. The granular temperature plays a role analogous to that of the molecular temperature in the kinetic theory of gases [*Chapman and Cowling*, 1970]. Like the molecular temperature of a gas, a higher granular temperature reduces bulk density and thereby enhances the ability of a granular mass to flow. However, a higher granular temperature also requires higher rates of energy dissipation, because grain velocity fluctuations cause inelastic grain collisions or intergranular fluid flow that dissipates energy. This energy dissipation has three important ramifications: (1) Granular media (and debris flows) cannot mimic the ability of a gas to maintain constant agitation and flow resistance in the absence of energy exchange with the environment. Instead, granular temperature requires bulk deformation and depends on flow interaction with boundaries that impart external forces. Granular temperatures and boundary forces cannot be specified independently but must be determined hand in hand as part of rigorous mathematical models [*Hui and Haff*, 1986]. (2) As granular temperature increases, stresses and flow resistance become increasingly rate dependent. At higher granular temperatures the mass acts more like a fluid and less like a frictional solid. (3) Formal application of kinetic theory to granular media results in severely mathematical formulations [e.g., *Lun et al.*, 1984], which have not been adapted to inertial flows of solid-fluid mixtures such as debris flows, although *Garcia-Aragon* [1995] has initiated work along these lines.

Granular temperature not only plays a key role in kinetic theories but also indicates whether the instantaneous, collisional grain interactions postulated in such theories are an appropriate idealization. Many dry granular flows involve enduring, frictional grain contacts as well as brief grain collisions [*Drake*, 1990; *Walton*, 1993], and even the most advanced theoretical descriptions of these types of flows are relatively rudimentary [*Anderson and Jackson*, 1992]. Enduring frictional contacts necessarily exist during at least part of a debris flow's duration, for contacts must be sustained as a flow mobilizes from a static mass or forms a static deposit [cf. *Zhang and Campbell*, 1992]. Moreover, at any instant, part of a debris flow may move in a collision-dominated mode, whereas other parts may be friction dominated. The relative importance of collisional, frictional, and fluid-mediated grain interactions is a central problem of debris flow physics and is analyzed in sections 4, 7, and 8.

Stress measurements at the bases of experimental debris flows at the USGS flume provide compelling evidence of nonzero granular temperatures. Both Figures 5 and 10 show fluctuations in total normal stress associated with grain agitation, although the fluctuations are difficult to interpret because a large sensing element (500 cm^2) measured the averaged effects of many ($\sim 10^5$) simultaneous grain interactions. However, contemporaneous measurements with a 1-cm^2 sensing element reveal stress fluctuations at a length scale close to that of the largest grains (gravel) in the experimental debris flow (Figure 11). Stress fluctuations detected by the 1-cm^2 sensor, but not those detected by the 500-cm^2 sensor, had amplitudes as large as or larger than the mean stress. The presence of these large-amplitude fluctuations, which apparently result from individual grains sliding, rolling, and bouncing irregularly along the bed and contacting the sensor, indicates that the effects of boundary slip on stresses can be substantial. If debris flows translated smoothly downslope as steady, laminar flows without boundary slip, no stress fluctuations would occur. If stress fluctuations resulted solely from fluctuations in mean flow quantities such as flow depth, the magnitude of the fluctuations relative to the mean stress would not change with the sensor size. Granular stress fluctuations necessarily are accompanied by grain-scale pore fluid pressure fluctuations [*Iverson and LaHusen*, 1989]. Furthermore, solid and fluid stress fluctuations with time and length scales much larger than those of individual grain interactions also may occur owing to development of interlocked grain clusters that move as more or less coherent blocks. Theoretical results [*Shen and Ackerman*, 1982], computational experiments [*Hopkins et al.*, 1993] and physical experiments [*Iverson and LaHusen*, 1989; *Drake*, 1990] all point to the existence of such clusters.

Pore fluid pressure and granular temperature play synergistic roles, as is indicated by the debris flow energy cascade described in section 2. The combined influence of granular temperature and pore pressure on flow resistance appears to control debris mobility. In turn, debris flow motion generates both granular temperature and nonequilibrium (nonhydrostatic) fluid pressures. A critical distinction exists between the means by which granular temperatures and nonequilibrium fluid pressures arise, however. Steady debris flow motion can produce and sustain granular temperatures by conversion of flow translational energy to grain fluctuation energy, whereas analogous conversion of flow energy to fluid pressure energy is problematic. The most generous estimate of such conversion assumes that all thermodynamic heat generated by debris flow motion produces fluid pressure. Then a typical debris flow heating rate of 0.005°C per meter of flow descent (see section 2) can be multiplied by the thermal pressurization factor for confined water at 20°C (6×10^5 Pa/°C) to estimate 3000 Pa or about 0.3 m of excess pressure head generated per meter of flow descent. However, such a generous estimate neglects the fact that water at 20°C can accommodate a temperature increase of 0.005°C by expanding only 0.0000001%, with no attendant pressure increase. In the agitated, unconfined environment of a debris flow, constraints on expansion are minimal, and substantial thermal pressurization of fluid thus appears unlikely. Yet fluid pressures $\sim\rho gh$ (roughly double the hydrostatic pore fluid pressure $\sim\rho_f gh$), high enough to liquefy the sediment mass, are common at the base of experimental debris flows (Figures 5 and 10). Sustained high fluid pressures reduce intergranular friction and influence grain collisions associated with high granular temperature. Understanding the origin and effects of high fluid pressures appears vital to understanding debris flow behavior.

An obvious possibility is that sediment consolidation produces high pore pressures in debris flows [cf. *Hutchinson*, 1986]. However, consolidation requires that the debris contract monotonically, a condition that cannot be sustained in steady debris flow motion. Thus the debris consolidation hypothesis is, at once, both routine and radical. If consolidation gives rise to high pore pressures in debris flows, then debris flows are fundamentally unsteady phenomena, and limited light can be shed on the phenomena by steady state rheometric experiments and theoretical models. Anecdotal evidence suggests that this may indeed be the case; steady debris flow motion is virtually never observed in nature, and steady motion of debris flow slurries is notoriously difficult if not impossible to achieve in experimental apparatus [e.g., *Phillips and Davies*, 1991; *Major and Pierson*, 1992]. Section 7 provides a detailed mechanical evaluation of hypothetical steady motion, and section 8 shows why unsteady debris flow motion appears more viable mechanically.

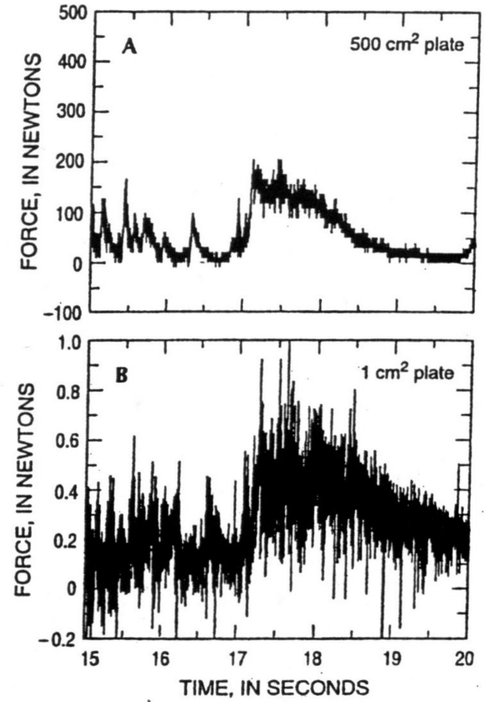

Figure 11. Contemporaneous measurements of bed normal force on (a) a 500-cm² plate and (b) a 1-cm² plate mounted flush with the flume bed. The scale for force in Figure 11b is 500 times the scale in Figure 11a, so that the scaled force amplitude is the same in each plot. The 1-cm² plate was located 0.5 m downslope from the 500-cm² plate, producing a small time lag between the measurements in Figures 11a and 11b. All data were sampled at 2000 Hz during the debris flow flume experiment of August 31, 1994 (see Figures 5 and 10).

3.4. Debris Flow Deposition

Deposition constitutes a special case of unsteady debris flow motion. Deposition occurs when all kinetic energy degrades to irrecoverable forms. Complete energy degradation occurs first when granular temperature falls to zero in the coarse-grained debris that collects at debris flow snouts and lateral margins, where levees may form. This coarse debris consequently composes the perimeter of most debris flow deposits (Figure 12). Deposited coarse debris lacks high pore pressures and typically forms a dam that impedes and eventually halts

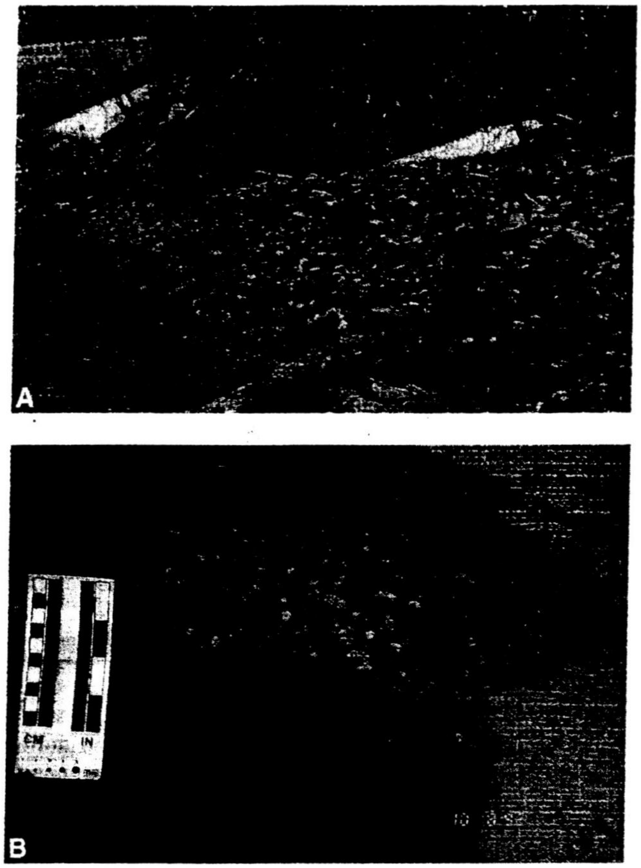

Figure 12. Photographs of snouts of debris flow deposits, which show concentrations of coarse clasts and bluntly tapered margin morphology. (a) Lobe of a small ($\sim$1000 m^3) debris flow that partly crossed the scenic highway near Benson State Park, Oregon, February 7, 1996. (b) Vertical cross section through a marginal lobe of an experimental debris flow at the USGS debris flow flume, October 8, 1992.

the motion of ensuing finer-grained debris that retains higher pore pressures. Alternatively, wetter, more mobile debris may have enough momentum to override or breach the dam of previously deposited debris, so that deposits can develop by a combination of forward pushing, mass "freezing," vertical accretion, and lateral shunting of previously deposited sediment [*Major*, 1997]. Experimental observations of idealized debris mixtures indicate that freezing generally occurs from the bottom up, rather than the top down, as debris comes to rest [*Vallance*, 1994]. Thus neither the thickness of deposited lobes nor that of levees provides a good indicator of the dynamic behavior of the moving debris as a whole [cf. *Johnson*, 1970]. Instead, the complex interplay between the resistance of the first-deposited debris and the momentum of subsequently arriving debris produces deposits that are initially dry and strong at their perimeter, wet and weak in their interior, and conspicuously heterogeneous in their resistance to motion. Indeed, pore fluid pressures in the center of a deposit can remain elevated well above hydrostatic levels and maintain the sediment in a nearly liquefied state long after deposition occurs (Figure 13) [*Major*, 1996] [cf. *Hampton*, 1979; *Pierson*, 1981]. Subsequent decay of interior pore pressures, with attendant consolidation (i.e., gravitational settling) of the solids and drainage of fluid, marks the final stages in a debris flow's transition from fluid-like to solid-like behavior.

The timescale for pore pressure decay is defined by the quotient of a pore pressure diffusion coefficient, $D = kE/\mu$, and the square of the characteristic drainage path length. Here E is the composite stiffness (reciprocal of the compressibility) of the debris mixture. Measurements and modeling by *Major* [1996] show that drainage is dominantly vertical in typical debris flow deposits, which have lengths and widths that greatly exceed their thickness h. Thus the characteristic drainage path length is h, which yields the pore pressure diffusion timescale

$$t_{\mathrm{dif}} = h^2\mu/kE \tag{8}$$

Because high pore pressures help sustain debris mobility, it is tempting to equate the diffusion timescale t_{diff} with the debris flow duration or timescale for which mobility is sustained, t_D [*Hutchinson*, 1986]. Three problems complicate this interpretation, however. First, pore fluid pressures are but one phenomenon that influences mobility; debris flow mixtures can flow in the absence of high pore pressure if they have sufficient granular temperature. Second, nonequilibrium pore pressures may be small or absent at the front of debris flow surges (Figures 5 and 10), so that pore pressure diffusion is locally irrelevant. Finally, the definition of t_{diff} includes a composite stiffness coefficient E, which has the properties of an elastic modulus in small-strain problems [*Biot*, 1941] but which has more complicated properties when deformations are large and irreversible [e.g., *Helm*, 1982]. Section 8 addresses this issue quantitatively and shows how the evolving compressibility of debris flow materials can influence pore pressure diffusion and play a key role in debris flow physics.

4. MOMENTUM TRANSPORT: SCALING AND DIMENSIONAL ANALYSIS

To build a quantitative background for analyzing debris flow physics, it is useful to ignore temporarily some of the complexities described in the preceding section and consider momentum transport during steady, simple shearing of an unbounded, uniform mixture of identical, dense spherical grains and water. Initially restricting attention to an unbounded domain and a single grain diameter δ vastly simplifies the analysis, because it unambiguously establishes the dominant length scale as δ. Scaling considerations then suffice to draw rudimentary conclusions about momentum transport and the attendant state of stress in the mixture. Associated dimensional analysis defines dimensionless parameters that can be used to classify debris flows and identify limiting

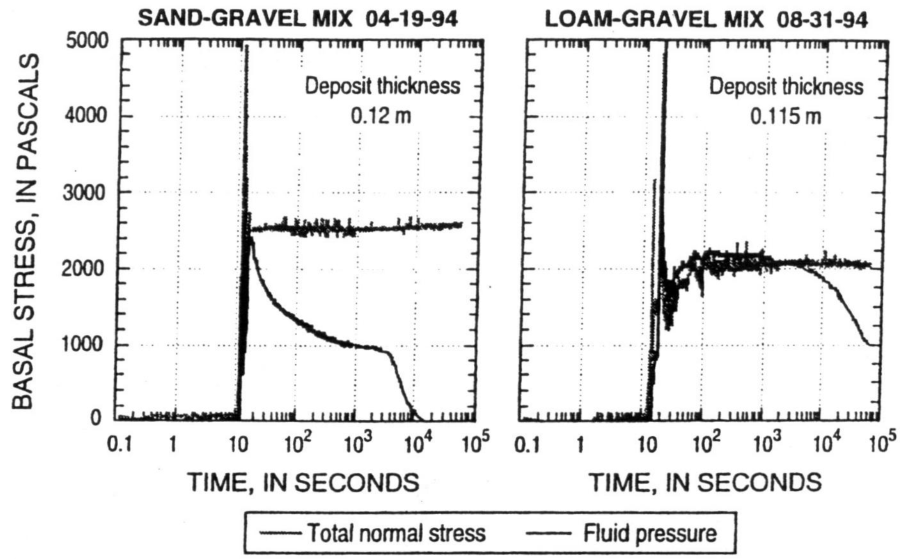

Figure 13. Measurements of total basal normal stress (on a 500-cm^2 plate) and basal pore pressure during deposition of debris flow sediments with different grain size distributions at the USGS debris flow flume. Measurements were made through ports in the runout pad at the flume base (Figure 4), and deposits were centered over the measurement ports. Deposit interiors were liquefied by high pore pressure at the time of emplacement, and pore pressures subsequently decayed. High pore pressures persisted much longer in the deposit that contained loam with about 6% (by weight) silt and clay-sized particles than in the deposit that lacked loam and contained about 2% (by weight) silt and clay-sized particles [after *Major*, 1996].

styles of behavior. The multiplicity of relevant dimensionless parameters also reveals why nearly intractable problems arise in attempts to "scale down" debris flow mixtures to the size of laboratory apparatus. Such scaling problems may partly explain why very divergent views about debris flow physics have arisen from different approaches to experimentation and modeling (see section 5).

Figure 14 depicts schematically a representative region within a uniform grain-water mixture undergoing steady, uniform shearing motion in a gravity field; the

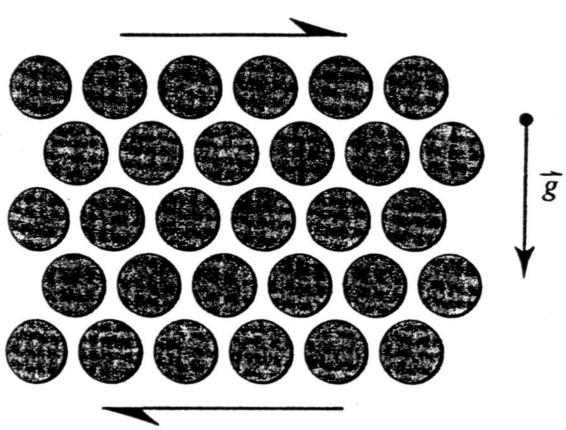

Figure 14. Schematic diagram of a steady, uniform, unbounded shear flow of identical solid spheres immersed in a Newtonian fluid. This flow is too simple to represent debris flows, but it provides a basis for assessing scaling parameters that influence stresses.

various stresses (solid grain shear and normal stress, fluid shear and normal stress, and solid-fluid interaction stress) that accompany momentum transport in the mixture are represented collectively by Σ. Adapting the approach used by *Savage* [1984] for dry grain flows, these stresses are postulated to depend functionally on the mixture shear rate $\dot{\gamma}$ and on 12 additional variables discussed in section 3 and listed in the notation section:

$$\Sigma = \mathcal{F}(\dot{\gamma}, \delta, \rho_s, \rho_f, g, \mu, k, T, E, \upsilon_s, \upsilon_f, \phi, e) \quad (9)$$

Variables not included in (9) might influence stresses also but are assumed to have less importance than those included.

As a preliminary step, dimensional analysis reorganizes (9) into a more fundamental and compact relationship that involves only dimensionless parameters. The first 10 variables in (9) have units comprising three physical dimensions: mass, length, and time. The last four variables in (9) are intrinsically dimensionless and are superfluous in dimensional analysis. According to the Buckingham II theorem [*Buckingham*, 1915], any physically meaningful relation between 10 variables comprising three dimensions must reduce to a relation between 7 (= 10 − 3) independent dimensionless parameters. Definition of these parameters depends on choices for the characteristic length, mass, and time. For the simple system depicted in Figure 14, the choices are obvious: the characteristic length is δ, the characteristic mass is $\rho_s\delta^3$, and the characteristic time is $1/\dot{\gamma}$. These, in turn, determine a characteristic velocity $v \sim \dot{\gamma}\delta$, which describes the speed at which grains move past one another and at which fluid moves to accommodate grain motion. With these choices, standard methods of dimensional analysis [e.g., *Bridgman*, 1922] applied to (9) yield

$$\frac{\Sigma}{\dot\gamma^2\delta^2\rho_s} = \mathcal{F}\left(\frac{\dot\gamma^2\delta}{g}, \frac{\dot\gamma\delta^2\rho_s}{\mu}, \frac{\rho_s}{\rho_f}, \frac{T}{\dot\gamma^2\delta^2}, \frac{k}{\delta^2}, \frac{E}{\dot\gamma^2\delta^2\rho_s}\right) \quad (10)$$

The right-hand side of this relation lists six dimensionless parameters that determine the dimensionless stresses, $\Sigma/\dot\gamma^2\delta^2\rho_s$. The significance of the first right-hand-side parameter was first enunciated by *Savage* [1984], and accordingly it has been dubbed the Savage number [*Iverson and LaHusen*, 1993]. The second parameter is a variation of a parameter first investigated by *Bagnold* [1954], commonly called the Bagnold number [*Hill*, 1966]. The third parameter is the ratio of solid density to fluid density, which ranges only from about 2 to 3 in debris flows. The fourth parameter is the granular temperature scaled by the square of the characteristic shear velocity $\dot\gamma\delta$ [cf. *Savage*, 1984]. The fifth parameter is the permeability divided by the grain diameter squared; it reflects the role that grain size and packing play in solid-fluid interactions. The sixth parameter is the composite mixture stiffness (resistance to dilation and contraction) divided by the characteristic stress $\dot\gamma^2\delta^2\rho_s$.

The significance of the parameters in (10) can be clarified by analyzing their relationship to estimates of solid, fluid, and solid-fluid interaction stresses in the mixture. These stresses have both shear and normal components; in turn, each of these components may have both quasi-static and inertial components. For brevity, this analysis will focus exclusively on shear components of stress, which are generally of greatest interest. A similar analysis is easily conducted for the normal stress components.

The solid inertial stress $T_{s(i)}$ and fluid inertial stress $T_{f(i)}$ both scale like the product of the mass (solid or fluid) per unit volume and the square of the characteristic velocity, $v^2 \sim \dot\gamma^2\delta^2$. Thus they may be estimated by

$$T_{s(i)} \sim \upsilon_s\rho_s\dot\gamma^2\delta^2 \quad (11)$$

$$T_{f(i)} \sim \upsilon_f\rho_f\dot\gamma^2\delta^2 \quad (12)$$

The first of these relationships shows that the characteristic stress used to scale Σ in (10) is essentially the solid grain inertia stress. This is the stress transmitted by grain collisions [cf. *Iverson and Denlinger*, 1987] and explicated by *Bagnold* [1954]. The second relationship shows that fluid can also sustain inertial stresses, in a manner roughly analogous to that of Reynolds stresses in turbulent flow of pure fluid. The fluid-inertia stress was ignored by *Bagnold* [1954].

The quasi-static solid stress $T_{s(q)}$ is associated with Coulomb sliding and enduring grain contacts (see equation (6)). This stress increases as depth below a horizontal datum increases but decreases if static pressure in the adjacent fluid increases independently. At depth $N\delta$ the quasi-static solid stress is estimated by

$$T_{s(q)} \sim N\upsilon_s(\rho_s - \rho_f)g\delta \tan\phi \quad (13)$$

where N, the number of grains above and including the layer of interest, accounts for the effects of the overburden load, and $\upsilon_s(\rho_s - \rho_f)g$ is the buoyant unit weight of this overburden. Additional (nonhydrostatic) fluid pressure may also mediate $T_{s(q)}$ but is characterized separately (below) by the solid-fluid interaction stress, T_{s-f}.

The quasi-static fluid stress derives from Newton's law of viscosity:

$$T_{f(q)} = \upsilon_f\dot\gamma\mu \quad (14)$$

In this equation, υ_f appears because only this fraction of the mixture undergoes viscous shear.

The solid-fluid interaction stress T_{s-f} results from relative motion of the solid and fluid constituents. Although T_{s-f} may involve both inertial and quasi-static (viscous drag) components, a detailed analysis by *Iverson* [1993] shows that viscous coupling surpasses inertial coupling in materials similar to those in debris flows, and that neglect of inertial coupling is generally justified. Viscous coupling results in drag that generates a force per unit volume of mixture $\sim v(\mu/k)$, which produces a stress $\sim v\delta(\mu/k)$. Thus, expressed in terms of the shear rate $\dot\gamma = v/\delta$, the interaction stress can be estimated as

$$T_{s\text{-}f} \sim \frac{\dot\gamma\mu\delta^2}{k} \quad (15)$$

This interaction stress results from grain-scale fluid flow driven by grain rearrangements during steady shearing motion at the rate $\dot\gamma$ [cf. *Iverson and LaHusen*, 1989]. If motion were unsteady and net volume change were to occur, an additional viscous interaction stress would arise in concert with net pore pressure diffusion (see discussion following equation (8)).

The chief significance of (11)–(15) lies in the ratios that they form. For example, division of the characteristic stress $T_{s(i)}$ by $T_{s(q)}$ shows that a Savage number N_{Sav} (here modified to account for the solid friction angle, overburden load, and hydrostatic buoyancy) may be defined by the ratio of inertial shear stress associated with grain collisions to quasi-static shear stress associated with the weight and friction of the granular mass

$$N_{Sav} = \frac{\dot\gamma^2\rho_s\delta}{N(\rho_s - \rho_f)g \tan\phi} \quad (16)$$

Similarly, division of $T_{s(i)}$ by $T_{f(q)}$ shows that a Bagnold number N_{Bag} may be defined by the ratio of inertial grain stress to viscous shear stress:

$$N_{Bag} = \frac{\upsilon_s}{1 - \upsilon_s}\frac{\rho_s\delta^2\dot\gamma}{\mu} \quad (17)$$

wherein the factor $\upsilon_s/(1 - \upsilon_s)$ results from the substitution $\upsilon_f = 1 - \upsilon_s$ and differs from the factor $\lambda^{1/2} =$

$[\upsilon_s^{1/3}/(\upsilon_*^{1/3} - \upsilon_s^{1/3})]^{1/2}$ originally used by *Bagnold* [1954] (υ_* is the maximum value of υ_s achievable in a dense-packed configuration). Division of $T_{s(i)}$ by $T_{f(i)}$ produces a "mass number" N_{mass} that describes the ratio of solid inertia to fluid inertia in the mixture:

$$N_{\text{mass}} = \frac{\upsilon_s}{1-\upsilon_s}\frac{\rho_s}{\rho_f} \tag{18}$$

Division of T_{s-f} by $T_{s(i)}$ produces a quantity here termed the "Darcy number,"

$$N_{\text{Dar}} = \frac{\mu}{\upsilon_s \rho_s \dot{\gamma} k} \tag{19}$$

which describes the tendency for pore fluid pressure developed between moving grains to buffer grain interactions. Furthermore, division of N_{Dar} by $E/(\dot{\gamma}^2\delta^2\rho_s)$ (which appears in (10)), yields $(\dot{\gamma}\mu\delta^2)/(\upsilon_s kE)$, a dimensionless parameter that describes the ratio of the timescale for diffusive pore pressure dissipation across the distance δ to the timescale for pore pressure generation by grain interactions, $1/\dot{\gamma}$ [cf. *Iverson and LaHusen*, 1989]. The diffusion timescale $\mu\delta^2/kE$ resembles the consolidation timescale defined in (8). The chief difference is that $\mu\delta^2/kE$ characterizes grain-scale diffusion in a flow that is macroscopically steady, whereas (8) characterizes diffusion during unsteady consolidation throughout the entire debris flow thickness.

Additional dimensionless parameters of interest can be obtained by forming ratios of the parameters defined in (16)–(19). For example, a version of the well-known grain Reynolds number can be expressed as

$$N_{\text{Rey}} = \frac{N_{\text{Bag}}}{N_{\text{mass}}} = \frac{\rho_f \dot{\gamma} \delta^2}{\mu} \tag{20}$$

and the ratio of the Bagnold number to Savage number forms a version of the friction number identified by *Iverson and LaHusen* [1993]:

$$N_{\text{fric}} = \frac{N_{\text{Bag}}}{N_{\text{Sav}}} = \frac{\upsilon_s}{1-\upsilon_s}\frac{N(\rho_s - \rho_f) g \delta \tan \phi}{\dot{\gamma}\mu} \tag{21}$$

This number expresses the ratio of shear stress borne by sustained grain contacts to viscous shear stress. It resembles the well-known Bingham number, which describes the ratio of stress borne by shear strength to stress borne by viscous flow in viscoplastic materials. The key difference between the friction number and Bingham number lies in the fact that the friction number characterizes stresses borne by distinct solid and fluid phases, whereas the Bingham number characterizes stresses in a one-phase material that exhibits both viscosity and strength.

The dimensionless groups defined by (16)–(21) distinguish five processes of momentum transport (i.e., stress generation) in a steady shear flow of a uniform mixture of identical grains and water: (1) inertial grain collisions, (2) grain contact friction, (3) viscous shear, (4) inertial (turbulent) fluid velocity fluctuations, and (5) solid-fluid interactions. At least this many processes must affect stresses in debris flows with more complicated constituents and kinematics [*Iverson and Denlinger*, 1987]. It thus appears unlikely that any simple rheological model can accurately represent all stresses in debris flows. Nonetheless, simple but valid approximations may be attainable if in some circumstances only a subset of these stresses dominate.

Rough but useful assessments of the relative importance of different stress generation mechanisms in debris flows can be accomplished by calculating representative values of the dimensionless parameters defined in (16)–(21) and comparing these values with those for simpler systems in which stress generation is better understood. This process is analogous to assessing open channel flow of water on the basis of Froude and Reynolds numbers. Table 5 lists values of (16)–(21) computed for a representative spectrum of debris flows, ranging from a 10-m^3 flow in the USGS flume to the prehistoric Osceola mudflow of $\sim 10^9$ m^3 (see Table 1). Values of some variables need to be estimated to make these computations. For example, Table 5 lists a fixed δ of 1 mm for all flows. Although all flows listed in Table 5 consisted predominantly of grains of about this size (sand), larger grains might be more significant in some instances (as in a boulder- or cobble-rich debris flow snout). Nonetheless, the values of (16)–(21) listed in Table 5 provide some idea of the range of values for a variety of debris flows.

Although interpretation of the values of (16)–(21) in Table 5 is limited by a dearth of relevant data, some guidelines exist. For example, *Savage and Hutter* [1989] reviewed a variety of experimental evidence and concluded that grain collision stresses dominate grain friction stresses in dry granular flows if N_{Sav} is greater than about 0.1. Similarly, *Bagnold*'s [1954] experiments demonstrated that in neutrally buoyant mixtures of spherical grains and liquid (where $N_{\text{Sav}} \rightarrow \infty$), collisional stresses dominate viscous stresses if N_{Bag} exceeds roughly 200. (This differs from *Bagnold*'s [1954] value of 450, because Bagnold included the factor $\lambda^{1/2}$ rather than $\upsilon_s/(1 - \upsilon_s)$ in his evaluation.) Apparently no experimental data bearing on transition values of N_{mass} are available, although the qualitative influence of N_{mass} is obvious from its definition: grain inertia becomes unimportant as the density or concentration of grains approaches zero. In contrast, many data pertain to grain Reynolds numbers, N_{Rey}. Typically, fluid flow with respect to grains begins to show inertial effects and deviate significantly from ideal viscous (Stokesian) behavior for $N_{\text{Rey}} > 1$ [*Vanoni*, 1975]. Fewer data are available for N_{fric} and N_{Dar}, although *Iverson and LaHusen* [1989] reported experiments with $1000 < N_{\text{Dar}} < 6000$, in which large fluid pressure fluctuations evidenced strong solid-fluid interactions. Values of N_{Dar} at least this large probably apply for most debris flows (Table 5).

With these guidelines for interpretation, the tabulated values of dimensionless parameters in Table 5

TABLE 5. Estimation of Dimensionless Parameters That Characterize Stresses in a Range of Prototypical Debris Flow Mixtures

Parameter	*Debris Flow Prototype* USGS Flume Experiment (Sand-Gravel)	Oddstad Debris Flow (Figure 1), Jan. 4, 1982	South Toutle River, May 18, 1980	Osceola Mudflow, circa 5700 B.P.
		Dimensional Parameters		
δ, m	0.001*	0.001*	0.001*	0.001*
$h = N\delta$, m	0.1	1	5	20
v, m/s	10	10	20	20
$\dot{\gamma}$, 1/s	100	10	4	1
ρ_s, kg/m^3	2700	2700	2700	2700
ρ_f, kg/m^3	1100	1100	1100	1200
μ, Pa s	0.001	0.01*	0.01*	0.1*
g, m/s^2	9.8	9.8	9.8	9.8
k, m^2	10^{-11}	10^{-11}*	10^{-12}	10^{-12}
E, Pa	10^4*	10^4*	10^4*	10^4*
v_s	0.6	0.6	0.6	0.6
v_f	0.4	0.4	0.4	0.4
ϕ, deg	40	30	30	30
		Dimensionless Parameters		
N_{Sav}	0.2	2×10^{-4}	6×10^{-6}	1×10^{-7}
N_{Bag}	400	4	0.2	0.4
N_{mass}	4	4	4	4
N_{Dar}	600	60,000	2×10^6	6×10^7
N_{Rey}	100	1	0.04	0.01
N_{fric}	2×10^3	2×10^4	3×10^4	4×10^5

Data sources for approximate range of values of dimensional parameters are as follows: h, v, and $\dot{\gamma}$, kinematic reconstructions and direct observations (see references cited in Table 1); ρ_f, ρ_s, μ, k, v_s, and v_f, Table 2, Table 4, and Figure 6 of this paper; δ, E, and ϕ, Figure 20 of this paper and data from *Major* [1996]. In all cases the typical shear rate $\dot{\gamma}$ is estimated from the quotient of the typical flow speed v and depth, h.

*Values of dimensional parameters for which the tabulated value may vary or err by more than an order of magnitude.

paint a reasonably consistent picture of the factors apt to influence stresses in debris flows. For thin, fast flows on steep slopes (e.g., flows at the USGS debris flow flume), high shear rates cause both the Savage number and Bagnold number to be moderately large; however, the tabulated values $N_{Sav} = 0.2$ and $N_{Bag} = 400$ approximate the respective transition values 0.1 and 200. Thus grain collisions might be expected to transmit most stress in such flows, but friction and viscosity also may contribute significantly. For larger flows with greater depths and smaller shear rates, the situation is more clear-cut. Small values of N_{Sav} and N_{Bag} indicate that collisions likely transmit negligible stress in such flows and that friction and viscosity dominate. Large values of the friction number suggest that frictional shear stresses probably exceed viscous shear stresses, but small grain Reynolds numbers and large values of N_{Dar} indicate that viscous drag associated with solid-fluid interactions is likely to be important. The picture changes in parts of debris flows (such as heads of surges) where grains coarser than sand predominate. If shear rates are constant and δ increases, friction increasingly dominates viscosity, but collisions increasingly dominate friction. Thus individual debris flows may include regions where different momentum transport processes dominate or where several processes contribute almost equally. With this knowledge, models that include only one or two processes of momentum transport (such as those described in sections 5 and 9) can be placed in an appropriate context.

In principle, the values of key dimensionless parameters also facilitate discrimination of debris flows from related phenomena. For example, by selecting the pa-

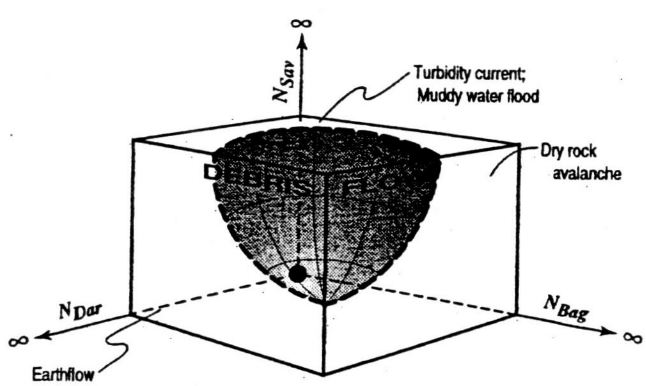

Figure 15. Classification scheme that distinguishes debris flows on the basis of values of the dimensionless parameters N_{Sav}, N_{Bag}, and N_{Dar}. Debris flows occupy a broad and imprecisely defined domain (shaded) in the center of this parameter space. If one or more of the parameters N_{Sav}, N_{Bag}, and N_{Dar} has a value either very large or small, debris flow may grade into other types of sediment transport processes, as indicated by labeled regions in the diagram.

TABLE 6. Comparison of Models' Ability to Explain Physical Phenomena That Typify Debris Flows

	Type of Model		
Phenomenon	*Bingham Viscoplastic*	*Bagnold Grain Flow*	*Coulomb Grain Flow With Variable Pore Pressure*
Flow mobilizes from rigid slope failure without changes in constitutive properties			X
Fluid pressures in flow can differ from the mean pressure and affect apparent strength or flow resistance			X
Flow can exhibit a "rigid" plug of undeforming material	X		X
Flow can lack a "rigid" plug of undeforming material		X	X
Flow is unsteady and nonuniform, with a blunt snout and tapered tail	X	X	X
Flow can transport large clasts that do not settle out	X	X	X
Flow produces grain size segregation			
Flow agitation can affect apparent strength or flow resistance		X	
Boundary slip occurs at the bed			X
Flow strengthens and halts rapidly when pore fluid is drained from beneath it			X
Deposit interior can remain weak and unable to support loads while deposit perimeter becomes rigid			X

"X" denote phenomena that can be explained at least qualitatively. Assessment of the Bingham and Bagnold models assumes that the standard forms as described by *Johnson* [1984] and *Takahashi* [1981] apply. The model of Coulomb grain flow with variable pore pressure is described in section 9 of this paper.

rameters N_{Sav}, N_{Bag}, and N_{Dar} as those most likely to vary significantly from flow to flow, a classification scheme such as that shown in Figure 15 can be devised. In this scheme various phenomena that can resemble and transform to or from debris flows, such as rock avalanches or turbidity currents, represent limiting cases in which one or more of the parameters N_{Sav}, N_{Bag}, and N_{Dar} has a value that is either very large or very small. The parameter space intermediate between these limiting cases includes the variety of behaviors that constitute the process of debris flow. At present, such a classification has utility chiefly as a conceptual tool; it illustrates the hybrid character of debris flows and indicates that debris flow behavior likely cannot be discriminated on the basis of a few simple measures, such as shear rate and solids concentration. A more rigorous interpretation remains elusive because the parameter space boundaries between various processes identified in Figure 15 remain vaguely defined.

Although the appeal of simple dimensional methods and classifications is clear, it is important to recognize their limitations. Because the foregoing dimensional analysis assumes very idealized kinematics (uniform simple shear flow), it neglects variations in granular temperature and volume fraction, and it neglects energy conversion and dissipation that necessarily occur at flow boundaries. Perhaps most importantly, it neglects that debris flows virtually always include grains of widely ranging sizes, develop pore pressures that exceed hydrostatic values, and occur as unsteady, nonuniform surges. Analyses more sophisticated than simple scaling and dimensional methods are therefore needed to develop better insight and appropriate models. The following sections describe traditional and more recent approaches to this problem.

5. TRADITIONAL (RHEOLOGICAL) MODELS OF MOMENTUM TRANSPORT

Models of two distinct types, viscoplastic and inertial grain flow, traditionally have provided the theoretical framework for most debris flow research. Each type of model postulates a unique rheological relation between the shear stress and shear strain rate in flowing debris mixtures. Such postulates conflict with data showing that solid and fluid stresses in debris flows vary asynchronously (Figures 5, 10, and 13) and with inferences that varying pore pressures and granular temperatures influence debris behavior. Consequently, this section avoids detailed review of traditional rheological models (provided previously by *Johnson* [1984] and *Takahashi* [1991]), and instead summarizes their strengths and shortcomings. Table 6 compares qualitative attributes of debris flows that can be explained with traditional models and a model that emphasizes solid-fluid interactions. Later sections of this paper provide a more quantitative perspective.

The first systematic efforts to develop a physical understanding of debris flows were those of *Johnson* [1965] and *Yano and Daido* [1965], who recognized independently that debris flows exhibit properties of both viscous fluids and plastic solids. This marked a significant step forward, because earlier, descriptive work did not clearly distinguish the mechanics of debris flows from those of muddy water floods. *Johnson* [1965, 1970, 1984] adopted the simplest mechanical model that combines plastic and viscous attributes: that of a Bingham, or viscoplastic, continuum [cf. *Bird et al.*, 1982]. This model describes a single-phase material that remains rigid or elastic unless deviatoric stresses exceed a threshold value, the plastic yield strength. Where stresses exceed the yield strength, the material flows like a viscous fluid. At a stress-free surface of an open channel flow such as a debris flow, a Bingham material translates like a rigid solid.

As was recognized by *Johnson* [1965, 1970, 1984], Bingham models for debris flows can be generalized to allow yield strength to depend on Coulomb friction (and hence on the mean stress) and viscosity to depend on deformation rate [*Iverson*, 1985; *Coussot and Piau*, 1994, 1995], but applications of Bingham models to debris flows have almost invariably assumed fixed viscosities and yield strengths [e.g., *Fink et al.*, 1981]. Most applications have also assumed steady, uniform flow. For example, steady state balances of driving and resisting force have been used to infer fixed yield strengths from the thickness of deposited debris flow lobes [*Johnson*, 1984; *Whipple and Dunne*, 1992]. Bingham strengths treated in this manner are equivalent both conceptually and mathematically to Coulomb strengths (equation (6)) in which $\phi = 0$ and cohesion alone controls yielding. If this equivalency has a sound physical basis, Bingham strengths should increase as the fines content of the debris increases, and small-scale experiments with debris mixtures composed of only fine sediment and water indeed produce this behavior [*Johnson*, 1970; *O'Brien and Julien*, 1988; *Major and Pierson*, 1992]. However, large-scale flume experiments with mixtures of predominantly sand, gravel, and water, with a fines content of only a few percent (comparable to most natural debris flow mixtures) show that increased fines content decreases lobe thickness and apparent strength, because the fines help sustain high pore pressures that reduce frictional resistance and enhance lobe spreading [*Major*, 1996]. This reveals a fundamental shortcoming of fixed-yield-strength Bingham models: such models simulate the rheology of the water-plus-fines fraction of debris-flow mixtures, whereas observations and data show that interactions of coarse sediment grains with one another and with adjacent fluid strongly affect debris flow behavior [cf. *Costa and Williams*, 1984; *Major and Pierson*, 1992].

Even if posed and used in a very general form [*Iverson*, 1985, 1986a, b], Bingham models have significant limitations [cf. *Johnson*, 1984]. They assume that momentum transport and energy dissipation in debris flows occurs exclusively by viscous shearing. They neglect the fact that rate-independent energy dissipation can occur when sediment grains contact one another or flow boundaries [e.g., *Adams and Briscoe*, 1994], and they neglect fluid flow relative to the granular assemblage. In this respect, Bingham models represent a limiting type of behavior in which $N_{\text{Bag}} \rightarrow 0$ and $N_{\text{Dar}} \rightarrow \infty$ (see Figure 15), which may provide an adequate description of phenomena such as slow, creeping earthflows but not of debris flows. Bingham models also generally employ fluid-mechanical no-slip boundary conditions. No-slip boundaries require a Bingham material to leave a continuous layer of deposited sediment along its path, but debris flow paths commonly lack such deposits. Instead, grains may slide, collide and roll along flow boundaries. Grains visible on the surface of debris flows may either jostle energetically or lock together to form an apparently rigid plug, depending on the granular temperature, which in turn depends on flow speed, composition, and boundary conditions. Realistic models of debris flow physics need to account for these phenomena.

To account for grain interactions, *Takahashi* [1978, 1980, 1981] exploited the seminal findings of *Bagnold* [1954] to develop an inertial grain flow model of debris flows. *Bagnold*'s [1954] experiments employed an enclosed annular shear cell to evaluate the effects of grain interactions in rapidly shearing, concentrated suspensions of uniform, solid spheres immersed in a Newtonian fluid of identical density. From his experiments and a simple analysis of binary grain collisions, Bagnold inferred that shear and normal stresses in the suspensions varied either quadratically or linearly with the shear rate, depending on the value of N_{Bag}. *Bagnold* [1954] used the terms "grain inertia" and "macroviscous," respectively, to describe the regimes where quadratic and linear stress–strain rate behavior obtained. Subsequent shear cell experiments by others largely confirmed Bagnold's results [e.g., *Savage and McKeown*, 1983] and also showed that the dynamic friction angle relating shear and normal stresses in rapidly shearing granular materials differed little from the static Coulomb friction angle described by (6) with $c = 0$ [e.g., *Hungr and Morgenstern*, 1984; *Savage and Sayed*, 1984; *Sassa*, 1985]. *Takahashi*'s [1978, 1980, 1981] influential contribution to debris flow physics involved application of Bagnold's stress–strain rate relations for the grain inertia regime. Other investigators [e.g., *Davies*, 1986] advocated *Bagnold*'s [1954] formulas for the macroviscous regime as a model for debris flows. Unfortunately, use of *Bagnold*'s [1954] formulas for either regime is problematic, for Bagnold's results reflect the special conditions of his experiments. Adoption of *Bagnold*'s [1954] formulas as constitutive equations for general flow fields leads to contradictory results.

Flow of a solid-fluid debris mixture in a channel enclosed by parallel, vertical plates illustrates the type of contradictions that can arise in applying *Bagnold*'s [1954] equations. Flow is driven by a longitudinal body force, such as that due to gravity. Regardless of flow rheology, symmetry dictates that the mixture's shear rate vanishes at the flow centerline (Figure 16). Bagnold's equations for both the grain inertia and macroviscous regimes then require that the normal and shear stress also vanish at the centerline. However, a vanishing normal stress contradicts the presence of the body force that drives the flow. Bagnold's experiments lacked this contradiction because granular pressure gradients due to gravity or other forces independent of shearing were absent in his apparatus. In Bagnold's experiments with neutrally buoyant spheres, he intentionally camouflaged the effect of gravity on the solid grains, imposed the shear rate, and measured the stress. In debris flows, in contrast, gravity imparts a stress that increases with depth below the surface, and the shear rate responds. Shearing, in turn, can modify the granular pressure gradient by influencing the local granular temperature, grain concentration, and possibly the pore-fluid pressure [cf. *Hui and Haff*, 1986; *Johnson et al.*, 1991]. Thus Bagnold's results, obtained with fixed concentrations and shear rates, provide valuable insight but not a valid constitutive equation for debris flows. Section 7 casts this interpretation quantitatively.

Takahashi's [1978, 1980, 1981] applications of *Bagnold*'s [1954] equations assume that $N_{Sav} \rightarrow \infty$, that no boundary slip occurs, that grains are uniformly dispersed in the flow, and that interstitial fluid sustains no excess pressure. As a consequence, grain collision stresses must increase linearly with depth to balance the gravitational stress. In turn, this requirement mandates a specific distribution of shear rate that excludes the possibility of "locked" or unyielding debris that does not shear [cf., *Iverson and Denlinger*, 1987]. Not only does this prediction contradict observations and the viscoplastic model, it also contradicts the fact that frictionally locked material must be present during the early and late stages of debris flows, when material is mobilized or deposited [*Iverson et al.*, 1997; *Major*, 1996].

Shortcomings of the viscoplastic and inertial grain flow models have motivated alternative approaches, but none has produced a widely embraced advance. One approach melds the equations of the viscoplastic and inertial grain flow models [*Chen*, 1987, 1988a, b]. This yields a formulation with numerous adjustable coefficients and with unresolved physical issues, described above, that lurk behind the mathematics. A similar approach combines the viscoplastic and grain inertia models in a linear sum without reconciling the models' physical contradictions [*O'Brien et al.*, 1993]. Other approaches abandon the effort to include detailed rheological descriptions, and adopt hydraulic approximations similar to that used in water flood routing. Traditional hydraulic approaches do not consider the dynamics of debris mobilization, deformation, and deposition, and instead use empirical coefficients to parameterize the momentum distribution and energy dissipation in reaches where debris flow is fully developed. Hydraulic formulations that employ depth-averaged "shallow water" momentum balances [*Macedonio and Pareschi*, 1992; *Caruso and Pareschi*, 1993; *Hunt*, 1994] as well as kinematic wave approximations [*Weir*, 1982; *Vignaux and Weir*, 1990; *Arratano and Savage*, 1994] have been presented. Calibrated hydraulic models hold promise for practical forecasts of debris flow speeds and shoreline inundation, but they necessarily neglect key facets of debris-flow behavior. Development of improved hydraulic models (section 9) requires explicit consideration of the physical processes that control mass, momentum, and energy fluxes in debris flows.

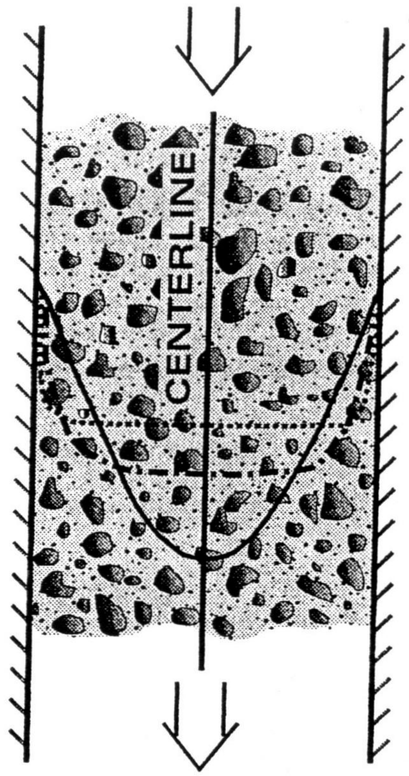

Figure 16. Schematic diagram depicting steady flow of a solid-fluid mixture between parallel vertical plates. A longitudinal body force (e.g., gravity) drives the flow. Depending on the distribution of granular temperature, a variety of velocity profiles are possible, including velocity profiles with an apparently rigid plug, as shown, but all velocity profiles must have a zero velocity gradient at the channel centerline [cf. *Hui and Haff*, 1986; *Johnson et al.*, 1991]. Consequent zero shear rate at the centerline invalidates use of *Bagnold*'s [1954] formulas as constitutive equations because the equations require zero normal stress in the presence of zero shear rate, which contradicts the presence of the body force that drives the flow.

6. MASS, MOMENTUM, AND ENERGY CONSERVATION IN DEBRIS FLOW MIXTURES

Mass and linear momentum balances for debris flows can be borrowed with only minor modification from the relatively mature field of continuum mixture theory [*Atkin and Craine*, 1976]. Under this rubric, separate but strongly coupled equations describe mass and momentum conservation for the debris flow's solid and fluid constituents, and the solid and fluid equations are assumed to apply at all locations simultaneously. Angular momentum equations can also be formulated but are rendered unnecessary by assuming all stress tensors to be symmetric. Similarly, balances of thermodynamic energy are rendered redundant by assuming the mixture is isothermal. However, an equation for grain fluctuation energy (granular temperature) may be necessary to describe solid phase motion, and fluid fluctuation energy (turbulence) may be embedded in the fluid momentum equation by including Reynolds stresses.

The mixture theory mass conservation equations for the solid and fluid constituents are, respectively,

$$\partial(\rho_s \upsilon_s)/\partial t + \nabla \cdot (\rho_s \upsilon_s \mathbf{v}_s) = m_s \tag{22a}$$

$$\partial(\rho_f \upsilon_f)/\partial t + \nabla \cdot (\rho_f \upsilon_f \mathbf{v}_f) = m_f \tag{22b}$$

in which $\mathbf{v}_s$ and $\mathbf{v}_f$ are the solid and fluid velocities, respectively, and m_s and m_f are the respective rates of solid and fluid mass addition, per unit volume. These equations are coupled because the volume fractions must obey $\upsilon_s + \upsilon_f = 1$. Addition of (22a) and (22b) yields an equivalent mass conservation equation for the mixture,

$$\partial\rho/\partial t + \nabla \cdot (\rho \mathbf{v}) = m_s + m_f \tag{23}$$

in which the mixture mass density ρ and velocity $\mathbf{v}$ are defined by

$$\rho = \rho_s \upsilon_s + \rho_f \upsilon_f \tag{24a}$$

$$\mathbf{v} = (\rho_s \upsilon_s \mathbf{v}_s + \rho_f \upsilon_f \mathbf{v}_f)/\rho \tag{24b}$$

These definitions show that the relevant mixture velocity is that of the center of mass, not volume, of a mixture volume element.

An important special case of mass conservation exists if no mass change occurs ($m_s = m_f = 0$) and the solid and fluid constituents are individually incompressible. Then addition of (22a) and (22b) results in the alternative forms

$$\nabla \cdot \upsilon_f(\mathbf{v}_f - \mathbf{v}_s) + \nabla \cdot \mathbf{v}_s = 0 \tag{25a}$$

$$\nabla \cdot \mathbf{v} = 0 \tag{25b}$$

Equation (25a) is noteworthy because if the standard expression for the fluid specific discharge $\mathbf{q} = \upsilon_f (\mathbf{v}_f - \mathbf{v}_s)$ is substituted in the first term, the equation matches the standard continuity equation for deforming porous media undergoing either quasi-static [*Bear*, 1972, p. 205] or inertial [*Iverson*, 1993] motion. Thus an analogy between debris flow mixtures and porous media can be exploited. Equation (25b) matches the standard continuity equation for an incompressible, single-phase continuum.

The mixture theory momentum conservation equations are

$$\rho_s \upsilon_s[\partial \mathbf{v}_s/\partial t + \mathbf{v}_s \cdot \nabla \mathbf{v}_s] = \nabla \cdot \mathbf{T}_s + \rho_s \upsilon_s \mathbf{g} + \mathbf{f} - m_s \mathbf{v}_s \tag{26a}$$

$$\rho_f \upsilon_f[\partial \mathbf{v}_f/\partial t + \mathbf{v}_f \cdot \nabla \mathbf{v}_f] = \nabla \cdot \mathbf{T}_f + \rho_f \upsilon_f \mathbf{g} - \mathbf{f} - m_f \mathbf{v}_f \tag{26b}$$

in which $\mathbf{g}$ is gravitational acceleration, $\mathbf{T}_s$ and $\mathbf{T}_f$ are the solid phase and fluid phase stress tensors, respectively, and $\mathbf{f}$ is the interaction force per unit volume that results from momentum exchange between the solid and fluid constituents. Sign conventions define normal stresses as positive in tension and $\mathbf{f}$ as positive when it acts on the solid. The last terms in (26a) and (26b) arise from the nonzero terms on the right-hand sides of (22a) and (22b) and account for momentum change due to mass change. However, they do not account for forces that enable mass change, and they assume that mass enters or leaves with zero momentum. Mixture theory equations similar to (22) and (26), but with $m_s = m_f = 0$, appear to have been first applied to phenomena like debris flows by *Shibata and Mei* [1986a, b].

Addition of the momentum conservation equations (26) for the solid and liquid constituents for the case $m_s = m_f = 0$ yields a momentum equation for the bulk mixture

$$\rho[\partial \mathbf{v}/\partial t + \mathbf{v} \cdot \nabla \mathbf{v}] = \nabla \cdot (\mathbf{T}_s + \mathbf{T}_f + \mathbf{T}') + \rho \mathbf{g} \tag{27a}$$

in which

$$\mathbf{T}' = -\rho_s \upsilon_s(\mathbf{v}_s - \mathbf{v})(\mathbf{v}_s - \mathbf{v}) - \rho_f \upsilon_f(\mathbf{v}_f - \mathbf{v})(\mathbf{v}_f - \mathbf{v}) \tag{27b}$$

is a contribution to the mixture stress that results from motion of the solid and fluid constituents relative to the mixture as a whole. Mathematically, $\mathbf{T}'$ arises because the convective acceleration terms on the left-hand sides of (26a) and (26b) do not sum to yield the mixture convective acceleration given by $\mathbf{v} \cdot \nabla \upsilon$ in (27a). Physically, $\mathbf{T}'$ indicates that stresses in a two-phase debris flow mixture represented as a one-phase material are more complicated than those obtained by summing the solid and fluid stresses, $\mathbf{T}_s + \mathbf{T}_f$. Except for the complicated stress term, the summed momentum conservation equation (27a) has the standard form for a single-phase continuum.

The basic mixture theory equations (22) and (26) hold three significant advantages over comparable single-phase equations: (1) They explicitly account for solid and fluid volume fractions and mass changes and thus can explicitly represent diverse or evolving debris flow compositions. (2) They include separate solid and fluid stress tensors, which have relatively straightforward physical interpretations. In contrast, single-phase models rely upon a stress tensor that amalgamates the effects of solids and fluids and their interactions. This amalgamated stress formulation may necessitate use of numerous poorly constrained parameters to describe the mixture rheology. (3) The mixture momentum equations contain an explicit solid-fluid interaction force. Such a force is lacking in single-phase models, which embed its effect in the amalgamated stress tensor. Because solid-fluid interactions differ from point to point within debris flows and play a key physical role (e.g., Figures 5, 10, and 13), explicit representation of their effects is desirable.

6.1. Quasi-Static Motion

Some properties of the interaction force as well as of the solid and fluid stresses can be clarified by considering the special case of quasi-static motion with incompressible constituents. Quasi-static motion occurs when the inertial (left-hand side) terms in (26) are negligible, which implies zero granular temperature. This would be the case, for example, during inception or cessation of debris flow motion. In these situations the mass change terms in (22) and (26) are likely negligible as well. Equations (22) then reduce to (25), and the momentum balances (26) reduce to

$$\nabla \cdot \mathbf{T}_s + \rho_s(1 - \upsilon_f)\mathbf{g} + \mathbf{f} = 0 \qquad (28a)$$

$$\nabla \cdot \mathbf{T}_f + \rho_f \upsilon_f \mathbf{g} - \mathbf{f} = 0 \qquad (28b)$$

Under quasi-static conditions in a granular medium, an appropriate constitutive equation for the pore fluid assumes that only isotropic fluid pressure p contributes to the fluid stress [*Bear*, 1972]. Thus

$$\mathbf{T}_f = -\upsilon_f \mathbf{I} p \qquad (29)$$

where $\mathbf{I}$ is the identity tensor and υ_f is included because p exists only within the fluid, whereas $\mathbf{T}_f$ is assumed to act throughout the mixture.

Even with specification of (29), to evaluate (28b) it is necessary to specify the interaction force $\mathbf{f}$. In the most general case of rapid motion, $\mathbf{f}$ might include a wide variety of phenomena such as buoyancy, drag, added mass, lift, and Basset, Faxen, and grain diffusion forces [*Johnson et al.*, 1990]. However, for analysis of quasi-static motion of debris flows, $\mathbf{f}$ depends chiefly on buoyancy and fluid drag that results from relative, creeping motion of the solid and fluid phases [cf. *Iverson*, 1993]:

$$\mathbf{f} = -p\nabla\upsilon_f + \frac{\mu \upsilon_f^2}{k}(\mathbf{v}_f - \mathbf{v}_s) \qquad (30)$$

Here the buoyancy force $-\rho_f \upsilon_s \mathbf{g}$ is included implicitly in the sum of $-p\nabla\upsilon_f$ and the gravity force $\rho_f \upsilon_f \mathbf{g}$, and the drag force is a function of fluid viscosity μ, granular phase hydraulic permeability k, fluid volume fraction υ_f, and relative velocity $\mathbf{v}_f - \mathbf{v}_s$ [cf. *Johnson et al.*, 1990].

The ramifications of (30) can be clarified by combining (28b), (29), and (30) and rearranging terms to yield

$$\mathbf{q} = \upsilon_f(\mathbf{v}_f - \mathbf{v}_s) = -\frac{k}{\mu}\nabla p_{\text{dev}} \qquad (31)$$

in which $p_{\text{dev}} = p - \rho_f g z$ is the fluid pressure deviation from the equilibrium or hydrostatic pressure $\rho_f g z$, where z is the vertical depth below a horizontal datum. Note that (31) is simply a statement of Darcy's law [*Bear*, 1972]. Substitution of (31) in (25) yields an equation that governs the nonequilibrium pore pressure

$$\nabla \cdot \frac{k}{\mu}\nabla p_{\text{dev}} = \nabla \cdot \mathbf{v}_s \qquad (32)$$

Solutions to (31) can be obtained if $\nabla \cdot \mathbf{v}_s$ is known or specified in terms of p_{dev}. Quasi-static stages of debris flow initiation and deposition each involve phenomena that allow this specification.

A useful form of the granular phase momentum equation for quasi-static conditions results from substitution of (29), (30), and (31) into (28a), which yields, after some algebraic manipulation

$$\nabla \cdot \mathbf{T}_e + (\rho_s - \rho_f)\upsilon_s \mathbf{g} - \nabla p_{\text{dev}} = 0 \qquad (33)$$

where $\mathbf{T}_e = \mathbf{T}_s + \mathbf{T}_f + p\mathbf{I}$ is the effective stress and $\mathbf{T}_s + \mathbf{T}_f$ is the total stress as classically defined by *Terzaghi* [1949]. This result implies that the total stress is related to the solid stress and pore fluid pressure by $\mathbf{T}_s + \mathbf{T}_f = \mathbf{T}_s - \upsilon_f \mathbf{I} p$. Moreover, (33) demonstrates that mixture theory subsumes the standard theory of quasi-static porous media as a special case. Thus standard theories for slope failure (which instigates debris flow) and deposit consolidation (which concludes debris flow) derive naturally from mixture theory. Single-phase theories of debris flow lack this generality and power of explanation.

Mathematical details of slope failure and deposit consolidation theories are too lengthy to present here, but some key concepts will be outlined to clarify how mixture theory provides a unifying framework. Prior to failure, granular slope debris may be regarded as static, and $\nabla \cdot \mathbf{v}_s = 0$ is satisfied. Then (32) reduces to a readily solved Laplace equation for p_{dev}, provided that k/μ is constant. This is the procedure used in most slope stability analyses [*Bromhead*, 1986]. Following determination of p_{dev}, effective stresses at failure must be calculated using (33) and an appropriate constitutive model, such as a Coulomb plasticity model (equation (6)) for effective stresses on prospective slip surfaces [*Savage and Smith*, 1986; *Iverson and Major*, 1986]. Alternatively, elasticity models can be used to determine a static effective stress field that can be used to infer the potential for Coulomb failures in slopes [*Iverson and Reid*, 1992; *Reid and Iverson*, 1992]. In either case, (32) and (33) provide the basic balance equations.

Mixture theory also subsumes the theory of consolidation of debris flow deposits. For small displacements the relation $\nabla \cdot \mathbf{v}_s = \partial\epsilon/\partial t$ applies, where ϵ is the volumetric strain (dilatation) of the solid phase. Employing this relation, a standard poroelastic constitutive equation that relates solid dilatation and pore pressure [*Biot*, 1941; *Rice and Cleary*, 1976] can then be substituted in (32) to yield a diffusion equation for nonequilibrium pore pressure. If the solid and fluid constituents are individually incompressible and k/μ is constant, the resulting diffusion equation has the simple form [*Chandler and Johnson*, 1981]

$$\frac{\partial p_{\text{dev}}}{\partial t} - \frac{kE}{\mu}\nabla^2 p_{\text{dev}} = 0 \qquad (34)$$

in which $E = K_b + 4G/3$ is a composite stiffness modulus that depends on the conventional elastic bulk (K_b) and shear (G) moduli of the granular composite. The group kE/μ serves as a pore pressure diffusivity and appears in the pore pressure diffusion timescale identified in (8). Modeling and measurements by *Major* [1996] confirm that this linear diffusion model represents postdepositional consolidation of debris flow deposits reasonably well (Figure 13). However, changes in permeability and stiffness may produce nonlinear behavior that is especially important in the early stages of consolidation, when the solid grains are loosely packed and the mixture undergoes large strains. This nonlinearity is analyzed in section 8.

6.2. Inertial Motion

The mixture theory approach provides a complete framework for predicting quasi-static phenomena during initiation and deposition of debris flows, but can the theory represent inertial debris flow motion with nonzero granular temperature? In kinetic theories of dry granular flow, the concept of granular temperature leads to a balance equation for the fluctuation energy of the solid grains, which must be satisfied along with momentum and mass balances. The physical motivation and interpretation of granular temperature equations were described by *Haff* [1983, 1986], and mathematical connections of such equations to classical kinetic theory were established by *Jenkins and Savage* [1983] and *Lun et al.* [1984]. A typical form of such an equation is given by *Campbell* [1990]:

$$\tfrac{1}{2}\rho_s\upsilon_s[\partial \mathrm{T}/\partial t + \mathbf{v}_s \cdot \nabla \mathrm{T}] = -\nabla \cdot \mathbf{j} - \mathbf{T}_s{:}\nabla \mathbf{v}_s - \Gamma \qquad (35)$$

wherein $\mathrm{T} = \langle \mathbf{v}_s'^2 \rangle$ is the granular temperature, $\mathbf{j}$ is the conductive flux of granular temperature from highly agitated to less-agitated regions within the flow, $\mathbf{T}_s{:}\nabla\mathbf{v}_s$ is the rate of generation of granular temperature via work performed by the stresses, $\mathbf{T}_s$, and Γ is the rate of degradation of granular temperature into thermodynamic heat as a result of dissipative grain interactions. An important implication of (35) is that grain fluctuation energy cannot be specified as a simple function of the local shear rate and solid volume fraction; instead, granular temperature is a field variable that may depend in a complicated way on boundary conditions and transport phenomena.

Rigorous application of (35) requires knowledge of a diffusion coefficient for $\mathbf{j}$ as well as appropriate boundary conditions and constitutive parameters to determine $\mathbf{T}_s$ and Γ. For purely collisional flows with identical spherical grains characterized only by their size (δ), density (ρ_s), and coefficient of restitution (e), the necessary information can be deduced from kinetic theory (see the review by *Campbell* [1990]). For flows in which enduring, frictional grain contacts may play an important role, the theory is less complete [*Anderson and Jackson*, 1992]. If, in addition, a viscous intergranular fluid is present, satisfactory theory is lacking entirely. However, hueristic analyses indicate that conduction of fluid pressure fluctuations that occur if there is nonzero granular temperature can play an important, perhaps dominant, role in mixture momentum transport when viscous fluid is present [*Jenkins and McTigue*, 1990; *McTigue and Jenkins*, 1992]. Thus although the effects of granular temperature on debris flow dynamics are not yet rigorously quantified, they are both theoretically and empirically identifiable. Section 7 provides further insight.

A better basis exists for evaluating the dynamic interaction force $\mathbf{f}$ during inertial debris flow motion. Drag arguably constitutes the most significant interaction force in most solid-fluid mixture flows [*Johnson et al.*, 1990]. Thus the Darcian drag described by (30) might represent the most important interactions in inertial as well as quasi-static stages of debris flows. Comparison of the experimental results of *Iverson and LaHusen* [1989] with calculations that use the model of *Iverson* [1993] show that Darcy coupling alone can yield excellent predictions of fluid pressures even when grain Reynolds numbers fall well above the Stokes flow limit. Moreover, an analysis by *DiFelice* [1994] of diverse experimental data on fluid drag forces in both dilute and concentrated suspensions of spheres shows that the total drag depends strongly on the solid volume fraction υ_s but surprisingly weakly on the grain Reynolds number over the range $10^{-2} < N_{\mathrm{Rey}} < 10^4$ (where N_{Rey} depends on the absolute value of the relative solid-fluid velocity, $\mathbf{v}_f - \mathbf{v}_s$). Thus, as a first approximation, a simple Darcy-drag model may be valid for debris flows.

Finally, appropriate boundary conditions as well as constitutive equations that relate the stresses $\mathbf{T}_f$ and $\mathbf{T}_s$ to the velocities $\mathbf{v}_f$ and $\mathbf{v}_s$ must in general be specified to solve the momentum equations (26). Appropriate constitutive equations for a Newtonian fluid phase are well known, but appropriate equations for the granular phase are lacking. Although beginnings have been made along these lines [e.g., *Shen and Ackermann*, 1982], rigorous formulations analogous to those for collisional dry grain flows [e.g., *Lun et al.*, 1984] have not been developed [cf. *Garcia-Aragon*, 1995]. To build insight, the next section considers solid, fluid, and boundary effects on momentum transport from the perspective of elementary mechanics.

7. GRAIN, FLUID, AND BOUNDARY INTERACTIONS: ANALYTICAL SOLUTIONS FOR IDEALIZED, STEADY FLOW

The balance equations of the preceding section provide a quantitative but rather general picture of debris flow mixture dynamics. To gain more detailed understanding, solutions and not merely balance equations must be investigated. Although solutions for quasi-static slope failure and deposit consolidation problems are abundant in the literature, solutions for boundary value problems that contain all the dynamic variables in (22), (26), and (35) are unavailable. This section therefore considers primitive forms of the balance equations that admit explicit analytical solutions. These solutions clarify physical effects of solid-fluid interactions and boundary conditions, and they reveal the significance of solid and fluid velocities normal to the bed, which are neglected in most practical models (see section 9). As a by-product, the solutions quantify the shortcomings of *Bagnold*'s [1954] formulas as constitutive equations for debris flows. They also indicate that presence of a viscous fluid phase reduces the net efficiency of steady, uniform motion of a granular material. This result contradicts the observation that viscous fluid enhances debris flow efficiency (sections 2 and 3), and thus reveals a limitation of steady state theories; it supports the idea that debris flows may be fundamentally unsteady phenomena.

Guidance for simplifying debris flow mixture theory comes from work on closely related granular flows. For example, *Anderson and Jackson* [1992] have shown that in steady, uniform, gravity-driven flows of dry grains that interact through both collisions and friction, significant variations in granular temperature, solid volume fraction, and mean grain velocity commonly occur only near the bed; grains far from the bed "lock" and translate as a rigid body if there is much dissipation and little conduction of granular temperature into the flow interior. *Jenkins and Askari* [1994] have exploited this fact to analyze the dynamics of unsteady, dry, granular flows with nonzero granular temperatures concentrated in a thin basal shear layer. Similar locking behavior necessarily occurs in debris flows during initiation and deposition and appears to occur when "rigid" plugs form during sustained debris flow motion [*Johnson*, 1984].

With this background, consider a hypothetical steady, uniform debris flow moving down a rough, impermeable, fixed bed of infinite extent and uniform inclination. By definition, no variation of any quantity occurs in directions parallel or transverse to the slope (Figure 17). The flow translates with velocity v_x and for simplicity has velocity fluctuations v' with only y components. A moving coordinate $x' = x - v_x t$ that translates with the steady flow in the x direction provides a convenient frame of reference. Shearing occurs only between the bed and a single layer of grains and fluid. A thick, locked layer of grains that moves downslope as a rigid body overlies the shearing layer. The goal is to understand how momentum communicated by the shear layer to the locked layer and bed is influenced by the shear rate and material properties such as solid and fluid densities, grain friction and restitution coefficients, and fluid viscosity. This understanding may then be extrapolated to more general cases where many layers of grains shear past one another.

Substantial simplification can be achieved with little sacrifice of relevance if the fluctuating motions of the shearing and locked layers occupy specified domains in y. It is convenient to define the boundary between these domains as $y = 0$. Thus in the coordinate system (x', y), assume that a shear layer grain with characteristic diameter δ and mass m_2 moves only in the domain between $y = 0$ and $y = -\delta - s$, where s can be viewed as the mean free path of grain oscillation. The overlying locked

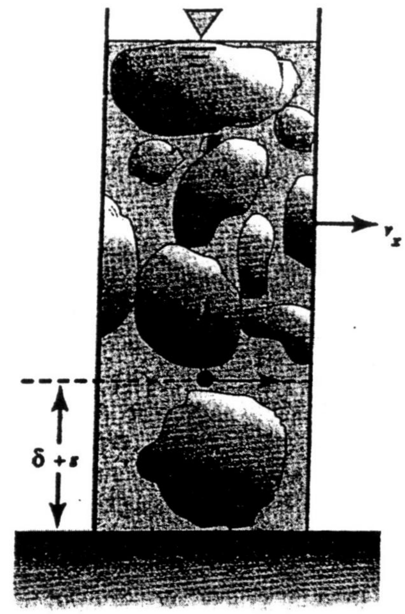

Figure 17. Schematic vertical cross section of a representative segment of an idealized debris flow (and translating coordinate system (x', y)) that move downstream with constant velocity v_x. Within the segment a single grain of mass m_2 exchanges momentum with the bed and the overlying grains, which have collective mass m_1. All momentum transfer and unsteady motion occur in the y direction. The fluctuating motion of m_2 is restricted to a vertical domain defined by the characteristic grain diameter δ and mean free path s. All grains are surrounded by fluid less dense than the grains. Gravity acts in the $-y$ direction.

layer of grains, of collective mass m_1 ($\gg m_2$), moves only between $y = 0$ and the upper flow surface (Figure 17). Interactions of the shear layer and locked layer occur exclusively at $y = 0$. No fluid or solid mass moves between the sheared and locked domains, and grains in both domains are rigid. These simplifications reduce the continuum-mixture problem to a discrete two-body problem that entails explicit analysis of momentum exchange at the domain boundary. The analysis parallels that of *Bagnold* [1954] but differs by including the effects of gravity, a free surface, and dissimilar masses m_1 and m_2, all of which exist in debris flows.

The idealization described above simplifies the governing equations substantially. Grain fluctuation energy is conducted from the basal shear layer to the locked layer by momentum exchange between the layers, but the time-averaged conduction does not change the granular temperature of either layer. Thus the fluctuation energy equation (35) becomes unnecessary; terms on both the left and right sides of (35) sum to zero for both the shear layer and the locked layer. Furthermore, the mass balance equations (22) applicable in each domain are satisfied trivially, and the x components of the momentum equations (26) reduce to simple steady state balances. The momentum equations for motion of the solids and fluid in the y direction reduce to

$$\rho_s \upsilon_s \frac{dv}{dt} = \upsilon_s(\rho_s - \rho_f) g_y - \frac{\mu \upsilon_f}{k} v \quad (36a)$$

$$0 = -\frac{dp}{dy} + \rho_f g_y + \frac{\mu \upsilon_f}{k} v \quad (36b)$$

in which v designates the solid fluctuation velocity in the y direction and g_y is the y component of $\mathbf{g}$. (Here primes and subscripts are omitted on v to simplify the notation.) No term involving the solid stress $\mathbf{T}_s$ appears in (36a) because the solid masses in each domain are treated as discrete bodies. Instead, the time-integrated grain inertia force $\int \rho_s \upsilon_s (dv/dt)\, dt$ communicated by impulses at domain boundaries predicts the time-averaged solid normal stress and obviates the need for a continuum stress term [cf. *Iverson*, 1993]. In addition, (36b) lacks fluid acceleration terms. This omission is justified if the dimensionless group $\mu \upsilon_f^2 \delta / k \rho_a \upsilon_x$ (where ρ_a is the added-mass density of solid grains accelerating through adjacent fluid) has a value substantially greater than 1, which indicates that solid-fluid interaction forces are dominated by viscous rather than inertial effects, a condition probably satisfied in many debris flows [*Iverson*, 1993]. Furthermore, (36a) and (36b) are only partly coupled; (36a) can be solved explicitly for the solid fluctuation velocity, which can then be input to (36b) to solve for the pore fluid pressure distribution. The pore fluid pressure gradient dp/dy is negative under static conditions ($v = 0$) because y is reckoned positive upward and g_y is negative; dp/dy increases when the solid fluctuation velocity v is positive and decreases when v is negative. However, (36b) shows that there is no tendency for net excess fluid pressures to develop if a net upward or downward solid velocity is absent. Fluid pressures that fluctuate so that the time-averaged excess pressure is zero have been measured in laboratory experiments with idealized debris flow mixtures [*Iverson and LaHusen*, 1989] and predicted with a model similar to (36) that couples inertial grain motion to pore pressure diffusion [*Iverson*, 1993].

Solutions of the y direction momentum equation for the solids (equation (36a)) hold the key to understanding this idealized debris flow and can be described best if the equation is first recast as

$$\frac{d^2u}{dt^2} + A\frac{du}{dt} = B \quad (37a)$$

in which $u = \int v\, dt$ is the solid displacement and A and B are defined by

$$A = \frac{\upsilon_f \mu}{\upsilon_s \rho_s k} \quad (37b)$$

$$B = \left(1 - \frac{\rho_f}{\rho_s}\right) g_y \quad (37c)$$

Note that B is generally negative because g_y is negative and $\rho_f < \rho_s$, but $B = 0$ if the solid grains are neutrally buoyant (the case of *Bagnold* [1954]). If the fluid is inviscid or absent, $A = 0$ as well.

Equation (37a) has the solution

$$u = -\frac{C_1}{A} \exp(-At) + \frac{B}{A} t + C_2 \quad (38)$$

in which C_1 and C_2 are constants determined by initial conditions. If $B = 0$, this solution lacks the second term, but if $A = 0$ (indicating an inviscid fluid), an entirely different solution applies:

$$u = \tfrac{1}{2}Bt^2 + C_1 t + C_2 \quad (39)$$

It is instructive to examine first the predictions of this solution for $A = 0$ and then to compare them with predictions of the more strongly nonlinear solution (38).

7.1. Inviscid Case ($A = 0$)

Initial conditions determine the values of C_1 and C_2 needed to complete the inviscid solution (39) for the motion of grain masses m_1 and m_2. For the upper, locked mass (m_1), appropriate initial conditions are

$$u(0) = 0 \quad (40a)$$

$$v(0) = du/dt(0) = v_0 \quad (40b)$$

which give $C_1 = v_0$, $C_2 = 0$, and the solutions for position and velocity

$$u = \tfrac{1}{2}Bt^2 + v_0 t \quad (41a)$$

$$v = Bt + v_0 \quad (41b)$$

These are simple ballistic trajectory equations for the oscillating motion of m_1, which is sustained by impulses from m_2. From (41a) it is easy to see that m_1 returns to its initial position, $u = 0$, after a time t_{cycle}:

$$t_{\text{cycle}} = -2(v_0/B) \quad (42)$$

At $t = t_{\text{cycle}}$, m_1 collides with m_2, and then repeats its trajectory.

The oscillations of m_2 are more complicated, because they must supply enough momentum to sustain the oscillations of m_1 and also satisfy (39), (42), and a condition for interaction with the bed, which includes both collisional dissipation and frictional dissipation due to slip at the bed. Thus for m_2, paired evaluations of (39) are required, one for upward motion and one for downward motion. Paired initial conditions are also needed, which can be written in terms of the grain position u; downward bound velocity v_{down}; upward bound velocity v_{up}; arrival time at the top of the domain boundary, t_{up}; and arrival time at the bottom of the domain boundary, t_{down}. The initial conditions are

Downward bound

$$u(t_{\text{up}}) = 0 \quad (43a)$$

$$v_{down}(t_{up}) = v_{0down} = -e\,v_{up}(t_{up}) \qquad (43b)$$

Upward bound

$$u(t_{down}) = -s \qquad (43c)$$

$$v_{up}(t_{down}) = v_{0up} = -e\,v_{down}(t_{down}) + \psi \qquad (43d)$$

in which v_{0up} and v_{0down} are the initial values of v_{up} and v_{down}, respectively, and ψ is a very important quantity with dimensions of velocity.

Values of ψ measure the net conversion of translational momentum $m_2 v_x$ into fluctuation momentum $m_2 v$ that results from interaction of m_2 with the rough bed (Figure 18). Grain fluctuation energy generated by working of the bed shear stress minus grain energy lost to inelastic collisions and bed friction equals $\frac{1}{2} m_2 \psi^2$. Because grain interactions with the bed and one another generally dissipate energy, a positive value of ψ is necessary to conduct fluctuation energy away from the bed and prevent the mass from locking frictionally.

The restitution coefficient e in (43b) applies to the collision of the shear layer grain m_2 and the overlying mass m_1. An exact analysis of the collision shows that e should be replaced by an effective coefficient of restitution which differs slightly from the true coefficient (Appendix A). However, for the condition $m_1 \gg m_2$ assumed here, the difference between the effective and true values of e is negligible.

Evaluation of (39) for the initial conditions (43) yields upward bound and downward bound solutions for the position and velocity of m_2, which at times t_{down} and t_{up} reduce to

$$\tfrac{1}{2}Bt_{down}^2 + v_{0down}t_{down} = -s \qquad (44a)$$

$$\tfrac{1}{2}Bt_{up}^2 + v_{0up}t_{up} = s \qquad (44b)$$

$$Bt_{down} + v_{0down} = -\frac{1}{e}\,v_{0up} + \frac{\psi}{e} \qquad (44c)$$

$$Bt_{up} + v_{0up} = -\frac{1}{e}\,v_{0down} \qquad (44d)$$

These four equations contain six unknowns, t_{up}, t_{down}, v_{0up}, v_{0down}, s and ψ; therefore two additional equations are required for closure. Constraints on collisions between m_2 and m_1 provide the necessary equations. Collisions occur at time t_{cycle}, as defined by (42), so it is necessary that

$$t_{up} + t_{down} = t_{cycle} = -2(v_0/B) \qquad (45)$$

Moreover, collisions must conserve momentum, which for $m_1 \gg m_2$ requires (Appendix A)

$$v_{0down} = \frac{-v_0 m_1(1+e) + (m_2 - e m_1)[-v_{0down}(1/e)]}{m_1 + m_2} \qquad (46)$$

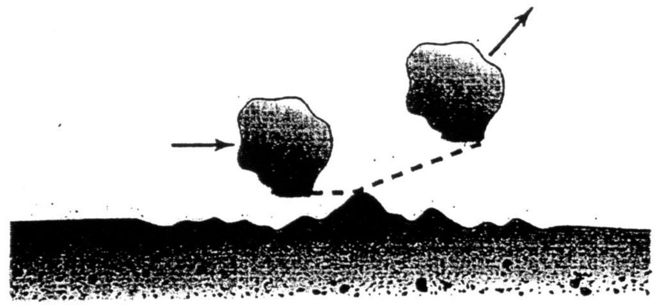

Figure 18. Schematic diagram depicting conversion of slope parallel translation velocity into slope normal fluctuation velocity as a grain interacts with a rough bed. The slope normal velocity generated minus velocity lost due to frictional and collisional energy dissipation determines ψ.

Thus (44), (45), and (46) form a closed, slightly nonlinear set of equations that can be solved explicitly.

Solutions of the set (44)–(46) yield key quantities such as s and ψ, and also facilitate evaluation of the granular temperature, granular stress and *Bagnold*'s [1954] "dispersive pressure." The exact solutions are algebraically cumbersome and are stated in Appendix B as equations (B1)–(B6). Valid approximations of (B1)–(B6) can be obtained by further exploiting the assumption $m_2/m_1 \ll 1$. As $m_2/m_1 \to 0$, the exact expression for ψ (equation (B6)) reduces to

$$\psi = v_0(m_1/m_2)(1 - e^2) \qquad (47a)$$

Substituting (47a) into (B1)–(B5) then yields the approximations

$$t_{up} = -\frac{1}{B}\,v_0\,\frac{2e}{1+e} \qquad (47b)$$

$$t_{down} = t_{up}/e \qquad (47c)$$

$$v_{0down} = -(m_1/m_2)e\,v_0 \qquad (47d)$$

$$v_{0up} = v_0\left(\frac{2e}{1+e} + \frac{m_1}{m_2}\right) \qquad (47e)$$

$$s = \frac{-2v_0^2 e}{B(1+e)}\left[\frac{1}{1+e} + \frac{m_1}{m_2}\right] \qquad (47f)$$

The approximation error is zero for all values of m_1/m_2 if $e = 1$ but grows as $e \to 0$.

The simple equations (47a)–(47f) describe the essential physics of the inviscid case; Table 7 lists some numerical values that satisfy the equations. The tabulated values demonstrate the following effects: (1) If v_0, B, e, and m_2 are held fixed, increased grain fluctuation speeds and increased mean free paths are required to sustain motion if the overburden mass m_1 is increased. Collision frequencies and t_{cycle} remain constant, but more fluctuation energy is required to support the increased overburden and prevent the entire mass from locking. (2) If $e = 1$, then $t_{up} = t_{down}$, and mean fluctuation speeds are identical in the upward and downward directions; no

TABLE 7. Examples of Parameter Values That Satisfy Equations (47)

	Specified Values				*Computed Values*					
Case	*e*	m_1/m_2	v_0, *m/s*	*B*, *m/s*^{2}	ψ, *m/s*	v_{0down}, *m/s*	v_{0up}, *m/s*	t_{up}, *s*	t_{down}, *s*	*s*, *m*
1	1	100	0.01	−5	0	−1	1.01	0.002	0.002	0.00201
2	1	1000	0.01	−5	0	−10	10.01	0.002	0.002	0.02001
3	0.5	1000	0.01	−5	7.5	−5.00	10.0067	0.00133	0.00267	0.013
4	0.9	1000	0.01	−5	1.9	−9.00	10.0095	0.00189	0.00211	0.019
5	0.9	1000	0.01	−1	1.9	−9.00	10.0095	0.00947	0.0105	0.095

Cases 1–5 were selected to illustrate the effects of variations in e, m_1/m_2, and B.

input of fluctuation energy from the bed is required, and $\psi = 0$. Values of e smaller than 1 produce asymmetrical fluctuations, in which mean upward speeds of grains exceed downward speeds. Then more input of fluctuation energy from the bed is needed to sustain motion, as is reflected by increased values of ψ. (3) Reductions in the magnitude of B, which reflect increased buoyancy forces, decrease the frequency of grain contacts but do not affect contact velocities. They increase the mean free path s, which reduces the solid volume fraction if all other factors are constant.

As characterized by this simple model, granular normal force, which can be equated with the "dispersive force" of *Bagnold* [1954], results from the time average of impulses due to grain interactions. This time average can be calculated using the impulse-momentum principle [e.g., *Spiegel*, 1967], which for the impulse communicated by m_1 during momentum exchange with m_2 can be written as

$$F_{\text{avg}} = \frac{1}{t_{\text{cycle}}} \int_{t_{\text{cycle}}} F\, dt = \frac{1}{t_{\text{cycle}}} [-m_1 v_0 - m_1 v_0] = B m_1 \tag{48}$$

where F_{avg} is the time-averaged impulse force and F is the instantaneous impulse force. According to (48) the time-averaged impulse is simply the buoyant weight of mass m_1. Consequently, the normal stress or dispersive force communicated by grain interactions depends on the buoyant weight of the overlying material, and it depends on grain dynamics only insofar as dynamics determine the mean free path of grain motion, s (see (47f)), or equivalently, v_s. In a "gravity-free" case such as that of *Bagnold* [1954], the solid mass concentration v_s is specified rather than determined by the physics of grain interactions, and the dispersive force need not balance the body force due to gravity.

A single quantity that summarizes how dispersive force depends on gravity can be calculated by adding (44c) and (44d) and then using (43b) and (43d) to eliminate $v_{0\text{down}}$ and $v_{0\text{up}}$ in favor of $v_{\text{up}}(t_{\text{up}})$ and $v_{\text{down}}(t_{\text{down}})$, yielding

$$v_{\text{up}}(t_{\text{up}}) + v_{\text{down}}(t_{\text{down}}) = \frac{1}{1+e}(Bt_{\text{cycle}} + \psi) \tag{49}$$

The sum $v_{\text{up}}(t_{\text{up}}) + v_{\text{down}}(t_{\text{down}})$ measures the asymmetry of the collision speed of a shear zone grain with the overlying mass and underlying bed. If grains are neutrally buoyant ($B = 0$) and the dissipation rate equals the rate of fluctuation energy generation by shearing ($\psi = 0$), this asymmetry is zero, and the collision speed depends only on shear kinematics. This is precisely the case investigated by *Bagnold* [1954]. However, in a debris flow with nonzero B and ψ, collisions are asymmetric except in the very special case that $\psi = -Bt_{\text{cycle}} = 2v_0$. This special case is similar to that in *Takahashi*'s [1978, 1980, 1981] application of Bagnold's equations; the application is appropriate only if the effects of gravity settling, as represented by the velocity Bt_{cycle}, are precisely offset by generation of fluctuation velocity, as represented by ψ. In the more general case of $\psi \neq -Bt_{\text{cycle}}$, asymmetry of grain interaction forces causes dispersive force to depend on all the kinematic phenomena and material properties that affect flow dynamics and granular temperature. *Bagnold*'s [1954] equations do not provide a valid description of flows in such circumstances.

Finally, the inviscid mixture formulation permits explicit evaluation of the granular temperature T, which depends on the temporal average of the grain fluctuation velocity v. This average is simply the quotient of the mean-free-path distance s and half the time required for one cycle of grain motion, t_{cycle}. Thus combining (7) and (45) yields an equation for granular temperature,

$$\text{T} = \langle v^2 \rangle = \left(\frac{2s}{t_{\text{cycle}}}\right)^2 = \left(\frac{-s}{v_0/B}\right)^2 \tag{50}$$

Alternatively, by substituting (B5) and (B6) into (50), the temperature can be expressed as a function of only the fundamental quantities ψ, e, and m_1/m_2,

$$\text{T} = \frac{4\psi^2 e^2}{(1-e)^2(1+e)^6}\left(\frac{m_2}{m_1} + 1 + e\right)^2 \tag{51}$$

which shows that the granular temperature increases as e, ψ, and m_2/m_1 increase. In the limiting case of $e \to 1$, $\text{T} \to \infty$ unless $\psi \to 0$ and friction due to bed slip dissipates fluctuation energy at the same rate it is generated.

7.2. Viscous Case ($A > 0$)

The viscous term A in the equation of motion (37a) adds mathematical complexity that reflects the physical complexity of debris flows. With $A > 0$, complete analytical results analogous to (47) cannot easily be attained, but quantitative inferences about the role of viscous intergranular fluid can nonetheless be drawn.

The appropriate initial conditions for the viscous case are the same as for the inviscid case. For the rigidly locked upper mass m_1, substitution of (40) and (43) in (38) leads to the position and velocity solutions

$$u = \frac{B/A - v_0}{A}[\exp(-At) - 1]] + \frac{B}{A}t \quad (52a)$$

$$v = (v_0 - B/A)[\exp(-At)] + B/A \quad (52b)$$

Like the solutions for the inviscid case (41), these equations describe ballistic paths, but they differ by including the effects of viscous drag. An important special case of (52b) occurs when At is large enough that $\exp(-At) \to 0$; then $v = B/A$ is a good approximation, which indicates that viscous and gravity forces balance and that solid grains descend at their terminal velocity. This is comparable to the settling velocity described in section 3 as a basis for distinguishing grains that act as discrete solids from those suspended as part of the fluid.

Further effects of viscous drag can be evaluated by noting that at time $t = t_{cycle}$, the mass m_1 returns to its original position, $u = 0$. Using these values in (52a) yields

$$\exp(-At_{cycle}) = \frac{Bt_{cycle}}{v_0 - B/A} + 1 \quad (53)$$

and substituting this result into (52b) yields the velocity of m_1 at time t_{cycle},

$$v(t_{cycle}) = Bt_{cycle} + v_0 \quad (54)$$

This equation matches the analogous equation for the inviscid case, (41b).

The fact that (54) applies in both the viscous and inviscid cases has significant implications, which are clarified by comparing viscous and inviscid mixtures moving at the same rate and undergoing similar internal motion. A reasonable criterion for identifying similar internal motion focuses on the momentum exchanged during collision of m_1 and m_2. This momentum exchange, described by (46), is the only facet of internal motion that can be characterized independently of viscosity; thus similar flows can be regarded as those for which v_x is identical and the values of m_1, m_2, e, v_{0down}, v_0 in (46) are identical. If v_0 is identical in the viscous and inviscid cases, then the magnitude of $v(t_{cycle})$ must be smaller in the viscous case because m_1 dissipates energy while it describes its ballistic trajectory in the viscous case, but not in the inviscid case. Thus (54) demonstrates that

$$t_{cycle}(\text{viscous}) < t_{cycle}(\text{inviscid}) \quad (55)$$

Consequently, increased viscosity reduces the average fluctuation velocity of m_1 but increases the frequency of collisions between m_1 and m_2, implying that the mean free path s of m_1 is reduced by the presence of viscous fluid. In turn, this result demonstrates that the viscous fluid decreases the granular temperature, as is expressed by (42) and (43). Reduction of granular temperature occurs because some of the grain fluctuation energy is converted to fluid pressure energy, which involves dissipative viscous forces.

If viscous forces dissipate energy, how does viscous fluid enhance debris flow efficiency? This question lies at the heart of debris flow physics. Viscosity causes grains to interact less energetically (with commensurately less dissipation) but more frequently, so the effect of viscosity on net dissipation due to grain interactions appears ambiguous. The issue can be clarified by assessing the rate of conversion of downslope translational momentum to grain fluctuation momentum that is required to sustain steady motion. To do so, an explicit expression for ψ/t_{cycle} must be obtained. This requires repetition of the steps used to obtain (44a)–(44d) for the shear zone grain m_2 in the inviscid case, which produces analogous expressions for the viscous case:

$$\frac{B/A - v_{0down}}{A}[\exp(-At_{down}) - 1] + \frac{B}{A}t_{down} = -s \quad (56a)$$

$$\frac{B/A - v_{0up}}{A}[\exp(-At_{up}) - 1] + \frac{B}{A}t_{up} = s \quad (56b)$$

$$(v_{0down} - B/A)\exp(-At_{down}) + B/A = -\frac{1}{e}v_{0up} + \frac{\psi}{e} \quad (56c)$$

$$(v_{0up} - B/A)\exp(-At_{up}) + B/A = -\frac{1}{e}v_{0down} \quad (56d)$$

In conjunction with (45) and (46), these four equations form a set of six equations in six unknowns, which determine the motion of m_2. This strongly nonlinear set does not admit simple, explicit solutions, but it does yield useful information. Expressions for $\exp(-At_{up})$ and $\exp(-At_{down})$ can be readily obtained from (56c) and (56d), and these can substituted into (56a) and (56b) to yield

$$(1/e)v_{0down} + v_{0up} + Bt_{up} = sA \quad (57a)$$

$$(1/e)v_{0up} + v_{0down} + Bt_{down} - \psi/e = -sA \quad (57b)$$

Addition of these two equations produces a simple and important result: an equation identical to (41) derived for the inviscid case. Combination of (41) with (43b) or (43d) and rearrangement of terms yields alternative expressions for ψ/t_{cycle}, one based on upward bound grain velocities from takeoff (v_{0up}) to impact ($v_{up}(t_{up})$) and one based on analogous downward bound velocities:

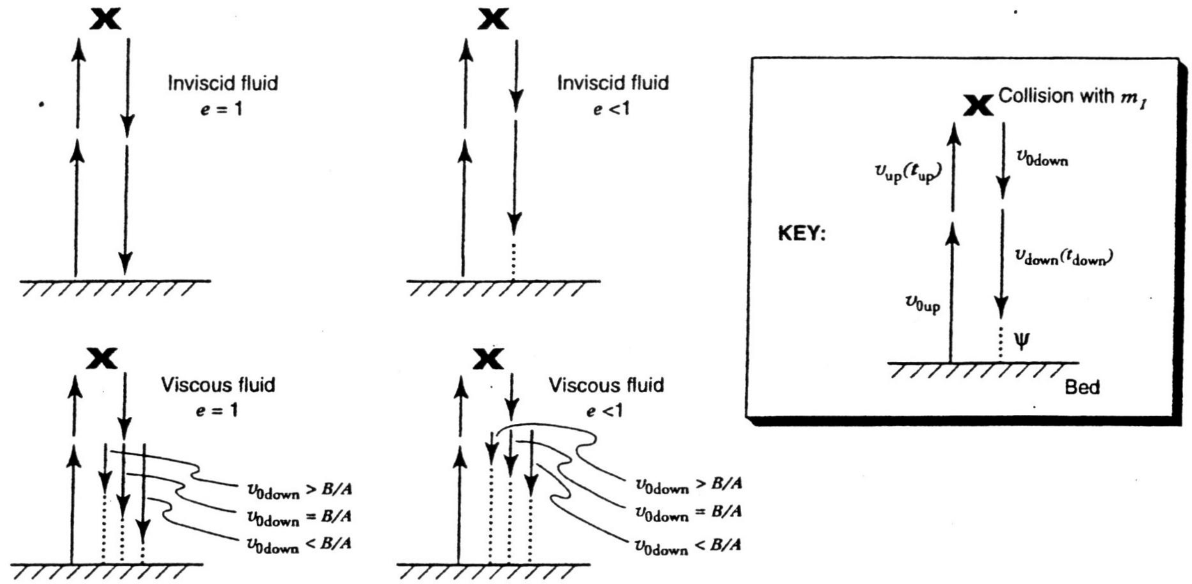

Figure 19. Pictorial summary of relative fluctuation velocities of grain m_2 during one cycle of vertical motion in mixtures of elastic ($e = 1$) and inelastic ($e < 1$) grains with viscous and inviscid fluids. Lengths of arrows depict the relative speeds of m_2: v_{0up} is the initial upward velocity of m_2 as it departs the bed, and $v_{up}(t_{up})$ is its upward velocity just before it contacts the overlying mass of grains, m_1; v_{0down} is the initial downward velocity of m_2 just after it contacts m_1, and $v_{down}(t_{down})$ is its downward velocity just before it contacts the bed. Dotted lines at the end of a motion cycle denote the deficit in fluctuation velocity (due to energy dissipation), which must be resupplied by ψ to sustain the fluctuating motion. B/A is the terminal descent velocity of m_2 in a viscous fluid.

$$\frac{\psi}{t_{cycle}} = -e\,\frac{(1+e)}{t_{cycle}}\left[v_{up}(t_{up}) - \frac{1}{e}\,v_{0up}\right] - eB \qquad (58a)$$

$$\frac{\psi}{t_{cycle}} = \frac{1+e}{t_{cycle}}\left[v_{down}(t_{down}) - \frac{1}{e}\,v_{0down}\right] - B \qquad (58b)$$

For both the viscous and inviscid cases, equations (58) quantify the rate of momentum conversion per unit mass needed to sustain steady motion. Terms on the right-hand sides of (58a) and (58b) distinguish the effects of fluid density (represented by B, which has a negative value) from those of viscosity. Increases in fluid density cause $B \to 0$, and this decreases the rate of momentum conversion ψ/t_{cycle} required to sustain steady motion.

Effects of viscosity enter (58a) and (58b) in a more complicated manner, through both t_{cycle} and the grain velocity terms in brackets. Increased viscosity decreases t_{cycle} and hence tends to increase ψ/t_{cycle}. In (58a) the term in brackets must be negative because v_{0up} must exceed $v_{up}(t_{up})$ unless there is no viscosity and no effective gravity ($A = 0$ and $B = 0$). This shows that ψ/t_{cycle} is positive unless $A = 0$ and $B = 0$. In (58b), however, the term in brackets can be either positive or negative, depending on whether the downward bound takeoff velocity v_{0down} exceeds the terminal velocity inferred from (56c), B/A. If v_{0down} exceeds the terminal fall velocity, then the grain decelerates as it descends toward the bed, the term in brackets in (58b) is positive, and the value of ψ/t_{cycle} increases. However, if v_{0down} is less than the terminal velocity, then the grain accelerates as it moves toward the bed, the term in brackets in (58b) is negative, ψ/t_{cycle} decreases, and some energy savings are accrued. The effect is most pronounced for large grains that have large terminal velocities, and it disappears as grain size diminishes. Moreover, the effect can occur only if $e < 1$, for equating (58a) and (58b) for the special case $e = 1$ leads to

$$-[v_{up}(t_{up}) - v_{0up}] = [v_{down}(t_{down}) - v_{0down}] \qquad (59)$$

which shows that the term in brackets in (58b) must be positive if $e = 1$. Thus only if grains are sufficiently large (i.e., have sufficiently large terminal velocities) can viscosity enhance efficiency, and this effect occurs only as grains move toward the bed. Figure 19 summarizes pictorially the various possibilities for energy savings and loss during grain velocity fluctuations for viscous and inviscid cases with $e = 1$ and $e < 1$. In all cases it is evident that the net effect of viscosity is increased dissipation.

The preceding analysis shows that viscous mediation of dissipative grain interactions cannot be expected to enhance the net efficiency of steady debris flow. This seems to contradict the most basic observation of debris flow behavior, that the interstitial liquid phase enhances net mobility (see section 2). However, the analysis also shows that increases in buoyancy (expressed by diminished magnitudes of B) can enhance efficiency. Indeed, as $B \to 0$, grain contact forces due to gravity diminish, and grain collision forces are increasingly buffered by viscosity. Pore fluid pressures that exceed hydrostatic pressures mimic the condition $B \rightarrow 0$, and pore pressures high enough to produce liquefaction and mimic the condition $B = 0$ have been measured in experimental debris flows (Figures 5, 10, and 13). However, (36b) indicates that such pressures can exist only transiently. Thus understanding unsteady behavior of debris flow mixtures appears vital for understanding debris flow motion.

8. UNSTEADY MOTION AND HIGH PORE PRESSURES

Previous sections point to two key phenomena that characterize unsteady, nonuniform debris flow motion: (1) Fluid pressures greater than hydrostatic pressures exist in debris flows and can enhance flow efficiency, but cannot exist during steady, uniform motion. (2) Debris flows move as a surge or series of surges, in which coarse-grained heads that lack high fluid pressure restrict the downslope motion of finer-grained debris that may be nearly liquefied by high fluid pressure (Figures 8, 9, and 10). A coherent theory that predicts the coupled evolution of these phenomena is currently unavailable. This section examines some rudiments of the individual phenomena without considering coupling.

8.1. Development and Diffusion of High Fluid Pressures

Momentum balances such as (36a) and (36b) imply that pore pressures greater than hydrostatic ($\sim\rho_f gh$) can persist only if the sediment mass contracts volumetrically or (in the one-dimensional case) if there is a net flux of sediment toward the bed. Bulk density and flow depth data from the USGS debris flow flume indicate that both of these phenomena are common. Debris flow elongation that causes a flux of sediment toward the bed involves a complicated combination of shear and normal strains that is difficult to assess. Contraction involves volumetric strains that lend themselves to straightforward analysis and are thus the focus here.

Contraction of a moving debris flow mass produces pore pressure diffusion analogous to that which occurs during consolidation of deposits. Consequently, a diffusion timescale like t_{diff} (equation (8)) describes the persistence of high pore pressures. If this timescale equals or exceeds the debris flow duration, then volumetric contraction (consolidation) and attendant pore pressure diffusion can explain the existence of locally high pore pressures. However, two factors complicate estimation of an appropriate diffusion timescale: (1) Consolidation in moving debris flows is resisted not only by pore fluid pressure but also by fluctuating grain motions (granular temperatures) that help keep the sediment dilated. (2) The dilated, highly compressible state of the moving debris virtually ensures that consolidation will be accompanied by large strains and attendant changes in permeability and compressibility, which can cause pore pressures to diffuse nonlinearly.

The effects of granular temperature and nonlinear diffusion on pore pressures in debris flows appear inextricably related. In a hypothetical steady debris flow such as that considered in section 7, brief or enduring interactions of fluctuating grains produce time-averaged contact forces that exactly balance the buoyant weight of the grains themselves (see equation (48)). Effects of the fluctuations on the distribution of normal stress in the mixture are straightforward: stronger fluctuations increase the fluid volume fraction and reduce the mixture bulk density [cf. *Jenkins*, 1994], and although fluctuations dilate the debris to a greater degree than is possible statically, the effect of fluctuations on the time-averaged stress distribution in the debris is identical to that of a static reduction in bulk density. Gravity-driven consolidation in the presence of grain fluctuations can therefore proceed much as it does in quasi-static sediment. Consolidation simply requires an attendant reduction of granular temperature. However, declining granular temperature with accompanying changes in fluid volume fraction can produce large changes in permeability and compressibility that render the ongoing consolidation strongly nonlinear. Thus it is reasonable, as a first approximation, to embed the effects of granular temperature implicitly in a nonlinear consolidation model. This approach is followed here.

Consider a debris mass moving sufficiently steadily that equations (28) are a good approximation to (26). This implies that bulk accelerations are negligible. Assume also that (29) and (30) provide an adequate description of fluid stresses and solid-fluid interaction forces. This implies that the fluid carries no shear stress and imparts force to the solids via buoyancy and Darcian drag only. Equation (32) then describes the relative solid-fluid motion that produces consolidation and pore pressure diffusion. It is convenient to work with a form of this equation in which the fluid volume fraction υ_f is the quantity that diffuses. This "porosity diffusion" is analogous to the diffusion of void ratio (υ_f/υ_s) used in classical analyses of soil consolidation, and it is coupled to pore pressure diffusion in a straightforward manner [*Gibson et al.*, 1967].

The first step in the analysis involves replacement of the solid velocity divergence $\nabla \cdot \mathbf{v}_s$ in (32) with a more useful quantity. If the solid and fluid densities are assumed constant, the mass-conservation equation for solids (22a) can be manipulated to yield $\nabla \cdot \mathbf{v}_s = (-1/\upsilon_s)(D\upsilon_s/Dt)$, in which D/Dt designates the material time derivative following the motion of the solids [*Bird et al.*, 1960; *Atkin and Craine*, 1976]. Then υ_s can be replaced by $1 - \upsilon_f$, and the resulting expression can be substituted into (32) to yield

$$(1 - \upsilon_f)\nabla \cdot \frac{k}{\mu} \nabla p_{\text{dev}} = \frac{D\upsilon_f}{Dt} \qquad (60)$$

For sediment-water mixtures under gravity loads, it is reasonable to assume that υ_f is a function of only the

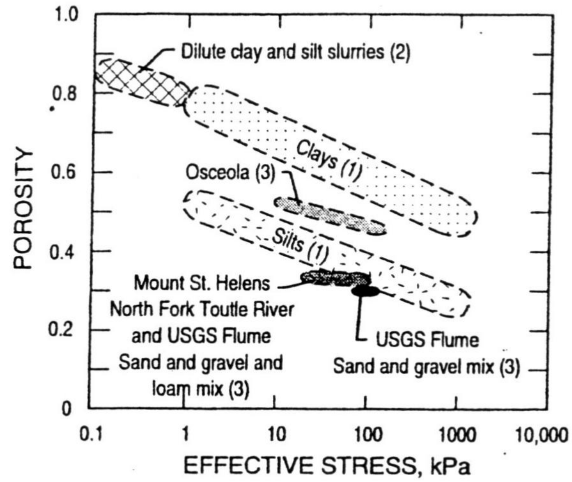

Figure 20. Data trends illustrating the approximate proportionality between fluid volume fraction (porosity) and the logarithm of effective stress in various soils and suspensions. Numbers identify data source: 1, *Lambe and Whitman* [1979]; 2, *Been and Sills* [1981]; 3, *Major* [1996].

effective stress, and thus of p_{dev}. Then application of the chain rule, $\nabla p_{dev} = (\partial p_{dev}/\partial \upsilon_f)\nabla \upsilon_f$, allows (60) to be recast as

$$\nabla \cdot \frac{k(1-\upsilon_f)}{\mu}\frac{\partial p_{dev}}{\partial \upsilon_f}\nabla \upsilon_f = \frac{D\upsilon_f}{Dt} \qquad (61)$$

in which the factor $\partial p_{dev}/\partial \upsilon_f$ plays the role of a stiffness modulus (reciprocal compressibility) of the mixture.

The conventional expression for the compressibility C of sediment-water mixtures describes the change in pore volume υ_f due to changes in effective stress, $C = -\partial \upsilon_f/\partial(\sigma - p)$. (Here σ is the total normal stress, defined as positive in compression, which is related to the stresses in section 6 by $\sigma = -\frac{1}{3}(\text{tr}\,\mathbf{T}_s + \text{tr}\,\mathbf{T}_f)$, where tr denotes the trace of the tensor.) For large strains, a reasonable postulate is that this compressibility varies inversely with the effective stress,

$$C \approx \kappa/(\sigma - p) \qquad (62)$$

where κ is a positive constant typically smaller than 1. Relationship (62) implies that the mixture grows progressively less compressible as consolidation proceeds and effective stress increases. Combining the definition $C = -\partial \upsilon_f/\partial(\sigma - p)$ with (62) and integrating the resulting equation shows that (62) also implies that the fluid volume fraction (porosity) declines logarithmically as effective stress increases:

$$\upsilon_f = \upsilon_{f0} - \kappa \ln|(\sigma - p)/(\sigma - p)_0| \qquad (63)$$

in which υ_{f0} and $(\sigma - p)_0$ are characteristic values of the fluid volume fraction and effective stress that derive from the stipulation that $\upsilon_f = \upsilon_{f0}$ when $\sigma - p = (\sigma - p)_0$. Data plotted in Figure 20 indicate that a logarithmic relationship such as (63) describes the volume change behavior of a variety of soils, slurries, and debris flow mixtures reasonably well [cf. *Lambe and Whitman*, 1979, p. 320; *Been and Sills*, 1981].

For problems of gravitational consolidation under constant load, the compressibility $\partial \upsilon_f/\partial p_{dev}$ in (61) matches the compressibility $C = -\partial \upsilon_f/\partial(\sigma - p)$ defined in terms of effective stress. This is apparent from the definition of effective stress, which can be written as

$$\sigma - p = \sigma - \rho_f g z - p_{dev} \qquad (64)$$

where the second term on the right-hand side is the hydrostatic component of the pore pressure, which remains constant. For estimation of consolidation behavior, the total stress σ can also be regarded as constant because the total stress changes little in comparison with the pore pressure during consolidation. Thus $\partial(\sigma - p) \approx \partial(-p_{dev})$, and the compressibility estimate defined by (62) can be substituted into (61), yielding

$$\nabla \cdot \frac{k(1-\upsilon_f)}{\mu C}\nabla \upsilon_f \approx \frac{D\upsilon_f}{Dt} \qquad (65)$$

This may be interpreted as an advection-diffusion equation for υ_f, in which the advection velocity is the velocity $\mathbf{v}_s$ of the reference frame for the material time derivative $D\upsilon_f/Dt$ [*Iverson*, 1993] [cf. *Atkin and Craine*, 1976]. Thus it is possible to exploit the fact that in a coordinate system that moves with velocity $\mathbf{v}_s$, (65) transforms into a standard diffusion equation that is readily solved [*Iverson*, 1993] [cf. *Ogata*, 1970].

The expression $k(1 - \upsilon_f)/\mu C$, which plays the role of the hydraulic diffusivity in (65), can be used to understand the character of nonlinear consolidation and estimate the timescale of nonlinear pore pressure diffusion. The expression can be written in a more explicit form by noting that the permeability of most sediment mixtures, including debris flow mixtures (Figure 6), is an exponential function of porosity or fluid volume fraction, $k = k_0 \exp(a\upsilon_f)$ [cf. *Lambe and Whitman*, 1979, p. 286; *Been and Sills*, 1981]. Use of this expression and (62) leads to an estimate of the hydraulic diffusivity D_h,

$$D_h = \frac{k(1-\upsilon_f)}{\mu C} = \frac{k_0(1-\upsilon_f)(\sigma - p)}{\kappa\mu}\exp(a\upsilon_f) \qquad (66)$$

which shows that the diffusivity is also an exponential function of fluid volume fraction. The implications of (66) can be clarified by noting that (63) can be used to rewrite the exponential function as

$$\begin{aligned}\exp(a\upsilon_f) &= \exp[a(\upsilon_{f_0} - \kappa \ln|(\sigma - p)/(\sigma - p)_0|)] \\ &= \exp(a\upsilon_{f_0})/[(\sigma - p)/(\sigma - p)_0]^{a\kappa}\end{aligned} \qquad (67)$$

Substituting (67) into (66) then yields

$$D_h = \frac{(1-\upsilon_f)k_0 \exp(a\upsilon_{f_0})}{\mu\kappa}(\sigma - p)_0^{a\kappa}(\sigma - p)^{1-a\kappa} \qquad (68)$$

An obvious implication of the last factor in (68) is that the character of pore pressure diffusion depends on

TABLE 8. Hydraulic Diffusivities D_h and Diffusion Timescales t_{diff} for Various Debris Flow Materials as Computed From Available Data and Equation (69)

Material	k_0, m^2	a	v_{f_0}	μ, Pa s	κ	$(\sigma - p)_0$, Pa	h, m	D_h, m^2/s	t_{diff}, s
USGS flume sand-gravel mix	10^{-13}	20	0.3	0.001	0.02	200	0.1	4×10^{-4}	20
USGS flume loam-gravel mix	10^{-13}	10	0.4	0.001	0.03	200	0.1	4×10^{-5}	300
Toutle River, May 18, 1980	10^{-14}	15	0.45	0.01	0.02	2000	1.0	9×10^{-5}	10,000 (3 hours)
Osceola, circa 5700 B.P.	10^{-14}	10	0.55	0.01	0.03	2000	1.0	2×10^{-5}	50,000 (14hours)

*For comparison, *Major* [1996] used quasi-static consolidation experiments to determine the following best fit values of hydraulic diffusivities: USGS flume loam-gravel mix, 1×10^{-6} m²/s; Toutle River debris flow, 2×10^{-6} m²/s; and Osceola mudflow, 4×10^{-7} m²/s.

whether or not $a\kappa > 1$. If $a\kappa > 1$, the diffusivity decreases as the effective stress increases because reduced permeability more than compensates for reduced compressibility. This is likely to be true for highly dilated, highly compressible sediment-water mixtures such as debris flow mixtures that are fully liquefied. In contrast, for $a\kappa < 1$, which is typical of less-dilated mixtures such as most soils, the diffusivity increases as effective stress increases, because reduced compressibility dominates reduced permeability. Values of a may be obtained from plots of permeability as a function of porosity or fluid volume fraction. For debris flow mixtures, such a plot (Figure 6) yields values of a that range from about 10 to 20 (Table 8). Values of κ may be obtained from (67) and plots of porosity (fluid volume fraction) as a function of effective stress (Figure 20), which show that values $0.02 < \kappa < 0.04$ are typical (Table 8). These values indicate that $a\kappa < 1$ probably characterizes most debris flow mixtures but that values of $a\kappa$ approach and might even exceed 1 when mixtures are highly dilated [cf. *Major*, 1996]. Values close to 1 imply that the diffusivity depends weakly on the effective stress and that a fixed diffusivity may provide reasonable estimates of consolidation behavior. This conclusion is supported by measurements and modeling of quasi-static consolidation of experimental debris flow deposits [*Major*, 1996].

Estimation of the timescale for consolidation in moving debris flows requires a characteristic value of the variable diffusivity given by (68), which can be obtained by assuming that the effective stress equals the characteristic effective stress $(\sigma - p)_0$ and that the fluid volume fraction equals the characteristic volume fraction v_{f_0}. Substitution of these values in (68) leads to the characteristic diffusivity

$$D_h = \frac{(1 - v_{f_0})k_0 \exp(a v_{f_0})}{\mu\kappa}(\sigma - p)_0 \qquad (69)$$

The timescale for consolidation of debris flow mixtures with this diffusivity is given by $t_{diff} \sim h^2/D_h$, where h is the debris flow thickness. Note that (69) implies that the effective compressibility of the debris flow mixture is given by $C = \kappa/(\sigma - p)_0$ (see (62)). By this definition, the effective compressibility of a debris flow body that is 1 m thick and 90% liquefied, for example, can be estimated from the typical values $\kappa \sim 0.04$ and $(\sigma - p)_0 \sim 2000$ Pa, which give $C \sim 2 \times 10^{-5}$ Pa^{-1}. This compressibility is roughly 1000 times greater than that of typical granular soil and many orders of magnitude greater than that of rock [cf. *Lambe and Whitman*, 1979].

Table 8 lists representative values of D_h and t_{diff} calculated using (69), data from Figures 6 and 20, and a representative range of debris flow materials and thicknesses. The pore pressure diffusion timescales range from tens of seconds to >10 hours, and they generally exceed the duration of motion of the corresponding debris flows. This result is noteworthy for two reasons. First, it demonstrates that consolidation provides a reasonable explanation for sustained high pore pressures in debris flows. Second, it demonstrates that the large compressibility of debris flow mixtures under low effective stress apparently contributes vitally to debris flow mobility by enabling effective hydraulic diffusivity values to be surprisingly low, much lower, for example, than those of most granular soils and fractured rocks [cf. *Li*, 1985; *Roeloffs*, 1996]. The large compressibility and low diffusivity result from the wide diversity of grain sizes in debris flows and from dilation of debris flow sediments that attends production of nonzero granular temperatures. Thus effects of widely ranging grain sizes, granular temperature, and high pore pressure may play synergistic and perhaps inseparable roles in sustaining debris flow mobility.

8.2. Debris Flow Surges With Nonuniform Fluid Pressures

Concentration of coarse clasts at the heads of debris flow surges gives them hydraulic diffusivities that may greatly exceed those of most debris flow material. This may explain, in part, why surge heads appear unsaturated and exhibit little or no pore fluid pressure (Figure 10). Interaction of surge heads with the nearly liquefied material behind them plays a key role in determining the unsteady, nonuniform character of debris flow motion and the extent of debris flow runout. Parts of debris flows that remain nearly liquefied provide little frictional resistance to motion, whereas surge heads can provide much frictional resistance. Other forms of flow resistance, associated with viscous flow of pore fluid and inelastic grain collisions, may also vary spatially, as is reflected by variations in Savage numbers and Bagnold numbers.

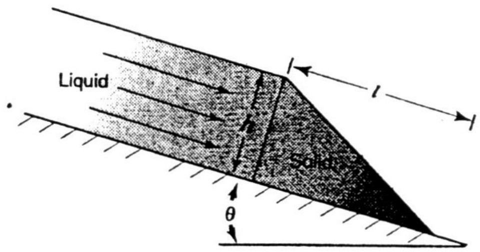

Figure 21. Schematic vertical cross section of the rigid body model of a debris-flow surge, with geometric parameters defined [cf. *Coleman*, 1993; *Whipple*, 1994].

Rigorous assessment of the interaction of relatively dry surge heads with nearly liquefied debris behind them requires numerical analysis of unsteady, nonuniform debris flow motion, as described in section 9. However, simple steady state analyses provide some insight into the problem and a framework for interpreting numerical results. Such analyses [*Coleman*, 1993; *Whipple*, 1994; *Major*, 1996] assume that the surge head acts as a translating rigid body, with Coulomb resistance at its base and a completely liquefied mass pushing it from behind. These analyses ignore other forms of resistance, including all resistance associated with internal deformation; they ignore all inertial and time-dependent effects, including the evolution of the debris flow shape; and they ignore multidimensional effects that cannot be represented with a one-dimensional force balance.

With the caveats described above, consider the simple model of a debris flow surge depicted in Figure 21. The surge moves steadily on a uniform slope inclined at the angle θ. The surge head has a triangular cross-sectional shape with height h equal to the debris flow thickness measured normal to the slope. The length l of the surge head is measured parallel to the slope. The mass of the surge head is then $\frac{1}{2}\rho_h l w$, where ρ_h is the bulk density of the head and w is its breadth normal to the plane of the page. The basal shear force τ and normal force σ due to the action of gravity on the head are simply $\tau = \frac{1}{2}\rho_h g h l w \sin\theta$ and $\sigma = \frac{1}{2}\rho_h g h l w \cos\theta$. Slope parallel Coulomb resistance to basal sliding of the head is described by $-\sigma \tan\phi$, and the slope parallel force of the liquefied debris flow body pushing against the upslope face of the head is described by $\frac{1}{2}\rho_b g h^2 w \cos\theta$, where ρ_b is the density of the liquefied body. This expression assumes that the streamlines of flow parallel the slope. Steady motion of the head then requires that the slope parallel forces acting on the head sum to zero:

$$\frac{1}{2}\rho_h g h l w \sin\theta - \frac{1}{2}\rho_h g h l w \cos\theta \tan\phi + \frac{1}{2}\rho_b g h^2 w \cos\theta = 0 \quad (70)$$

Combination of terms reduces (70) to [cf. *Whipple*, 1994]

$$\frac{h}{l} = \frac{\rho_h}{\rho_b}(\tan\phi - \tan\theta) \quad (71)$$

Furthermore, $\rho_h \approx \rho_b$ is usually a reasonable approximation for debris flows, so that (71) can be expressed as

$$h/l \approx \tan\phi - \tan\theta \quad (72)$$

Although quantitative predictions of (71) and (72) must be interpreted with great caution owing to the many factors neglected in the analysis, qualitative trends predicted by (71) and (72) provide some insight for interpreting both debris flow behavior and predictions of more elaborate models. For example, (72) shows that on steep slopes (where $\theta \to \phi$), $h/l \to 0$ is required to sustain steady motion; this implies that debris flow surges will accelerate on steep slopes unless the length of the surge head is very long in relation to its height. Moreover, for surges with identical values of l, surges with the largest h will accelerate fastest and overtake smaller surges, which may help explain surge coalescence. On low-angle slopes, where $\theta \to 0$, $h/l \to \tan\phi$ is required to sustain steady motion; this implies that surges will decelerate and stop on low-angle slopes unless $h/l > \tan\phi$ can be maintained, which requires surge heads to be short and steep. Typically $\phi \sim 30°$, so that l greater than about $h/0.6$ suffices to stop motion. Data such as those of Figures 5 and 10 indicate that the length of surge heads typically exceeds $h/0.6$, so that the frictional resistance of surge heads appears capable of halting debris flow motion as slope angles decline toward zero. Data such as those of Figures 5 and 10 also reveal the oversimplification of the rigid surge head model, however. More realistic assessment of the role of surge heads requires a model such as that described in the next section.

9. HYDRAULIC MODELING AND PREDICTION OF DEBRIS FLOW MOTION

Models that employ hydraulic theory simplifications provide the most sophisticated tool for practical forecasts of debris flow runout and inundation limits. Such models also have scientific importance, for at present they constitute the state-of-the-art method for predicting unsteady, nonuniform motion, one of debris flows' most obvious and readily measured attributes. Hydraulic models are distinguished primarily by the use of depth-averaged equations of motion, which omit some key physical phenomena. In particular, because such models ignore velocity components normal to the bed, they can include solid-solid and solid-fluid interaction effects in only a rudimentary way. This precludes rigorous treatment of the evolution of granular temperatures and nonhydrostatic pore pressures (see sections 7 and 8). Efforts to build more sophistication into hydraulic models continue [e.g., *Jenkins and Askari*, 1994].

To date, several types of hydraulic models have been presented. They differ primarily in the type of slope parallel momentum balance employed. The simplest approach uses the kinematic wave approximation, in which a steady state momentum balance replaces the dynamic momentum balance for unsteady flow [e.g., *Weir*, 1982; *Arratano and Savage*, 1994]. More elaborate dynamic wave models retain the full momentum balance [e.g., *Yamashita and Miyamoto*, 1991; *Macedonio and Pareschi*, 1992; *Hunt*, 1994; *Shieh et al.*, 1996] but differ in their representation of stresses that resist motion. Most begin with the one-phase Bingham or Bagnold model described in section 5 but ultimately lump the Bingham and Bagnold stresses into a bulk flow resistance coefficient (e.g., Manning's n) similar to those used in water flood routing. Bulk resistance coefficients have been thoroughly calibrated for water floods but not for debris flows. Calibration is problematic for debris flows because the mechanisms of momentum transport and energy dissipation in debris flows (solid friction, inelastic collisions, pore fluid flow) may differ significantly between events, whereas the chief mechanism in water floods (hydrodynamic turbulence) is universal. Moreover, Manning-type flow resistance coefficients amalgamate the effects of internal and boundary resistance and cannot represent static resistance that is present during debris flow initiation and deposition. Indeed, the fact that debris flows exhibit both solid and fluid behavior means that debris flow models require initial and boundary conditions that differ fundamentally from those for water floods.

To account for debris flows' variable composition, the possibility of boundary slip, and the mechanics of initiation and deposition as well as flow, the hydraulic model described here uses internal and basal friction angles and pore fluid viscosity to characterize flow resistance. This facilitates rigorous model tests because values of friction angles and fluid viscosity can be measured independently rather than calibrated. Fluid effects also enter the model by mediating internal and basal friction. Stress due to grain collisions is neglected, so the model does not represent the full spectrum of debris flow behavior depicted in Figure 15. The mathematical formulation and solution technique are based on a modification of the hydraulic theory for dry granular flows developed by *Savage and Hutter* [1989, 1991]. *Hungr* [1995] has described an approach that is in some respects similar.

9.1. Relationship to Mixture Theory

To clarify the assumptions of the hydraulic formulation, it is useful to establish its relationship to the mixture theory described in section 6. Simplification of the mixture momentum equations (26) can be achieved by focusing on the motion of the solids and analyzing the motion of the fluid relative to that of the solids, just as in quasi-static porous media problems [e.g., *Bear*, 1972]. Then the pertinent fluid velocity is the specific discharge divided by the fluid volume fraction, $\mathbf{q}/\upsilon_f = \mathbf{v}_f - \mathbf{v}_s$. Substituting this expression in the fluid momentum equation (26b) yields, for the special case in which ρ_s and ρ_f as well as the total debris flow mass and density are constant,

$$\rho_f\upsilon_f\left[\frac{\partial}{\partial t}(\mathbf{q}/\upsilon_f + \mathbf{v}_s) + \frac{\mathbf{q}}{\upsilon_f}\cdot\nabla(\mathbf{q}/\upsilon_f + \mathbf{v}_s) + \mathbf{v}_s\cdot\nabla(\mathbf{q}/\upsilon_f + \mathbf{v}_s)\right] = \nabla\cdot\mathbf{T}_f + \rho_f\upsilon_f\mathbf{g} - \mathbf{f} \quad (73)$$

Darcy's law provides an estimate of the largest plausible $\mathbf{q}$ in (73) because data (Figures 5, 10, and 13) show that hydraulic head gradients in debris flows commonly approach but seldom exceed liquefaction-inducing gradients, which roughly equal 1. Thus the hydraulic conductivity $K = \rho_f gk/\mu$ provides a good estimate of the maximum magnitude of $\mathbf{q}$, and the conductivity rarely exceeds ~0.01 m/s for debris flow materials (see Table 3 and Figure 6). In contrast, $\mathbf{v}_s$ typically exceeds 1 m/s. By this rationale, $\mathbf{v}_s$ generally exceeds $\mathbf{q}/\upsilon_f$ by more than an order of magnitude, and discarding terms in (73) that contain $\mathbf{q}/\upsilon_f$ in favor of those containing $\mathbf{v}_s$ yields the approximation

$$\rho_f\upsilon_f[\partial\mathbf{v}_s/\partial t + \mathbf{v}_s\cdot\nabla\mathbf{v}_s)] = \nabla\cdot\mathbf{T}_f + \rho_f\upsilon_f\mathbf{g} - \mathbf{f} \quad (74)$$

This equation implies that inertial forces affecting fluid motion are practically indistinguishable from those affecting solid motion, except insofar as the fluid and solid masses per unit volume of mixture differ. Small differences in solid and fluid velocities can nonetheless have very significant (albeit noninertial) effects.

A simplified momentum equation for the solid-fluid mixture results from adding (74) and (26a). This yields

$$\rho[\partial\mathbf{v}_s/\partial t + \mathbf{v}_s\cdot\nabla\mathbf{v}_s] = \nabla\cdot(\mathbf{T}_s + \mathbf{T}_f) + \rho\mathbf{g} \quad (75)$$

in which ρ is the mixture density defined by (24a). The solid-fluid interaction force $\mathbf{f}$ does not appear explicitly in this equation but resides implicitly in the combined solid-fluid stress tensor, $\mathbf{T}_s + \mathbf{T}_f$.

The assumption $\mathbf{q}/\upsilon_f \ll \mathbf{v}_s$ also produces a simplified mass-balance equation from (25a),

$$\nabla\cdot\mathbf{v}_s = 0 \quad (76)$$

Thus (75) and (76) constitute approximate governing equations for debris flows that maintain constant mass and density as they move. These equations differ from analogous equations governing motion of a one-phase granular solid in only two respects: they involve the total mixture density ρ and the influence of fluid stress $\mathbf{T}_f$.

The relative simplicity of (75) and (76) simplifies subsequent manipulations, which consist of specializing the equations to two spatial coordinates, followed by scaling and depth averaging. The steps are essentially identical to those described by *Savage and Hutter* [1989, 1991], who additionally generalized the equations to accommodate curvilinear coordinates. The steps can also be generalized to three spatial coordinates [*Lang and Leo*, 1994], but for brevity only the two-dimensional approach is summarized here. For two-dimensional flow

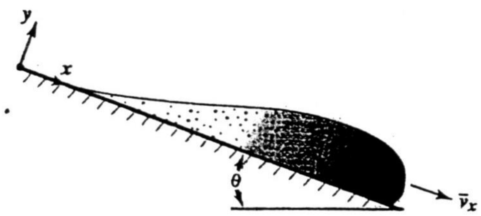

Figure 22. Schematic vertical cross section of an unsteady, deforming debris flow surge moving down an inclined plane. The flow depth h and depth-averaged velocity $\bar{v}_x$ vary as functions of x and t.

across an infinitely wide planar surface that slopes at the angle θ (Figure 22), (75) and (76) reduce to

$$\frac{\partial v_x}{\partial x} + \frac{\partial v_y}{\partial y} = 0 \qquad (77a)$$

$$\rho\left(\frac{\partial v_x}{\partial t} + v_x\frac{\partial v_x}{\partial x} + v_y\frac{\partial v_x}{\partial y}\right) = -\frac{\partial T_{s(xx)}}{\partial x} - \frac{\partial T_{s(yx)}}{\partial y} - \frac{\partial T_{f(xx)}}{\partial x} - \frac{\partial T_{f(yx)}}{\partial y} + \rho g \sin\theta \qquad (77b)$$

$$\rho\left(\frac{\partial v_y}{\partial t} + v_y\frac{\partial v_y}{\partial y} + v_x\frac{\partial v_y}{\partial x}\right) = -\frac{\partial T_{s(yy)}}{\partial y} - \frac{\partial T_{s(xy)}}{\partial x} - \frac{\partial T_{f(yy)}}{\partial y} - \frac{\partial T_{f(xy)}}{\partial x} - \rho g \cos\theta \qquad (77c)$$

To streamline the presentation, these and subsequent equations incorporate several changes in notation. They omit the subscript s that denotes solid phase velocities, because all v refer to the solid phase; velocity subscripts x and y denote slope parallel and slope normal Cartesian components, respectively (Figure 22). Sign conventions for stress components have been reversed so that compression and left-lateral shear are positive, following *Savage and Hutter* [1989]. Subscripts in parentheses denote the Cartesian components of the solid and fluid stresses; the first subscript indicates the normal to the plane upon which the stress component acts, and the second subscript indicates the direction of action. The shear stress subscripts (xy) and (yx) are interchangeable, however, because stress tensors are assumed to be symmetric.

9.2 Normalization, Depth Averaging, and Constitutive Assumptions

A key step in simplifying (77a)–(77c) involves scaling that is similar but not identical to the well-known shallow water or Saint-Venant scaling [cf. *Vreugdenhil*, 1994]. As described by *Savage and Hutter* [1989] and *Iverson* [1997], two length scales exist, the characteristic flow length $\bar{l}$ in the x direction and the characteristic flow depth $\bar{h}$ in the y direction. The parameter $\epsilon = \bar{h}/\bar{l}$ describes the ratio of these length scales and is deemed generally much smaller than 1. The characteristic time-scale is that of free fall in the x direction, $(\bar{l}/g)^{1/2}$, because the potential for free fall drives debris flow motion. These time and length scales in turn lead to differing velocity scales for the x direction, $(g\bar{l})^{1/2}$, and y direction, $\epsilon(g\bar{l})^{1/2}$, which imply that $v_x \gg v_y$. The scales for stresses are the stresses that would exist at the base of a steady, uniform flow of depth $\bar{h}$, $\rho g\bar{h}\sin\theta$ for shear stress and $\rho g\bar{h}\cos\theta$ for normal stress and pore pressure.

Scaled (i.e., normalized) equations result from multiplying each term of (77a) by $(\bar{l}/g)^{1/2}$, dividing each term of (77b) and (77c) by ρg, and taking the limit as $\epsilon \to 0$. This yields governing equations that differ from equation (2.10) of *Savage and Hutter* [1989] only by including fluid stresses,

$$\frac{\partial v_x}{\partial x} + \frac{\partial v_y}{\partial y} = 0 \qquad (78a)$$

$$\frac{\partial v_x}{\partial t} + v_x\frac{\partial v_x}{\partial x} + v_y\frac{\partial v_x}{\partial y} = \sin\theta\left(1 - \frac{\partial T_{s(yx)}}{\partial y} - \frac{\partial T_{f(yx)}}{\partial y}\right) + \epsilon\cos\theta\left(-\frac{\partial T_{s(xx)}}{\partial x} - \frac{\partial T_{f(xx)}}{\partial x}\right) \qquad (78b)$$

$$0 = \cos\theta\left(-1 - \frac{\partial T_{s(yy)}}{\partial y} - \frac{\partial T_{f(yy)}}{\partial y}\right) \qquad (78c)$$

In these equations and all subsequent equations, all quantities are normalized by the appropriate scaling variables, as described above, but for brevity the original (dimensional) notation is retained [cf. *Iverson*, 1997]. Equations (78) have two key properties: (1) The y direction momentum balance (78c) has a simple form identical to that for steady, uniform flow; integration of (78c) shows that the total normal stress at any depth is simply the static stress $\rho g(h - y)\cos\theta$. (2) The x direction momentum balance (78b) includes longitudinal normal stress gradient terms preceded by the small parameter ϵ, which apparently indicates that such terms can be neglected. However, as was explained by *Savage and Hutter* [1989], neglect of longitudinal normal stress gradients is untenable because it produces a stress field identical to that for steady, uniform flow, which negates any hope of modeling surge-like motion. The physical rationale for retaining this term becomes more apparent when the equations are integrated over the flow depth.

The final step in simplifying the governing equations involves depth integration, which incorporates constitutive assumptions about stresses and produces equations without explicit y dependence. The process is reasonably straightforward but rather protracted, and the results are simply summarized here. The process involves repeated application of Leibniz's rule for integrating derivatives and incorporates kinematic boundary conditions, which state that mass neither enters nor leaves at the free surface (where $y = h$) and bed (where $y = 0$),

$$\frac{\partial h}{\partial t} + v_x\frac{\partial h}{\partial x} - v_y = 0 \quad \text{at} \quad y = h(x, t) \qquad (79a)$$

$$v_y = 0 \quad \text{at} \quad y = 0 \tag{79b}$$

It also involves the assumption that the debris flow surface is free of all stresses,

$$T_{s(xx)} = T_{s(yy)} = T_{s(yx)} = T_{f(xx)} = T_{f(yy)} = T_{f(yx)} = 0 \quad \text{at} \quad y = h(x,t) \tag{80}$$

and it employs depth-averaged velocities and normal stresses defined by

$$\overline{v_x} = \frac{1}{h}\int_0^h v_x \, dy \tag{81a}$$

$$\overline{T_{s(xx)}} = \frac{1}{h}\int_0^h T_{s(xx)} \, dy \tag{81b}$$

$$\overline{T_{s(yy)}} = \frac{1}{h}\int_0^h T_{s(yy)} \, dy \tag{81c}$$

$$\overline{T_{f(xx)}} = \frac{1}{h}\int_0^h T_{f(xx)} \, dy \tag{81d}$$

$$\overline{T_{f(yy)}} = \frac{1}{h}\int_0^h T_{f(yy)} \, dy \tag{81e}$$

$$\overline{v_x^2} = \frac{1}{h}\int_0^h v_x^2 \, dy = \xi \overline{v_x}^2 \tag{81f}$$

As was noted by *Savage and Hutter* [1989], values of ξ in (81f) that deviate from unity provide information about the deviation of the vertical velocity profile from uniformity. If a debris flow moves exclusively by basal slip, $\xi = 1$ applies. At the other extreme, $\xi = 6/5$ applies for a debris flow with no basal sliding and a parabolic velocity profile indicative of laminar viscous flow. As a result, the assumption $\xi \approx 1$ appears generally justified.

More important than the details of the internal velocity field is the constitutive description of stresses in (78b). For the granular solids the stress model used here is the simple Coulomb rule given by (6). The appropriate nondimensional form of the Coulomb rule is

$$T_{s(yx)} = -\text{sgn}\,(v_x) T_{s(yy)} \cot\theta \tan\phi_{\text{bed/int}} \tag{82}$$

in which $\phi_{\text{bed/int}}$ indicates the appropriate friction angle for bed slip or internal deformation and sgn (v_x) denotes the sign (+ or −) of v_x. In (82), cot θ appears because of the different scalings for shear and normal stress components. Although (82) does not contain pore pressure effects explicitly, it does so implicitly because $T_{s(yy)}$ and $T_{f(yy)}$ are related by (78c). Thus as fluid pressures $T_{f(yy)}$ grow in magnitude, the magnitudes of $T_{s(yy)}$ and $T_{s(yx)}$ diminish.

The Coulomb rule also leads directly to an expression relating $T_{s(xx)}$ to $T_{s(yy)}$, obtained from classical *Rankine* [1857] earth pressure theory. Earth pressure theory applies to effective stresses borne by the solid constituents [*Lambe and Whitman*, 1979] and presumes a relation

$$T_{s(xx)} = k_{\text{act/pass}} T_{s(yy)} \tag{83}$$

in which $k_{\text{act/pass}}$ is an earth pressure coefficient that has different values depending on whether the flow is "actively" extending ($\partial\overline{v_x}/\partial x > 0$) or "passively" compressing ($\partial\overline{v_x}/\partial x < 0$). For deformation that includes both bed slip and internal slip, earth pressure theory leads to the expression for $k_{\text{act/pass}}$ presented without derivation by *Savage and Hutter* [1989],

$$k_{\text{act/pass}} = 2\,\frac{1 \mp [1 - \cos^2\phi_{\text{int}}(1 + \tan^2\phi_{\text{bed}})]^{1/2}}{\cos^2\phi_{\text{int}}} - 1 \tag{84}$$

and derived in Appendix C. The "−" in "∓" applies to the active coefficient, and the "+" applies to the passive. *Hungr* [1995] suggested that the earth pressure relation (83) might be generalized by including the effects of elastic compliance, but noted that the elastic modulus has negligible influence on model predictions.

Equations (78)–(84) provide all information necessary to complete the formulation of the hydraulic equations. Integration of (78a) from $y = 0$ to $y = h$, with application of the kinematic boundary conditions (79), produces a depth-averaged mass conservation equation,

$$\frac{\partial h}{\partial t} + \frac{\partial (h\overline{v_x})}{\partial x} = 0 \tag{85}$$

Integration of (78c) from $y = 0$ to $y = h$ yields a steady momentum balance in the y direction, which states that the sum of the nondimensional solid and fluid stress balances the y component of the nondimensional total mixture weight

$$T_{s(yy)} + T_{f(yy)} = h(x,t) - y \tag{86}$$

This in turn leads to nondimensional expressions for the total (solid plus fluid) normal stress at the bed and for the y direction depth-averaged total normal stress,

$$T_{s(yy)} + T_{f(yy)} = h \quad \text{at} \quad y = 0 \tag{87}$$

$$\overline{T_{s(yy)}} + \overline{T_{f(yy)}} = \frac{1}{h}\int_0^h (h - y)\, dy = \tfrac{1}{2}h \tag{88}$$

Integration of the normalized x direction momentum equation (78b) from $y = 0$ to $y = h$ yields the result [cf. *Savage and Hutter*, 1989, equation (2.24)]

$$\frac{\partial}{\partial t}(h\overline{v_x}) + \frac{\partial}{\partial x}(\xi h \overline{v_x}^2) = h \sin\theta$$
$$+ (T_{s(yx)}|_{y=0}) \sin\theta + (T_{f(yx)}|_{y=0}) \sin\theta$$
$$- \epsilon \cos\theta \frac{\partial}{\partial x}(h\overline{T_{s(xx)}}) - \epsilon \cos\theta \frac{\partial}{\partial x}(h\overline{T_{f(xx)}}) \quad (89)$$

Terms on the right-hand side of (89) can be interpreted as follows. The first term represents the gravitational driving stress. The second term represents frictional resistance to slip at the base of the flow and can be evaluated by applying the Coulomb equation (82) and the normal stress equation (87) at the flow base,

$$(T_{s(yx)}|_{y=0}) \sin\theta = -\mathrm{sgn}\,(\overline{v_x})(h - p_{\mathrm{bed}}) \cos\theta \tan\phi_{\mathrm{bed}} \quad (90)$$

where $h - p_{\mathrm{bed}}$ is the nondimensional basal effective stress and $p_{\mathrm{bed}} = T_{f(yy)}|_{y=0}$ is the nondimensional basal pore pressure. The third term on the right-hand side of (89) represents flow resistance due to shear of the fluid at the flow base. It can be evaluated using Newton's law of viscosity (14), which yields

$$[(T_{f(yx)})|_{y=0}] \sin\theta = -\upsilon_f \bar{\mu} (\partial v_x/\partial y)|_{y=0} \quad (91)$$

where $\bar{\mu}$ is the appropriate, nondimensional depth-averaged viscosity, given by $\bar{\mu} = \mu/[\rho g \bar{h}^2/(g\bar{l})^{1/2}]$. Application of (91) requires knowledge of the fluid velocity gradient at the bed, $(\partial v_x/\partial y)|_{y=0}$, which is generally unknown but can be obtained from estimates of the vertical velocity profile. The estimates are constrained by assuming no slip of fluid at the bed and a mean fluid velocity of $\overline{v_x}$. For example, if the velocity profile is linear, then $(\partial v_x/\partial y)|_{y=0} = \overline{v_x}/h$. If the velocity profile is parabolic, then a simple analysis of laminar flow down an incline shows that $(\partial v_x/\partial y)|_{y=0} = 3\overline{v_x}/h$ [cf. *Bird et al.*, 1960, pp. 37–40]. If the velocity profile is blunt, with shear strongly concentrated near the bed, a good descriptor is $(\partial v_x/\partial y)|_{y=0} = (n + 2)(\overline{v_x}/h)$, where $n = 1$ indicates a parabolic profile and $n > 1$ indicates blunter profiles; this form is used below. The fourth term on the right-hand side of (89) represents the longitudinal stress gradient due to interaction of solid grains. It can be evaluated using (83) and (88), yielding

$$-\epsilon \cos\theta \frac{\partial}{\partial x}(h\overline{T_{s(xx)}})$$
$$= -\epsilon k_{\mathrm{act/pass}} \cos\theta \frac{\partial}{\partial x}\left(\frac{h^2}{2} - h\overline{T_{f(yy)}}\right) \quad (92)$$

As is indicated by the presence of $\overline{T_{f(yy)}}$ in (92), the longitudinal solid stress gradient is mediated by fluid pressure. The final term in (89) represents the longitudinal stress gradient due to the fluid pressure alone. Because fluid pressure is isotropic, it can be rewritten with $\overline{T_{f(yy)}}$ in place of $\overline{T_{f(xx)}}$,

$$-\epsilon \cos\theta \frac{\partial}{\partial x}(h\overline{T_{f(xx)}}) = -\epsilon \cos\theta \frac{\partial}{\partial x}(h\overline{T_{f(yy)}}) \quad (93)$$

The utility of (92) and (93) is enhanced by evaluating the integral (81e) to calculate $\overline{T_{f(yy)}}$ for a condition in which the fluid pressure increases linearly from zero at the debris flow surface to a maximum of p_{bed} at the bed (a condition consistent with the hydraulic theory assumptions). The integration shows that $\partial(h\overline{T_{f(yy)}})/\partial x = h(\partial p_{\mathrm{bed}}/\partial x)$, and this substitution is used in (94) below.

9.3. Governing Equations and Auxiliary Conditions

The final form of the x direction momentum equation results from incorporating (85) and (90)–(93) in (89), assuming $\xi = 1$, collecting and cancelling like terms, and dividing by h, which yields

$$\frac{\partial \overline{v_x}}{\partial t} + \overline{v_x}\frac{\partial \overline{v_x}}{\partial x} = \sin\theta - \mathrm{sgn}\,(\overline{v_x})\left(1 - \frac{p_{\mathrm{bed}}}{h}\right)\cos\theta \tan\phi_{\mathrm{bed}}$$
$$- \upsilon_f \bar{\mu}(n+2)\left(\frac{\overline{v_x}}{h^2}\right)$$
$$- \epsilon \cos\theta \frac{\partial}{\partial x}[k_{\mathrm{act/pass}}(h - p_{\mathrm{bed}}) + p_{\mathrm{bed}}] \quad (94)$$

Together, (94) and (85) form a set of two equations in two unknowns, $\overline{v_x}(x, t)$ and $h(x, t)$, which can be solved provided that the basal pore fluid pressure $p_{\mathrm{bed}}(x, t)$ and the necessary initial and boundary conditions are specified. The need to specify rather than predict basal pore pressures is inherent to the hydraulic model; fluid pressure deviations from hydrostatic values result from velocity components normal to the bed (see section 8), and neglect of such velocities in (78c) precludes the possibility of predicting nonhydrostatic pressures. Thus inclusion of nonhydrostatic pressures $p_{\mathrm{bed}}(x, t)$ may seem to contradict the hydraulic model assumptions. The inclusion is justified, however, on the grounds that the consolidation process responsible for generating nonhydrostatic fluid pressures (section 8) typically operates on timescales substantially longer than the debris flow duration (Table 8). Thus as a first approximation, high pore pressures, once established, may be assumed to persist in debris flows, and pore pressures may be treated as parameters in hydraulic model calculations.

Inspection of the individual terms in (94) reveals how the hydraulic model encapsulates debris flow physics. The inertial terms on the left-hand side of (94) show that both rigid body accelerations and convective accelerations may be important. On the right-hand side of (94), if the first two terms are viewed in isolation, they depict a static balance of forces identical to that used in infinite slope stability analyses for cases in which there is zero cohesion and an arbitrary distribution of pore pressure [cf. *Iverson*, 1990, 1992]. If the last term on the right-hand side is included, this static force balance assumes a form comparable to that of two-dimensional slope stability analyses that use methods of slices, and in this case the interslice forces are represented by depth-averaged Rankine stresses. Thus the model subsumes classical models of the statics of landslides with spatially varied pore pressures as a limiting case, which applies to incipient debris flow motion. The third term on the right-hand side of (94) represents the effects of shear resistance due to fluid viscosity. The motion of a frictionless but viscous mass is represented by the special case where $\phi_{bed/int} = 0$ or, alternatively, $p_{bed} = h$ (in which case the mass is completely liquefied by pore pressure).

The final term is perhaps the most interesting and important term in (94), for it describes the longitudinal stress variation that accompanies variations in flow depth and surge-like motion. The term shows that a great change in debris flow behavior occurs as p_{bed} ranges from 0 to h. If $p_{bed} = h$ and the sediment mass behaves like a liquid, normal stresses are isotropic, equal to the static pressure, and independent of the local style of deformation. If $p_{bed} = 0$ and the debris behaves like a Coulomb solid, normal stresses are anisotropic, and the longitudinal normal stress depends strongly on whether the sediment mass is locally extending ($\partial \overline{v_x}/\partial x > 0$) or compressing ($\partial \overline{v_x}/\partial x < 0$) as it deforms and moves downslope. For example, in a typical case with $\phi_{int} = 40°$ and $\phi_{bed} = 30°$, (84) indicates that the value of the active (extending) and passive (compressing) earth pressure coefficients are 0.82 and 4.0, respectively. In this case, longitudinal stresses in regions of extending flow will be 18% less than in a liquid of density ρ, but longitudinal stresses in regions of compressing flow will be 4 times greater than in a liquid. Consequently, the model predicts that strong local gradients in the longitudinal normal stress can occur for two reasons: either the style of deformation changes locally from extending to compressing, or the pore pressure varies locally from high to low. Thus, depending on the deformation style and pore pressure distribution, the model expressed by (85) and (94) can represent unsteady flow behavior that ranges from that of a granular avalanche, as modeled by *Savage and Hutter* [1989, 1991], to that of a liquid surge, as modeled by *Hunt* [1994]. Furthermore, the front of a fully developed debris flow may act like a compressing granular solid and support high lateral stresses, while the trailing flow acts more like a fluid. This phenomenon explains how debris flow surges with steep snouts and gradually tapered tails can move downstream with only modest attenuation.

The initial and boundary conditions used in conjunction with (85) and (94) are identical to those described by *Savage and Hutter* [1989]. The initial conditions specify the zero velocity and static geometry of the mass that mobilizes into a debris flow,

$$\overline{v_x}(x, 0) = 0 \tag{95a}$$

$$h(x, 0) = h_0(x) \tag{95b}$$

Boundary conditions stipulate that the height of the deforming mass is zero at the front margin ($x = x_F$) and rear margin ($x = x_R$),

$$h(x_F, t) = 0 \tag{96a}$$

$$h(x_R, t) = 0 \tag{96b}$$

These zero-depth boundary conditions are connected to the velocities at the front and rear flow margins by the relations

$$\overline{v_{x_F}} = dx_F/dt \tag{97a}$$

$$\overline{v_{x_R}} = dx_R/dt \tag{97b}$$

Finally, the pore pressure distribution $p_{bed}(x, t)$ must be specified.

9.4. Solutions and Comparisons With Data

In general, the nonlinearity of the equation set (85) and (94) necessitates numerical solutions. The numerical solutions summarized here employed the Lagrangian finite difference scheme developed for dry Coulomb flows by *Savage and Hutter* [1989, 1991], who determined that this scheme was superior to various Eulerian methods. The Lagrangian scheme was modified to account for the effects of pore fluid pressure, as represented in (94), but the viscous shear term involving $\bar{\mu}$ in (94) was omitted for three reasons. (1) Scaling analyses [*Iverson*, 1997] indicate that this term is commonly orders of magnitude smaller than other terms in (94). (2) Lack of knowledge of the appropriate n value makes evaluation of the viscous shear term uncertain, and it is undesirable to introduce a poorly constrained "fitting" parameter in the model. (3) Omission of the viscous shear term reduces the model to a straightforward force balance in which Coulomb friction provides all resistance to motion, and fluid stresses merely mediate the Coulomb friction. This facilitates comparison of model results with those for the dry Coulomb flows of *Savage and Hutter* [1989, 1991]. Moreover, because the Coulomb bed friction and internal friction angles can be measured independently and the pore pressure distribution can be measured during debris flow flume experiments, the model provides true predictions of experimentally observed flow velocities and depths and not merely calibrated fits of data. Comparison of predictions and data then indicate whether the omitted viscous shear term might be essential.

To make predictions for debris flow flume experiments with sediment mixtures containing about 2% silt and clay, 43% sand, and 55% gravel by weight, the values $\phi_{int} = 42°$ and $\phi_{bed} = 28°$ were inferred from quasi-static measurements of the critical angles for motion of dry sediment on a tilting table. The bed friction angle was established as the mean of numerous measurements of the tilt required for basal slip of a tabular sediment mass placed on a concrete slab with a surface texture identical to that of the flume bed. The internal friction angle was

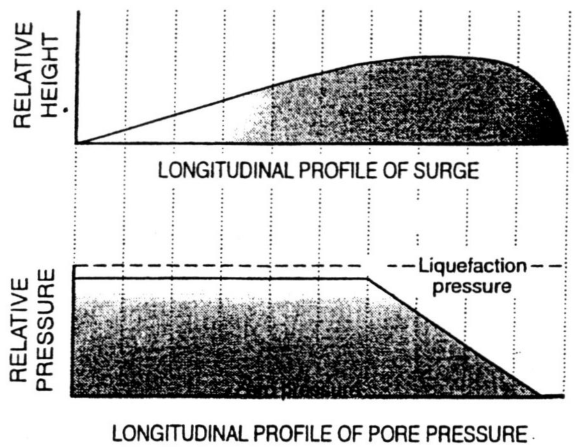

Figure 23. Spatial distribution of basal pore fluid pressures in a moving surge (expressed as a fraction of the pressure required for complete liquefaction) used in model calculations for nodes where $\overline{v_x} > 0$. The pore pressure distribution elongates with the surge, but the pressure magnitude (relative to the liquefaction pressure) remains constant.

established in a similar way from measurements in which the slip was constrained to occur within the sediment mass by barriers that prevented basal slip [*Lill*, 1993]. Following *Savage and Hutter*, [1989], the measured static friction angles were assumed to be good approximations of the applicable dynamic friction angles. Measurements of pore fluid pressures showed them to be hydrostatic at the time of flow release but to rise within a few seconds to near-liquefaction levels [*Iverson et al.*, 1997] and to then evolve to a state of near-zero pressure at the flow snout and near-liquefaction pressure in the flow body (Figures 5, 10, and 11). Figure 23 depicts the distribution of pore fluid pressures, relative to total basal normal stress, used in model calculations for all nodes where $\overline{v_x} > 0$. This distribution mimics, in a simplified way, measured pore pressure distributions. Pore pressures were assumed to be hydrostatic where $\overline{v_x} = 0$.

A strong tendency existed for numerical solutions to exhibit oscillatory behavior, even when the Lagrangian scheme was optimized to suppress numerical instability by including a small numerical viscosity as described by *Savage and Hutter* [1989]. The "best," or least oscillatory, solutions were obtained by using a discretization that included about 80 space nodes and a dimensionless time step size of about 0.001. For a typical flume experiment, in which the debris flow length is of the order of 10 m, this translates to a dimensional time step of about 0.001 s and space discretization of about 0.1 m. About 30,000 time steps were needed to simulate a typical flume experiment.

To facilitate comparisons with experimental data, model predictions are presented in terms of dimensional rather than normalized variables. Comparisons with data from the USGS flume experiment of July 24, 1995, are emphasized because this experiment was representative of many others but was distinguished by particularly high resolution measurements of $\overline{v_x}$ and h. The model initial conditions simulated the July 24, 1995, conditions prior to flow release: a 9.4-m^3 heap of sediment with a vertical downslope face and a gently sloping surface had a dry bulk density of 1800 kg/m^3 and was saturated with water at hydrostatic pressure.

Figure 24 illustrates the predicted evolution of the speed and shape of the debris flow surge that developed when the 9.4-m^3 mass of water-saturated sediment was released from the gate. Predictions indicate that a blunt snout quickly develops and attenuates only modestly as the debris flow advances downslope. In contrast, simulations with spatially uniform pore pressures or with no pore pressures produce a finely tapered leading edge rather than a blunt snout [cf. *Savage and Hutter*, 1989]. The snout accelerates as long as it travels on the uniformly inclined 31° slope. However, the nearly liquefied tail behind the snout elongates markedly and accelerates less rapidly than the snout. This causes the surge profile to stretch in length and attenuate in height with increasing time and travel distance, as commonly observed in experiments and in nature (see Figure 3). The simulated surge subsequently compresses as the debris flow decelerates and comes to rest on the flatter runout surface. One test of model performance involves comparison of the predicted and observed time and distance of runout. The distal limit of the experimental flow was 101 m from the flume gate, or 18.5 m across the runout surface before stopping, whereas the model predicted that the flow would stop after traveling a total distance of 91 m, or 8.5 m across the runout surface. The experimental flow required about 11 s to reach its distal limit, whereas the model predicted that 9.5 s would be required to reach the distal limit. A cause of the model's overprediction of average flow front speed and underprediction of the flow front runout is visible in videotape and photographic recordings of the experiment: as it pro-

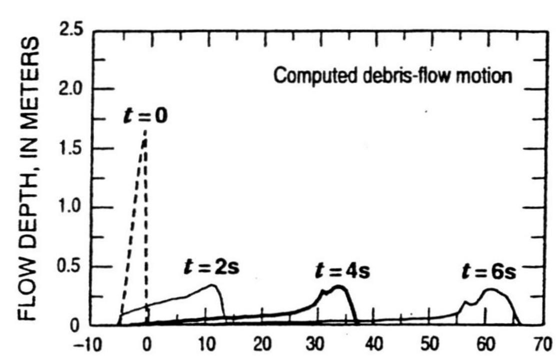

Figure 24. Predicted vertical cross-sectional profiles of the experimental debris flow of July 24, 1995. Profiles illustrate continuous acceleration and elongation of the debris flow surge during 6 s of motion down a uniform 31° slope. The profile of the static sediment heap denoted by $t = 0$ represents the initial condition. Vertical exaggeration is 20×.

gressed downslope, the flow segregated into three major surges plus several minor surges (Figure 25), whereas the model simulates one coherent surge only. Segregation into multiple surges appears to retard the average speed of the flow front but increase its ultimate runout. Depleted in size and momentum by loss of mass to the trailing surges, the flow front decelerates quickly on the runout surface. Succeeding surges overtake the decelerating front and impart momentum that pushes the front forward and delays its stoppage.

More quantitative tests of the model can be made by comparing predicted and measured graphs of flow depth as a function of time at fixed measurement cross sections. Figure 25 compares predictions with records of flow depth measured at three downstream cross sections during the flume experiment of July 24, 1995. Measurements at a cross section 2 m downslope from the release gate were made with an ultrasonic transceiver that produced data with a time resolution of about 0.1 s and depth resolution of about 0.05 m. Measurements at cross sections 33 m and 67 m downslope were made with high-precision laser triangulation systems that provided a time resolution of 0.001 s (the sampling frequency) and depth resolution of 0.001 m. Comparison of the data and model predictions show that the model predicts the speed of the advancing debris flow front very well and the overall shape of the debris flow surge reasonably well. However, it fails to predict some important details. The model underestimates the attenuation of the surge front, it overestimates the attenuation of the waveform tail, and it does not simulate breakup of the surge into multiple surges. The first two difficulties might be partially remedied by including the viscous shear term in the model, and this is a logical next step. Accurate simulation of the instability that causes a single surge to devolve into multiple surges is more difficult because it requires unambiguous distinction between numerical and physical instabilities. This will likely require a new type of analysis.

Overall, the success of the simple model that employs (85) and (94) as governing equations appears better than expected. The relatively rapid, thin debris flows in the USGS flume are characterized by moderately large Savage numbers and Bagnold numbers (Table 5), so a model that emphasizes Coulomb friction and excludes explicit treatment of grain collisions might be expected to perform poorly. However, collision-dominated flows obey a relation between shear and normal stresses that mimics the quasi-static Coulomb equation [*Savage and Hutter*, 1991]. The ratio of shear to normal stresses, rather than their absolute magnitudes, determines the value of $k_{act/pass}$ in (94), and the term containing $k_{act/pass}$ establishes the surge-like character of the flow. Therefore although Coulomb stresses lack the shear rate dependence of collisional stresses, they can mimic the effects of collisional stresses in some respects. A momentum equation as simple as (94), with appropriate accounting for viscous shear effects, might provide an adequate model for predicting bulk motion of debris flows. The model may be especially appropriate for less energetic debris flows in which shear rates are lower and grain collisions figure less prominently than in the high-speed flows at the USGS flume.

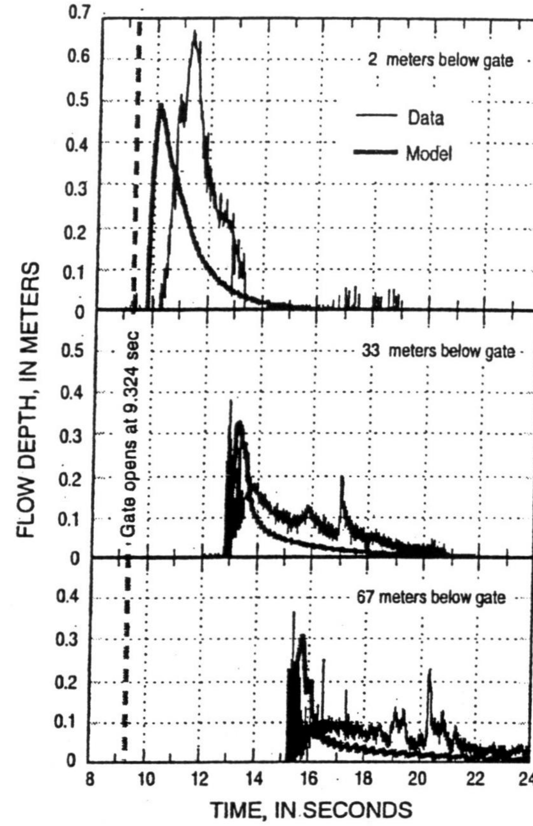

Figure 25. Comparison of measured and predicted flow depths as a function of time for the experimental debris flow of July 24, 1995. Predictions and data are shown for three cross sections, 2 m, 33 m, and 67 m downslope from the gate at the flume head. Flow commenced at the recorded time $t = 9.324$ s, and flow through all cross sections was on a uniform 31° slope.

10. CONCLUSION

Debris flows are gravity-driven surges of roughly equal volumes of water and poorly sorted sediment, thoroughly mixed and agitated. Phenomena such as fine-sediment gravity currents or wet rock avalanches can superficially resemble debris flows but lack the strong solid-fluid interactions that produce debris flows' unique attributes. Interaction of solids and fluid gives debris flows bulk mobilities (L/H) that commonly exceed those of comparably sized rock avalanches by 100%. Juxtaposition of solid and fluid forces allows debris flow materials to slide or lock frictionally as well as to flow. Most debris flows commence as landslides triggered by increased pore water pressures, and most terminate as slowly consolidating sediment deposits. Between these quasi-static stages of motion, debris flow behavior typically is influenced by inertial forces and by a combination of grain friction, grain collisions, and viscous fluid flow. Investigations of these influences indicate that traditional Bingham and Bagnold models of debris behavior should be supplanted by models that account for interactions of solid and fluid constituents.

Data from large-scale flume experiments provide clues to the character of momentum transfer in debris flows. Measured stresses at the base of debris flows change rapidly, and the relative magnitude of stress fluctuations increases as the area of the measurement surface decreases. This indicates that individual grains or groups of grains and adjacent fluid interact dynamically with the flow boundary, and probably with one another, and corroborates the visual impression that debris flows can violate no-slip boundary conditions and develop substantial grain fluctuation energy, or granular temperature. Measured basal fluid pressures, which change asynchronously relative to the basal total stresses, indicate that heads of debris flow surges generally lack much fluid pressure, whereas the finer-grained tails of surges are nearly liquefied by high fluid pressure. Interior fluid pressures remain elevated at near-liquefaction levels even during deposition, indicating that deposition results mainly from resistance at flow heads and margins.

Mixture theory provides an appropriate mathematical framework for investigating debris flows. It indicates that fluid pressures greater than hydrostatic cannot persist during steady, uniform debris motion. Instead, high fluid pressures result from debris contraction (consolidation), which must be accompanied by local reduction of granular temperature and by globally unsteady motion. This suggests that debris flow motion may be a fundamentally unsteady phenomenon. As yet, however, no comprehensive model exists to calculate the coupled, simultaneous evolution of pore pressures and granular temperatures in unsteady debris flows. Nonetheless, estimates of characteristic timescales for dissipation of excess pore fluid pressures in debris flows show that they typically exceed flow durations. Depth-averaged models of debris flow motion can therefore exploit the assumption that pore fluid pressures remain elevated for the duration of an event. A model of this type, derived by generalizing the Savage-Hutter model of dry flows of Coulomb material, predicts the behavior of experimental debris flows reasonably well.

Experimental debris flows, like many in nature, typically have included no clasts with dimensions comparable to or greater than the flow depth and have been confined to channels with simple geometries. Models based on classical continuum mechanics appear to work well for describing such flows. However, natural debris flows may encounter channels so tortuous or entrain boulders so large that continuum mechanical assumptions fail. Discrete particle models, comparable to the dry avalanche model of *Cleary and Campbell* [1993], might be required to understand debris flow behavior in such circumstances. Furthermore, the apparent sensitivity of debris flow motion to nuances in the positioning of individual boulders or flow path obstacles hints that debris flow motion may be mechanistically chaotic, at least in some instances. Deterministic prediction of some aspects of debris flow behavior may therefore prove impossible.

Future experimentation and modeling can probably illuminate at least six key aspects of debris-flow physics without resolving the possibility of chaos or adopting the methodology of discrete-particle modeling:

1. Flow regimes in which grain friction, grain collisions, and fluid viscosity dominate can in principle be discriminated on the basis of transition values of dimensionless parameters such as N_{Bag}, N_{Sav}, and N_{Dar}. Rigorous experiments, in which one parameter is systematically varied while others are held constant, should help define the transition values. Once defined, these values can guide application of simplified models of debris flows dominated by only one or two types of momentum transfer.

2. Development of physically based understanding and modeling of mass gain and loss by moving debris flows is essential for realistic predictions in many circumstances. Incorporating mass change terms in mathematical models is straightforward, but how to predict the magnitudes of mass change on the basis of boundary and flow properties remains unclear. Better understanding of erosion and sedimentation by debris flows will probably require systematic experimentation.

3. Debris flows can move as a single surge, but they commonly break into a series of surges of roughly similar magnitude. Surge fronts carry the largest percentage of large clasts and commonly form the deepest part of the flow, and formation and segregation into multiple surges therefore have great implications for hazards due to impact and inundation. Although development of surges from infinitesimal flow perturbations has been observed under various field and experimental conditions, the physics remain poorly understood. More experiments and analyses are needed.

4. Pore-fluid pressures exert a strong influence on debris flow mechanics. The influence can be modeled simplistically by including realistic pore pressure distributions in appropriately formulated hydraulic models (e.g., section 9). However, a rigorous understanding of pore pressure effects requires a fully coupled model in which pore pressures and granular temperatures evolve contemporaneously from initiation through inertial motion and subsequent deposition.

5. Grain size sorting that selectively moves the largest clasts to the surface and front of debris flow surges may play an essential role in controlling the pore pressure distribution. Sophisticated continuum models may be able to account for sorting phenomena.

6. Models and experimental tests that provide understanding of debris flows' response to three-dimen-

sional topography are necessary for hazard forecasts in many areas. Quasi-three-dimensional models that capture some elements of debris flow behavior have been developed recently by *O'Brien et al.* [1993], *Lang and Leo* [1994], and *Hungr* [1995], but further work to expand upon these models and include the effects of solid-fluid interactions is desirable.

APPENDIX A: DERIVATION OF EQUATION (46)

Conservation of linear momentum by m_2 during collision with m_1 can be expressed with good approximation by (46) if $m_1 \gg m_2$. The approximation can be derived from exact equations for momentum conservation during collision of two inelastic bodies traveling in colinear paths, which may be stated as [*Spiegel*, 1967, p. 200–201]:

$$v_0 = \frac{(m_1 - em_2)(-v_0) + m_2(1+e)v_{\mathrm{up}}(t_{\mathrm{up}})}{m_1 + m_2} \tag{A1}$$

$$v_{0\mathrm{down}} = \frac{m_1(1+e)(-v_0) + (m_2 - em_1)v_{\mathrm{up}}(t_{\mathrm{up}})}{m_1 + m_2} \tag{A2}$$

Here m_1 has velocity v_0 prior to the collision and $-v_0$ after the collision; m_2 has velocity $v_{\mathrm{up}}(t_{\mathrm{up}})$ prior to the collision and $v_{0\mathrm{down}}$ after the collision.

An effective coefficient of restitution e' for behavior of m_2 during the collision may be defined exactly as

$$e' = -\frac{v_{0\mathrm{down}}}{v_{\mathrm{up}}(t_{\mathrm{up}})} \tag{A3}$$

An exact expression for e' may be obtained by first solving (A1) for $v_{\mathrm{up}}(t_{\mathrm{up}})$, which yields

$$v_{\mathrm{up}}(t_{\mathrm{up}}) = v_0\left(\frac{2m_1}{m_2(1+e)} + \frac{1-e}{1+e}\right) \tag{A4}$$

Substituting (A4) into (A2) then yields an expression for $v_{0\mathrm{down}}$ that is linear in v_0. Then substituting both this expression for $v_{0\mathrm{down}}$ and (A4) into (A3) yields, after some manipulation,

$$e' = \frac{-2 + 2e[2 + (m_1/m_2)]}{2(m_1/m_2) + 3 - e + (1-e)(m_2/m_1)} \tag{A5}$$

This equation is exact. Simplified versions of (A5) exist for the special case wherein $m_1 = m_2$, which leads to the result

$$e' = \frac{3e - 1}{3 - e} \tag{A6}$$

and for the special case $m_1 \gg m_2$, which gives the result

$$e' \approx e \tag{A7}$$

This approximation neglects all terms in (A5) that are of the order of 1 and smaller and retains terms of the order of m_1/m_2.

TABLE A1. Values of e' Calculated From (A5) for Various Values of e and m_1/m_2

Value of m_1/m_2	*Value of* e'			
	$e = 0.1$	$e = 0.5$	$e = 0.9$	$e = 1.0$
10	0.017	0.443	0.886	1.0
100	0.091	0.494	0.899	1.0
1000	0.099	0.499	0.900	1.0

Comparison of the tabulated e' values with the associated e values shows the error of the approximation $e = e'$.

Equation (46) is obtained from (A2) by using (A7) and replacing $v_{\mathrm{up}}(t_{\mathrm{up}})$ with the equivalent expression $-v_{0\mathrm{down}}(1/e)$. The validity of the approximation can be investigated empirically by comparing values of e with those of e' calculated using (A5) (Table A1). The tabulated values indicate that the approximation error increases as values of m_1/m_2 and e decline. The error is less than 2%, however, if $m_1/m_2 > 10$ and $e > 0.9$, or if $m_1/m_2 > 1000$ and $e > 0.1$. The approximation appears useful as long as these or comparable conditions are satisfied.

APPENDIX B: EXACT SOLUTIONS FOR BEHAVIOR OF GRAIN m_2

Exact, simultaneous solution of (44a)–(44d), (45), and (46) yields

$$t_{\mathrm{up}} = -\frac{1}{B}\left(v_0\left[\frac{2e}{1+e} + (e-1)\frac{m_1}{m_2}\right] + \frac{\psi}{1+e}\right) \tag{B1}$$

$$t_{\mathrm{down}} = -\frac{1}{B}\left(v_0\left[\frac{2}{1+e} - (e-1)\frac{m_1}{m_2}\right] - \frac{\psi}{1+e}\right) \tag{B2}$$

$$v_{0\mathrm{down}} = -(m_1/m_2)ev_0 \tag{B3}$$

$$v_{0\mathrm{up}} = ev_0\left(\frac{2}{1+e} + \frac{m_1}{m_2}\right) + \frac{\psi}{1+e} \tag{B4}$$

$$s = -\frac{1}{2B}\left[\left(\frac{2v_0 - \psi}{1+e} + v_0\frac{m_1}{m_2}\right)^2 - e^2v_0^2\left(\frac{m_1}{m_2}\right)^2\right] \tag{B5}$$

$$\psi = v_0(1-e)\left(2\frac{m_2}{m_1}\frac{1+e}{1+e^2} + 2 + \frac{m_1}{m_2}(1+e)\right) \cdot \left(2\frac{m_2}{m_1}\frac{1+e}{1+e^2} + 1\right)^{-1} \tag{B6}$$

The equation for ψ, (B6), is critical because ψ appears in most of the other equations and has great physical significance. If $e = 1$, then $\psi = 0$, which implies that grain fluctuation energy lost to bed friction exactly balances the production of fluctuation energy by working of the bed shear stress. If $e < 1$, as is true for inelastic sediment grains, then $\psi > 0$, which implies that production of fluctuation energy must more than compensate

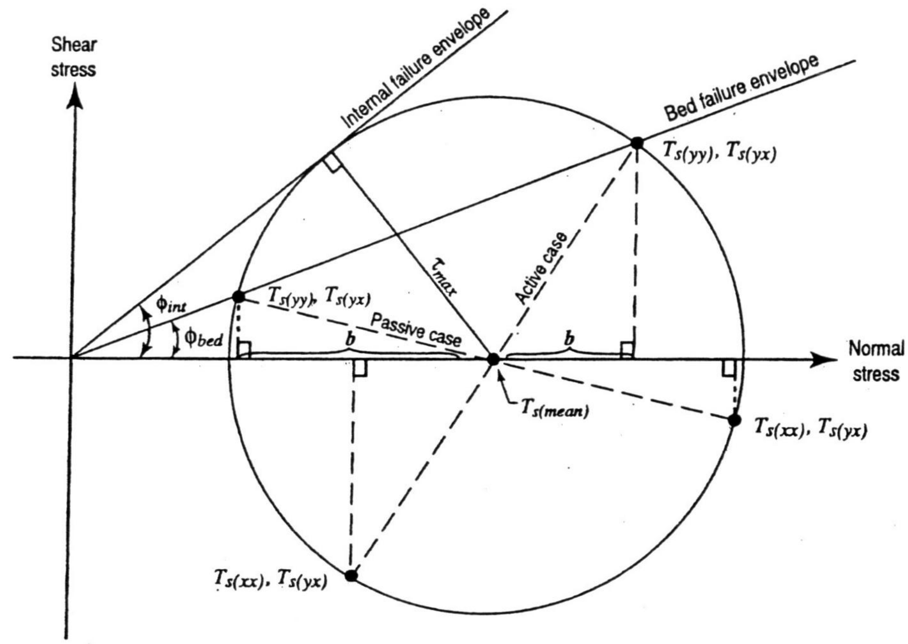

Figure C1. Mohr stress circle and Coulomb failure envelopes for a granular material that is simultaneously slipping along a bed and failing internally. The radius of the stress circle defines the maximum internal shear stress, τ_{max}.

for bed friction in order to sustain the oscillating motion of grain m_2.

APPENDIX C: DERIVATION OF EQUATION (84)

The earth pressure coefficient equation (84) can be derived with reference to the Mohr stress circle and Coulomb failure envelopes depicted in Figure C1 [cf. *Savage and Hutter*, 1989]. The diagram illustrates the state of stress in a Coulomb mass that is simultaneously sliding along the bed, where the friction angle is ϕ_{bed}, and failing internally, where the friction angle is ϕ_{int}. The basic equations necessary to obtain the expression for $k_{act/pass}$ are

$$T_{s(yx)} = T_{s(yy)} \tan \phi_{bed} \tag{C1}$$

$$\tau_{max} = T_{s(mean)} \sin \phi_{int} \tag{C2}$$

$$T_{s(mean)} + b = T_{s(yy)} \tag{C3}$$

$$b^2 + T_{s(yx)}^2 = \tau_{max}^2 \tag{C4}$$

$$k_{act/pass} = \frac{T_{s(xx)}}{T_{s(yy)}} = -1 + 2\frac{T_{s(mean)}}{T_{s(yy)}} \tag{C5}$$

Equations (C1) and (C2) state the Coulomb failure rule for bed slip and internal slip, respectively. Equations (C3) and (C4) state simple geometric relations evident in Figure C1. Like (C1) and (C2), (C3) and (C4) apply for both the active (extensional) and passive (compressional) failure states. Equation (C5) provides a useful alternative definition of $k_{act/pass}$ in terms of the mean normal stress, $T_{s(mean)} = \frac{1}{2}(T_{s(xx)} + T_{s(yy)})$. This quantity, like the quantities b and τ_{max}, is defined graphically in Figure C6. Physically, τ_{max} is the maximum shear stress attainable in the failing mass, and b is the difference between the y direction normal stress $T_{s(yy)}$ and the mean normal stress.

The initial steps in the derivation consist of substituting (C4) into (C2), substituting (C1) into the resulting equation, and then substituting (C3) into this equation. This produces the result

$$[T_{s(yy)} - T_{s(mean)}]^2 = T_{s(mean)}^2 \sin^2 \phi_{int} - T_{s(yy)}^2 \tan^2 \phi_{bed} \tag{C6}$$

Regrouping terms in this equation, using the identity $1 - \sin^2 \phi_{int} = \cos^2 \phi_{int}$, and dividing all terms by $T_{s(yy)}^2(1 + \tan^2 \phi_{bed})$ then yields

$$\frac{\cos^2 \phi_{int}}{1 + \tan^2 \phi_{bed}} \left(\frac{T_{s(mean)}}{T_{s(yy)}}\right)^2 - \frac{2}{1 + \tan^2 \phi_{bed}} \left(\frac{T_{s(mean)}}{T_{s(yy)}}\right) + 1 = 0 \tag{C7}$$

This is a quadratic equation in $T_{s(mean)}/T_{s(yy)}$, which may be solved by the standard quadratic formula, yielding

$$\frac{T_{s(mean)}}{T_{s(yy)}} = \frac{1 \mp [1 - \cos^2 \phi_{int}(1 + \tan^2 \phi_{bed})]^{1/2}}{\cos^2 \phi_{int}} \tag{C8}$$

which is obtained after some algebraic simplification. Substitution of (C8) into (C5) then yields (84). Note that this derivation and Figure C1 assume $\phi_{bed} < \phi_{int}$; otherwise, ϕ_{bed} is irrelevant because all deformation occurs internally. In the event that $\phi_{bed} > \phi_{int}$, the term involving ϕ_{bed} in (C8) and (84) can be ignored, and (84) reduces to the standard form of the Rankine equation for deforming granular media without basal sliding [e.g., *Lamb and Whitman*, 1979, p. 164].

NOTATION

a factor characterizing dependence of permeability on porosity.
A viscous relaxation rate, equal to $\upsilon_f\mu/\upsilon_s\rho_s k$, $1/T$.
b difference between y direction and mean normal stress, M/LT^2.
B buoyancy-adjusted gravity, equal to $(1 - \rho_f/\rho_s)g_y$, L/T^2.
c cohesive strength, M/LT^2.
C mixture compressibility, LT^2/M.
C_1 constant of integration, L/T.
C_2 constant of integration, L.
d total derivative operator.
D material derivative operator (following motion of solids).
D_h hydraulic diffusivity, L^2/T.
e coefficient of restitution of solid grains.
E composite mixture stiffness, equal to $1/C$, M/LT^2.
$\mathbf{f}$ solid-fluid interaction force per unit volume of mixture, M/L^2T^2.
F magnitude of instantaneous grain impulse force, ML/T^2.
F_{avg} time-averaged value of F, ML/T^2.
$\mathbf{g}$ gravitational acceleration, L/T^2.
g magnitude of $\mathbf{g}$, L/T^2.
g_y y component of $\mathbf{g}$, L/T^2.
h debris flow thickness normal to bed, L.
$\bar{h}$ characteristic value of h, L.
H vertical distance of debris flow descent from source area, L.
i subscript denoting inertial component of stress.
$\mathbf{I}$ identity tensor.
$\mathbf{j}$ conductive flux of granular temperature per unit volume, M/T^3.
k hydraulic permeability, L^2.
$k_{\text{act/pass}}$ Rankine earth pressure coefficient.
K hydraulic conductivity, L/T.
l length of head of debris flow surge, L.
$\bar{l}$ characteristic length (parallel to bed) of debris flow surge, L.
L horizontal distance of debris flow runout from source area, L.
m_s mass influx rate of solids per unit debris flow volume, M/TL^3.
m_f mass influx rate of fluid per unit debris flow volume, M/TL^3.
m_1 mass of grains overlying basal shear zone, M.
m_2 mass of grain within basal shear layer, M.
M total mass of debris flow, M.
n viscous power law coefficient.
N number of grains above slip surface.
N_{Bag} Bagnold number.
N_{Dar} Darcy number.
N_{fric} friction number.
N_{mass} mass number.
N_{Rey} grain Reynolds number.
N_{Sav} Savage number.
p pore fluid pressure, M/LT^2.
p_{bed} normalized pore fluid pressure at bed.
p_{dev} deviation of p from hydrostatic value, M/LT^2.
q subscript denoting quasi-static component of stress.
$\mathbf{q}$ Darcian specific discharge of pore fluid, L/T.
R bulk flow resistance coefficient.
s mean free path of grain motion, L.
t time, T.
t_D time duration of debris flow from initiation to deposition, T.
t_{diff} timescale for pore pressure diffusion, T.
t_{up} time of upward motion of grain m_2 between successive contacts, T.
t_{down} time of downward motion of grain m_2 between successive contacts, T.
t_{cycle} $t_{\text{up}} + t_{\text{down}}$, T.
$\mathbf{T}_s$ solid phase stress tensor, M/LT^2.
$\mathbf{T}_f$ fluid phase stress tensor, M/LT^2.
$\mathbf{T}_{s-f}$ solid-fluid interaction stress tensor, M/LT^2.
$\mathbf{T}_e$ effective stress tensor, M/LT^2.
$\mathbf{T}'$ extra stress tensor in solid-fluid mixture modeled as single phase, M/LT^2.
$\bar{T}$ depth-averaged stress component, M/LT^2.
u displacement of solid grain from initial position, L.
v velocity magnitude, L/T.
$\mathbf{v}$ mixture velocity, L/T.
$\mathbf{v}_s$ solid phase velocity, L/T.
$\mathbf{v}_f$ fluid phase velocity, L/T.
$\overline{\mathbf{v}_s}$ time-averaged mean value of $\mathbf{v}_s$, L/T.
$\mathbf{v}_s'$ fluctuation of $\mathbf{v}_s$ about its mean value, L/T.
v_y component of $\mathbf{v}_s$ normal to bed, L/T.
v_x component of $\mathbf{v}_s$ parallel to bed, L/T.
$\overline{v_x}$ depth-averaged value of v_x, L/T.
v_{set} grain settling velocity, L/T.
v_0 initial velocity of grain m_1 following contact with m_2, L/T.
v_{up} upward-bound velocity of grain m_2, L/T.
v_{down} downward-bound velocity of grain m_2, L/T.
$v_{0\text{up}}$ initial value of v_{up} following grain contact with bed, L/T.
$v_{0\text{down}}$ initial value of v_{down} following grain contact with overlying mass, L/T.
w debris flow width, L.
x coordinate directed parallel to bed, L.
x' x coordinate that translates downslope with velocity $\overline{v_x}$, L.
y coordinate directed normal to bed, L.
z vertical coordinate, L.

α mass percentage of fines in sediment mixture.
$\dot{\gamma}$ shear strain rate, $1/T$.
Γ rate of degradation of granular temperature to heat per unit volume, M/LT^3.
$\hat{\delta}$ characteristic grain diameter, L.
ϵ debris flow aspect ratio, equal to $\bar{h}/\bar{l}$.
θ slope angle.
κ sediment-water mixture compression coefficient.
λ *Bagnold*'s [1954] linear concentration of solids.
μ dynamic viscosity of pore fluid with suspended fine sediment, M/LT.
μ_w dynamic viscosity of pure water, M/LT.
ξ momentum distribution coefficient for depth-averaged flow.
ρ mass density of debris flow mixture, M/L^3.
ρ_a added-mass density of solids accelerating through fluid, M/L^3.
ρ_b mass density of body of debris flow surge, M/L^3.
ρ_f mass density of debris flow fluid constituents, M/L^3.
ρ_h mass density of head of debris flow surge, M/L^3.
ρ_s mass density of debris flow solid constituents, M/L^3.
ρ_w mass density of pure water, M/L^3.
ρ_{dry} dry (dehydrated) bulk density of debris flow mixture, M/L^3.
σ total normal compressive stress, M/LT^2.
Σ stress (generic), M/LT^2.
τ shear stress, M/LT^2.
τ_{max} maximum shear stress, M/LT^2.
T granular temperature, L^2/T^2.
υ_f volume fraction of pore fluid, (equal to porosity in saturated mixture).
υ_s volume fraction of granular solids ($\upsilon_s + \upsilon_f = 1$ in saturated mixture).
υ_{fines} volume fraction of fine grains (silt plus clay).
ϕ bulk friction angle.
ϕ_g grain friction angle.
ϕ_{bed} friction angle for sliding along bed.
ϕ_{int} friction angle for internal deformation.
ψ fluctuation velocity generated by grain interaction with bed, L/T.
∇ gradient operator, $1/L$.
$\nabla\cdot$ divergence operator, $1/L$.
∂ partial derivative operator.
$\mathcal{F}$ functional operator (generic).
0 subscript denoting reference state.
: scalar product of tensors and dyads [cf. *Bird et al.*, 1960].

ACKNOWLEDGMENTS. Rick LaHusen was instrumental in devising and implementing electronic data collection systems at the USGS debris flow flume. Jon Major collected and consolidated the data on debris flow deposits formed during flume experiments. Dave McTigue, Jon Major, Joe Walder, Mark Reid, Jim Vallance, Bill Savage, Ron Shreve, Stephen Grand, Neal Iverson, and Sue Knight provided useful critiques of the manuscript.

James A. Smith was the editor responsible for this paper. He thanks Dave McTigue, William Savage, and Ronald Shreve for their technical reviews and Steven Grand for serving as a cross-disciplinary referee.

REFERENCES

Abbott, J., L. A. Mondy, A. L. Graham, and H. Brenner, Techniques for analyzing the behavior of concentrated suspensions, in *Particulate Two-Phase Flow*, edited by M. C. Roco, pp. 3–32, Butterworth-Heinemann, Newton, Mass., 1993.

Acrivos, A., The rheology of concentrated suspensions of non-colloidal particles, in *Particulate Two-Phase Flow*, edited by M. C. Roco, pp. 169–189, Butterworth-Heinemann, Newton, Mass., 1993.

Adams, M. J., and B. J. Briscoe, Deterministic micromechanical modeling of failure or flow in discrete planes of densely packed particle assemblies: Introductory principles, in *Granular Matter*, edited by A. Mehta, pp. 259–291, Springer-Verlag, New York, 1994.

Anderson, K. G., and R. Jackson, A comparison of some proposed equations of motion of granular materials for fully developed flow down inclined planes, *J. Fluid Mech.*, *241*, 145–168, 1992.

Anderson, S. A., and N. Sitar, Analysis of rainfall-induced debris flows, *J. Geotech. Eng.*, *121*, 544–552, 1995.

Arattano, M., and W. Z. Savage, Modelling debris flows as kinematic waves, *Bull. Int. Assoc. Eng. Geol.*, *49*, 3–13, 1994.

Atkin, R. J., and R. E. Craine, Continuum theories of mixtures: Basic theory and historical development, *Q. J. Mech. Appl. Math., Part 2*, *29*, 209–244, 1976.

Bagnold, R. A., Experiments on a gravity-free dispersion of large solid spheres in a Newtonian fluid under shear, *Proc. R. Soc. London, Ser. A*, *225*, 49–63, 1954.

Batchelor, G. K., and J. T. Green, The determination of the bulk stress in a suspension of spherical particles to order c^2, *J. Fluid Mech.*, *56*, 401–427, 1972.

Bear, J., *Dynamics of Fluids in Porous Media*, 764 pp., Dover, Mineola, N. Y., 1972.

Been, K., and G. C. Sills, Self-weight consolidation of soft soils: An experimental and theoretical study, *Geotechnique*, *31*, 519–535, 1981.

Beverage, J. P., and J. K. Culbertson, Hyperconcentrations of suspended sediment, *J. Hydraul. Div. Am. Soc. Civ. Eng.*, *90*(HY6), 117–128, 1964.

Biot, M. A., General theory of three-dimensional consolidation, *J. Appl. Phys.*, *12*, 155–164, 1941.

Bird, R. B., W. E. Stewart, and E. N. Lightfoot, *Transport Phenomena*, 780 pp., John Wiley, New York, 1960.

Bird, R. B., G. C. Dai, and B. J. Yaruso, The rheology and flow of viscoplastic materials, *Rev. Chem. Eng.*, *1*, 1–70, 1982.

Bishop, A. W., The stability of tips and spoil heaps, *Q. J. Eng. Geol.*, *6*, 335–376, 1973.

Blake, G. R., Bulk density, in *Methods of Soil Analysis*, edited by C. A. Black et al., pp. 374–390, Am. Soc. of Agron., Madison, Wis., 1965.

Bridgman, P. W., *Dimensional Analysis*, Yale Univ. Press, New Haven, Conn., 1922.

Bridgwater, J., M. H. Cooke, and A. M. Scott, Inter-particle percolation: Equipment development and mean percolation velocities, *Trans. Inst. Chem. Eng.*, *56*, 157–167, 1978.

Bromhead, E. N., *The Stability of Slopes*, 374 pp., Chapman and Hall, New York, 1986.

Buckingham, E., Model experiments and the form of empirical equations, *Trans. ASME*, *37*, 263, 1915.

Campbell, C. S., Rapid granular flows, *Annu. Rev. Fluid Mech.*, *22*, 57–92, 1990.

Cannon, S. H., and W. Z. Savage, A mass-change model for the estimation of debris-flow runout, *J. Geol.*, *96*, 221–227, 1988.

Caruso, P., and M. T. Pareschi, Estimation of lahar and lahar-runout flow hydrograph on natural beds, *Environ. Geol.*, *22*, 141–152, 1993.

Casagrande, A., Liquefaction and cyclic deformation of sands—A critical review, *Harvard Soil Mech. Ser.*, *88*, 51 pp., 1976.

Chandler, R. N., and D. L. Johnson, The equivalence of quasi-static flow in fluid-saturated porous media and Biot's slow wave in the limit of zero frequency, *J. Appl. Phys.*, *52*, 3391–3395, 1981.

Chapman, S., and T. G. Cowling, *Mathematical Theory of Nonuniform Gases*, 3rd ed., 423 pp., Cambridge Univ. Press, New York, 1970.

Chen, C., Comprehensive review of debris flow modeling concepts in Japan, in *Debris Flows/Avalanches: Process, Recognition, and Mitigation, Rev. Eng. Geol.*, vol. 7, edited by J. E. Costa and G. F. Wieczorek, pp. 13–29, Geol. Soc. of Am., Boulder, Colo., 1987.

Chen, C., Generalized viscoplastic modeling of debris flow, *J. Hydraul. Eng.*, *114*, 237–258, 1988a.

Chen, C., General solutions for viscoplastic debris flow, *J. Hydraul. Eng.*, *114*, 259–282, 1988b.

Cleary, P. W., and C. S. Campbell, Self-lubrication by long runout landslides: Examination by computer simulation, *J. Geophys. Res.*, *98*(B12), 21,911–21,924, 1993.

Coleman, P. F., A new explanation for debris flow surge phenomena (abstract), *Eos Trans. AGU*, *74*(16), Spring Meet. Suppl., 154, 1993.

Costa, J. E., Physical geomorphology of debris flows, in *Developments and Applications of Geomorphology*, edited by J. E. Costa and P. J. Fleisher, pp. 268–317, Springer-Verlag, New York, 1984.

Costa, J. E., and G. F. Wieczorek (Eds.), *Debris Flows/Avalanches: Process, Recognition, and Mitigation, Rev. Eng. Geol.*, vol. 7, 239 pp., Geol. Soc. of Am., Boulder, Colo., 1987.

Costa, J. E., and G. P. Williams, Debris-flow dynamics (videotape), *U.S. Geol. Surv. Open File Rep.*, *84-606*, 22 min., 1984.

Coussot, P., Structural similarity and transition from Newtonian to non-Newtonian behavior for clay-water suspensions, *Phys. Rev. Lett.*, *74*, 3971–3974, 1995.

Coussot, P., and J.-M. Piau, On the behavior of fine mud suspensions, *Rheol. Acta*, *33*, 175–184, 1994.

Coussot, P., and J.-M. Piau, The effects of an addition of force-free particles on the rheological properties of fine suspensions, *Can. Geotech. J.*, *32*, 263–270, 1995.

Coussot, P., and S. Proust, Slow unconfined spreading of a mudflow, *J. Geophys. Res.*, *101*(B11), 25,217–25,229, 1996.

Daido, A., On the occurrence of mud-debris flow, *Bull. Disaster Prev. Res. Inst. Kyoto Univ.*, *Part 2*, *21*(187), 109–135, 1971.

Davies, T. R. H., Spreading of rock avalanche debris by mechanical fluidization, *Rock Mech.*, *15*, 9–24, 1982.

Davies, T. R. H., Large debris flows: A macroviscous phenomenon, *Acta Mech.*, *63*, 161–178, 1986.

Davies, T. R. H., Debris-flow surges—A laboratory investigation, *Mitt. 96*, 122 pp., Versuchsanst. für Wasserbau, Hydrologie und Glaziologie, Zürich, Switzerland, 1988.

Davies, T. R. H., Debris-flow surges—Experimental simulation, *N. Z. J. Hydrol.*, *29*, 18–46, 1990.

DiFelice, R., The voidage function for fluid-particle interaction systems, *Int. J. Multiphase Flow*, *20*, 153–159, 1994.

Drake, T. G., Structural features in granular flows, *J. Geophys. Res.*, *95*(B6), 8681–8696, 1990.

Eckersley, D., Instrumented laboratory flowslides, *Geotechnique*, *40*, 489–502, 1990.

Einstein, A., A new determination of molecular dimensions (in German), *Ann. Phys.*, *19*, 289–306, 1906. (English translation by A. D. Cowper in *Investigations on the Theory of Brownian Movement*, edited by R. Furth, pp. 38–62, Dover, Mineola, N. Y., 1956.)

Ellen, S. D., and R. W. Fleming, Mobilization of debris flows from soil slips, San Francisco Bay region, California, in *Debris Flows/Avalanches: Process, Recognition, and Mitigation, Rev. Eng. Geol.*, vol. 7, edited by J. E. Costa and G. F. Wieczorek, pp. 31–40, Geol. Soc. of Am., Boulder, Colo., 1987.

Erlichson, H., A mass-change model for the estimation of debris-flow runout, A second discussion: Conditions for the application of the rocket equation, *J. Geol.*, *99*, 633–634, 1991.

Fairchild, L. H., and M. Wigmosta, Dynamic and volumetric characteristics of the 18 May 1980 lahars on the Toutle River, Washington, in *Proceedings of the Symposium on Erosion Control in Volcanic Areas Tech. Mem. 1908*, pp. 131–153, Jpn. Public Works Res. Inst., Min. of Constr., Tokyo, 1983.

Fink, J. H., M. C. Malin, R. E. D'Alli, and R. Greeley, Rheological properties of mudflows associated with the spring 1980 eruptions of Mount St. Helens volcano, Washington, *Geophys. Res. Lett.*, *8*, 43–46, 1981.

Frankel, N. A., and A. Acrivos, On the viscosity of a concentrated suspension of solid spheres, *Chem. Eng. Sci.*, *22*, 847–853, 1967.

Garcia-Aragon, J. A., Granular-fluid chute flow: Experimental and numerical observations, *J. Hydraul. Eng.*, *121*, 355–364, 1995.

Gibson, R. E., G. L. England, and M. J. L. Hussey, The theory of one-dimensional consolidation of saturated clays, 1, Finite nonlinear consolidation of thin homogeneous layers, *Geotechnique*, *17*, 261–273, 1967.

Haff, P. K., Grain flow as a fluid-mechanical phenomenon, *J. Fluid Mech.*, *134*, 401–430, 1983.

Haff, P. K., A physical picture of kinetic granular fluids, *J. Rheol.*, *30*, 931–948, 1986.

Hampton, M. A., Buoyancy in debris flows, *J. Sediment. Petrol.*, *49*, 753–758, 1979.

Hampton, M. A., H. J. Lee, and J. Locat, Submarine landslides, *Rev. Geophys.*, *34*, 33–59, 1996.

Hanes, D. M., and D. L. Inman, Experimental evaluation of a dynamic yield criterion for granular fluid flows, *J. Geophys. Res.*, *90*(B5), 3670–3674, 1985.

Hayashi, J. N., and S. Self, A comparison of pyroclastic flow and debris avalanche mobility, *J. Geophys. Res.*, *97*(B6), 9063–9071, 1992.

Heim, A., *Bergsturz und Menschenleben*, 218 pp., Fretz und Wasmuth, Zürich, Switzerland, 1932.

Helm, D. C., Conceptual aspects of subsidence due to fluid withdrawal, in *Recent Trends in Hydrogeology*, edited by T. N. Narasimhan, *Spec. Pap. Geol. Soc. Am.*, *189*, 103–139, 1982.

Henderson, F. M., *Open Channel Flow*, 522 pp., Macmillan, New York, 1966.

Hill, H. M., Bed forms due to a fluid stream, *J. Hydraul. Div. Am. Soc. Civ. Eng.*, *92*, 127–143, 1966.

Hooke, R. L., Mass movement in semi-arid environments and the morphology of alluvial fans, in *Slope Stability—Geotechnical Engineering and Geomorphology*, edited by M. G. Anderson and K. S. Richards, pp. 505–529, John Wiley, New York, 1987.

Hopkins, M. A., J. T. Jenkins, and M. Y. Louge, On the structure of three-dimensional shear flows, *Mech. Mater.*, *16*, 179–187, 1993.

Howard, T. R., J. E. Baldwin II, and H. F. Donley, Landslides in Pacifica, California, caused by the storm, in *Landslides, Floods and Marine Effects of the Storm of January 3–5, 1982, in the San Francisco Bay Region, California*, edited by S. D. Ellen and G. F. Wieczorek, *U.S. Geol. Surv. Prof. Pap., 1434*, 163–184, 1988.

Hsu, K. J., Catastrophic debris streams (sturzstroms) generated by rockfalls, *Geol. Soc. Am. Bull., 86*, 129–140, 1975.

Hui, K., and P. K. Haff, Kinetic grain flow in a vertical channel, *Int. J. Multiphase Flow., 12*, 289–298, 1986.

Hungr, O., A mass-change model for the estimation of debris-flow runout: A discussion, *J. Geol., 98*, 791, 1990.

Hungr, O., A model for the runout analysis of rapid flow slides, debris flows, and avalanches, *Can. Geotech. J., 32*, 610–623, 1995.

Hungr, O., and N. R. Morgenstern, High velocity ring shear tests on sand, *Geotechnique, 34*, 415–421, 1984.

Hunt, B., Newtonian fluid mechanics treatment of debris flows and avalanches, *J. Hydraul. Eng., 120*, 1350–1363, 1994.

Hutchinson, J. N., A sliding-consolidation model for flow slides, *Can. Geotech. J., 23*, 115–126, 1986.

Hutter, K., B. Svendsen, and D. Rickenmann, Debris-flow modeling: A review, *Continuum Mech. Thermodyn., 8*, 1–35, 1996.

Innes, J. L., Debris flows, *Prog. Phys. Geogr., 7*, 469–501, 1983.

Iverson, R. M., A constitutive equation for mass-movement behavior, *J. Geol., 93*, 143–160, 1985.

Iverson, R. M., Unsteady, nonuniform landslide motion, 1, Theoretical dynamics and the steady datum state, *J. Geol., 94*, 1–15, 1986a.

Iverson, R. M., Unsteady, nonuniform landslide motion, 2, Linearized theory and the kinematics of transient response, *J. Geol., 94*, 349–364, 1986b.

Iverson, R. M., Groundwater flow fields in infinite slopes, *Geotechnique, 40*, 139–143, 1990.

Iverson, R. M., Sensitivity of stability analyses to groundwater data, in *Landslides (Proceedings of the Sixth International Symposium on Landslides, 1)*, edited by D. H. Bell, pp. 451–457, A. A. Balkema, Rotterdam, Netherlands, 1992.

Iverson, R. M., Differential equations governing slip-induced pore-pressure fluctuations in a water-saturated granular medium, *Math. Geol., 23*, 1027–1048, 1993.

Iverson, R. M., Hydraulic modeling of unsteady debris-flow surges with solid-fluid interactions, in *Proceedings of the First International Conference on Debris-Flow Hazards Mitigation*, Am. Soc. of Civ. Eng., New York, in press, 1997.

Iverson, R. M., and R. P. Denlinger, The physics of debris flows—A conceptual assessment, in *Erosion and Sedimentation in the Pacific Rim*, edited by R. L. Beschta et al., *IAHS Publ., 165*, 155–165, 1987.

Iverson, R. M., and R. G. LaHusen, Dynamic pore-pressure fluctuations in rapidly shearing granular materials, *Science, 246*, 769–799, 1989.

Iverson, R. M., and R. G. LaHusen, Friction in debris flows: Inferences from large-scale flume experiments, *Hydraulic Engineering '93 (Proceedings of the 1993 Conference of the Hydraulics Division of the American Society of Civil Engineers)*, vol. 2, 1604–1609, Am. Soc. of Civ. Eng., New York, 1993.

Iverson, R. M., and J. J. Major, Groundwater seepage vectors and the potential for hillslope failure and debris flow mobilization, *Water Resour. Res., 22*, 1543–1548, 1986.

Iverson, R. M., and M. E. Reid, Gravity-driven groundwater flow and slope failure potential, 1, Elastic effective-stress model, *Water Resour. Res., 28*, 925–938, 1992.

Iverson, R. M., J. E. Costa, and R. G. LaHusen, Debris-flow flume at H. J. Andrews Experimental Forest, Oregon, *U.S. Geol. Surv. Open File Rep., 92-483*, 2 pp., 1992.

Iverson, R. M., M. E. Reid, and R. G. LaHusen, Debris-flow mobilization from landslides, *Ann. Rev. Earth Planet. Sci., 25*, 85–138, 1997.

Jaeger, H. M., and S. R. Nagel, Physics of the granular state, *Science, 255*, 1523–1531, 1992.

Jahns, R. H., Desert floods, *Contrib. 499*, pp. 10–15, Calif. Inst. of Technol., Pasadena, 1949.

Jenkins, J. T., Rapid granular flow down inclines, *Appl. Mech. Rev., Part 2, 47*(6), S240–S244, 1994.

Jenkins, J. T., and E. Askari, Hydraulic theory for a debris flow supported by a collisional shear layer, *Proceedings of the International Association for Hydraulic Research International Workshop on Floods and Inundations Related to Large Earth Movements, Trent, Italy, 1994*, A6.1–A6.10, Int. Assoc. for Hydraul. Res., Delft, Netherlands, 1994.

Jenkins, J. T., and D. F. McTigue, Transport processes in concentrated suspensions: The role of particle fluctuations, in *Two Phase Flows and Waves*, edited by D. D. Joseph and D. G. Schaeffer, pp. 70–79, Springer-Verlag, New York, 1990.

Jenkins, J. T., and S. B. Savage, A theory for the rapid flow of identical, smooth, nearly elastic particles, *J. Fluid Mech., 130*, 187–202, 1983.

Johnson, A. M., A model for debris flow, Ph.D. dissertation, Pa. State Univ., State College, 1965.

Johnson, A. M., *Physical Processes in Geology*, 557 pp., W. H. Freeman, New York, 1970.

Johnson, A. M., Debris flow, in *Slope Instability*, edited by D. Brunsden and D. B. Prior, pp. 257–361, John Wiley, New York, 1984.

Johnson, G., M. Massoudi, and K. R. Rajagopal, A review of interaction mechanisms in fluid-solid flows, *Tech. Rep. DOE/PETC/TR-90/9*, U.S. Dep. of Energy, 54 pp., Pittsburgh Energy Technol. Cent., Pittsburgh, Pa., 1990.

Johnson, G., M. Massoudi, and K. R. Rajagopal, Flow of a solid-fluid mixture between flat plates, *Chem. Eng. Sci., 46*, 1713–1723, 1991.

Khegai, A. Y., N. V. Popov, P. A. Plekhanov, and V. A. Keremkulov, Experiments at the Chemolgan debris-flow testing ground, Kazakhstan, *Landslide News, 6*, 27–28, Jpn. Landslide Soc., Kyoto, 1992.

Kytomaa, H. K., and C. M. Atkinson, Sound propagation in suspensions and acoustic imaging of their microstructure, *Mech. Mater., 16*, 189–197, 1993.

Lambe, T. W., and R. V. Whitman, *Soil Mechanics, SI Version*, 553 pp., John Wiley, New York, 1979.

Lang, R. M., and B. R. Leo, Model for avalanches in three spatial dimensions, *CRREL Rep. 94-5*, 23 pp., U.S. Army Corps of Eng. Cold Reg. Res. and Eng. Lab., Hanover, N. H., 1994.

Lee, J., S. C. Cowin, and J. S. Templeton III, An experimental study of the kinematics of flow through hoppers, *Trans. Soc. Rheol., 18*, 247–269, 1974.

Li, J., and J. Yuan, The main features of the mudflows in Jiang-Jia Ravine, *Z. Geomorphol., 27*, 326–341, 1983.

Li, T., A model for predicting the extent of a major rockfall, *Z. Geomorphol., 27*, 473–482, 1983.

Li, V. C., Estimation of in-situ hydraulic diffusivity of rock masses, *Pure Appl. Geophys., 122*, 545–559, 1985.

Lighthill, M. J., and G. B. Whitham, On kinematic waves, 1, Flood movement in long rivers, *Proc. R. Soc. London, Ser. A, 229*, 281–316, 1955.

Lill, T., A critical evaluation of a new method for determining the angle of internal friction for cohesionless sediments, B.S. thesis, 37 pp., Beloit Coll., Beloit, Wis., 1993.

Lun, C. K., S. B. Savage, D. J. Jeffrey, and N. Chepurny, Kinetic theories for granular flow: Inelastic particles in Couette flow and slightly inelastic particles in a general flow field, *J. Fluid Mech., 140*, 223–256, 1984.

Macedonio, G., and M. T. Pareschi, Numerical simulation of some lahars from Mount St. Helens, *J. Volcanol. Geotherm. Res.*, *54*, 65–80, 1992.

Major, J. J., Experimental studies of deposition by debris flows: Process, characteristics of deposits and effects of pore-fluid pressure, 341 pp., Ph.D. dissertation, Univ. of Wash., Seattle, 1996.

Major, J. J., Depositional processes in large-scale debris-flow experiments, *J. Geol.*, *105*, 345–366, 1997.

Major, J. J., and T. C. Pierson, Debris flow rheology: Experimental analysis of fine-grained slurries, *Water Resour. Res.*, *28*, 841–857, 1992.

Major, J. J., and B. Voight, Sedimentology and clast orientations of the 18 May 1980 southwest-flank lahars, Mount St. Helens, Washington, *J. Sediment. Petrol.*, *56*, 691–705, 1986.

Malekzadeh, M. J., Flow of liquid-solid mixtures down inclined chutes, Ph.D. thesis, 212 pp., McGill Univ., Montreal, Que., Canada, 1993.

McTigue, D. F., and J. T. Jenkins, Channel flow of a concentrated suspension, in *Advances in Micromechanics of Granular Materials*, edited by H. H. Shen, pp. 381–390, Elsevier, New York, 1992.

Middleton, G., Experimental studies related to the problem of flysch sedimentation, *Geol. Assoc. Can. Spec. Pap.*, *7*, 253–272, 1970.

Mitchell, J. K., *Fundamentals of Soil Behavior*, 422 pp., John Wiley, New York, 1976.

Miyamoto, K., and S. Egashira, Mud and debris flows, *J. Hydrosci. Hydraul. Eng. Jpn. Soc. Civ. Eng.*, *SI-2*, 1–19, 1993.

Mohrig, D., G. Parker, and K. X. Whipple, Hydroplaning of subaqueous debris flows (abstract), *Eos Trans. AGU*, *76*(46), Fall Meet. Suppl., F277, 1995.

Morton, D. M., and R. H. Campbell, Spring mudflows at Wrightwood, southern California, *Q. J. Eng. Geol.*, *7*, 377–384, 1974.

O'Brien, J. S., and P. Y. Julien, Laboratory analysis of mudflow properties, *J. Hydraul. Eng.*, *114*, 877–887, 1988.

O'Brien, J. S., P. Y. Julien, and W. T. Fullerton, Two-dimensional water flood and mudflow simulation, *J. Hydraul. Eng.*, *119*, 244–261, 1993.

Ogata, A., Theory of dispersion in a granular medium, *U.S. Geol. Surv. Prof. Pap.*, *411-I*, 34 pp., 1970.

Ogawa, S., Multitemperature theory of granular materials, in *Proceedings of the U.S.-Japan Seminar on Continuum-Mechanics and Statistical Approaches to the Mechanics of Granular Materials*, pp. 208–217, Gukujutsu Bunken Fukyukai, Tokyo, 1978.

Ohsumi Works Office, *Debris Flow at Sakurajima*, *2*, 81 pp., Jpn. Min. of Constr., Kagoshima, 1995.

Okuda, S., H. Suwa, K. Okunishi, K. Yokoyama, and M. Nakano, Observations on the motion of a debris flow and its geomorphological effects, *Z. Geomorphol.*, suppl. 35, 142–163, 1980.

Onada, G. Y., and E. G. Liniger, Random loose packings and the dilatancy onset, *Phys. Rev. Lett.*, *64*, 2727–2730, 1990.

Passman, S. L., and D. F. McTigue, A new approach to the effective stress principle, in *Compressibility Phenomena in Subsidence*, edited by S. K. Saxena, pp. 79–91, Eng. Found., New York, 1986.

Phillips, C. J., and T. R. H. Davies, Determining rheological properties of debris flow material, *Geomorphology*, *4*, 101–110, 1991.

Pierson, T. C., Erosion and deposition by debris flows at Mt. Thomas, North Canterbury, New Zealand, *Earth Surf. Processes*, *5*, 227–247, 1980.

Pierson, T. C., Dominant particle support mechanisms in debris flows at Mt. Thomas, New Zealand, and implications for flow mobility, *Sedimentology*, *28*, 49–60, 1981.

Pierson, T. C., Initiation and flow behavior of the 1980 Pine Creek and Muddy river lahars, Mount St. Helens, Washington, *Geol. Soc. Am. Bull.*, *96*, 1056–1069, 1985.

Pierson, T. C., Flow behavior of channelized debris flows, Mount St. Helens, Washington, in *Hillslope Processes*, edited by A. D. Abrahams, pp. 269–296, Allen and Unwin, Winchester, Mass., 1986.

Pierson, T. C., Flow characteristics of large eruption-triggered debris flows at snow-clad volcanoes: Constraints for debris-flow models, *J. Volcanol. Geotherm. Res.*, *66*, 283–294, 1995.

Pierson, T. C., and J. E. Costa, A rheologic classification of subaerial sediment-water flows, in *Debris Flows/Avalanches: Process, Recognition, and Mitigation*, *Rev. Eng. Geol.*, vol. 7, edited by J. E. Costa and G. F. Wieczorek, pp. 1–12, Geol. Soc. of Am., Boulder, Colo., 1987.

Pierson, T. C., and K. M. Scott, Downstream dilution of a lahar: Transition from debris flow to hyperconcentrated streamflow, *Water Resour. Res.*, *21*, 1511–1524, 1985.

Pierson, T. C., R. J. Janda, J. C. Thouret, and C. A. Borrero, Perturbation and melting of snow and ice by the 13 November 1985 eruption of Nevado del Ruiz, Colombia, and consequent mobilization, flow, and deposition of lahars, *J. Volcanol. Geotherm. Res.*, *41*, 17–66, 1990.

Plafker, G., and G. E. Ericksen, Nevado Huascaran avalanches, Peru, in *Rockslides and Avalanches*, vol. 1, *Natural Phenomena*, edited by B. Voight, pp. 277–314, Elsevier, New York, 1978.

Poletto, M., and D. D. Joseph, Effective density and viscosity of a suspension, *J. Rheol.*, *39*, 323–343, 1995.

Prior, D. B., and J. M. Coleman, Submarine Slope Instability, in *Slope Instability*, edited by D. Brunsden and D. B. Prior, pp. 419–455, John Wiley, New York, 1984.

Rankine, W. J. M., On the stability of loose earth, *Philos. Trans. R. Soc. London*, 1857.

Reid, M. E., and R. M. Iverson, Gravity-driven groundwater flow and slope failure potential, 2, Effects of slope morphology, material properties, and hydraulic heterogeneity, *Water Resour. Res.*, *22*, 939–950, 1992.

Rice, J. R., and M. P. Cleary, Some basic stress diffusion solutions for fluid-saturated elastic porous media with compressible constituents, *Rev. Geophys.*, *14*, 227–241, 1976.

Rodine, J. D., and A. M. Johnson, The ability of debris heavily freighted with coarse clastic materials to flow on gentle slopes, *Sedimentology*, *23*, 213–224, 1976.

Roeloffs, E., Poroelastic techniques in the study of earthquake-induced hydrologic phenomena, *Adv. Geophys.*, *37*, 133–195, 1996.

Rogers, C. D. F., T. A. Dijkstra, and I. J. Smalley, Particle packing from an Earth science viewpoint, *Earth Science Reviews*, *36*, 59–92, 1994.

Rosato, A., K. J. Strandburg, F. Prinz, and R. H. Swendsen, Why the Brazil nuts are on top: Size segregation of particulate matter by shaking, *Phys. Rev. Lett.*, *25*, 1038–1040, 1987.

Sabo Publicity Center, Debris flow at Sakurajima Volcano, videotape with audio in English, Ohsumi Work Off., Kyushu Reg. Constr. Bur., Jpn. Min. of Constr., Kagoshima, 1988.

Sassa, K., The mechanism starting liquefied landslides and debris flows, in *Proceedings of the Fourth International Symposium on Landslides*, vol. 2, pp. 349–354, Int. Soc. for Soil Mech. and Found. Eng., Toronto, Ont., Canada, 1984.

Sassa, K., The mechanism of debris flow, in *Proceedings of the Eleventh International Conference on Soil Mechanics and Foundation Engineering*, pp. 1173–1176, A. A. Balkema, Rotterdam, Netherlands, 1985.

Savage, S. B., The mechanics of rapid granular flows, *Adv. Appl. Mech.*, *24*, 289–366, 1984.

Savage, S. B., Interparticle percolation and segregation in granular materials: A review, in *Developments in Engineering Mechanics*, edited by A. P. S. Selvadurai, pp. 347–363, Elsevier, New York, 1987.

Savage, S. B., Mechanics of debris flows, in *Hydraulic Engineering '93 (Proceedings of the 1993 Conference of the Hydraulics Division of the American Society of Civil Engineers)*, vol. 2, 1402–1407, Am. Soc. of Civ. Eng., New York, 1993.

Savage, S. B., and K. Hutter, The motion of a finite mass of granular material down a rough incline, *J. Fluid Mech.*, *199*, 177–215, 1989.

Savage, S. B., and K. Hutter, The dynamics of avalanches of granular materials from initiation to runout, I, Analysis, *Acta Mech.*, *86*, 201–223, 1991.

Savage, S. B., and S. McKeown, Shear stresses developed during rapid shear of dense concentrations of large spherical particles between concentric cylinders, *J. Fluid Mech.*, *127*, 453–472, 1983.

Savage, S. B., and M. Sayed, Stresses developed in dry cohesionless granular materials sheared in an annular shear cell, *J. Fluid Mech.*, *142*, 391–430, 1984.

Savage, W. Z., and W. K. Smith, A model for the plastic flow of landslides, *U.S. Geological Survey Prof. Pap.*, *1385*, 32 pp., 1986.

Scheidegger, A. E., On the prediction of the reach and velocity of catastrophic landslides, *Rock Mech.*, *5*, 231–236, 1973.

Scott, K. M., J. W. Vallance, and P. T. Pringle, Sedimentology, behavior, and hazards of debris flows at Mount Rainier, Washington, *U.S. Geol. Surv. Prof. Pap.*, *1547*, 56 pp., 1995.

Sharp, R. P., and L. H. Nobles, Mudflow of 1941 at Wrightwood, southern California, *Geol. Soc. Am. Bull.*, *64*, 547–560, 1953.

Shen, H., and N. L. Ackerman, Constitutive relationships for solid-fluid mixtures, *J. Eng. Mech. Div. Am. Soc. Civ. Eng.*, *108*, 748–763, 1982.

Shibata, M., and C. C. Mei, Slow parallel flows of a water-granule mixture under gravity, I, Continuum modeling, *Acta Mech.*, *63*, 179–193, 1986a.

Shibata, M., and C. C. Mei, Slow parallel flows of a water-granule mixture under gravity, II, Examples of free surface and channel flows, *Acta Mech.*, *63*, 195–216, 1986b.

Shieh, C.-L., Jan, C.-D., and Y.-F. Tsai, A numerical simulation of debris flow and its application, *Nat. Hazards*, *13*, 39–54, 1996.

Shlemon, R. J., R. H. Wright, and D. R. Montgomery, Anatomy of a debris flow, Pacifica, California, in *Debris Flows/Avalanches: Process, Recognition, and Mitigation, Rev. Eng. Geol.*, vol. 7, edited by J. E. Costa and G. F. Wieczorek, pp. 181–200, Geol. Soc. of Am., Boulder, Colo., 1987.

Siebert, L., Large volcanic debris avalanches; Characteristics of source areas, deposits, and associated eruptions, *J. Volcanol. Geotherm. Res.*, *22*, 163–197, 1984.

Sitar, N., S. A. Anderson, and K. A. Johnson, Conditions for initiation of rainfall-induced debris flows, in *Stability and Performance of Slopes and Embankments II Proceedings*, pp. 834–849 Geotech. Eng. Div., Am. Soc. of Civ. Eng., New York, 1992.

Skempton, A. W., Long-term stability of clay slopes, *Geotechnique*, *14*, 75–101, 1964.

Skempton, A. W., Residual strength of clays in landslides, folded strata and the laboratory, *Geotechnique*, *35*, 3–18, 1985.

Spiegel, M. R., *Theoretical Mechanics, Schaum's Outline Series*, 368 pp., McGraw-Hill, New York, 1967.

Suwa, H., Focusing mechanism of large boulders to a debris-flow front, *Trans. Jpn. Geomorphol. Union*, *9*, 151–178, 1988.

Takahashi, T., Mechanical characteristics of debris flow, *J. Hydraul. Div. Am. Soc. Civ. Eng.*, *104*, 1153–1169, 1978.

Takahashi, T., Debris flow on prismatic open channel, *J. Hydraul. Div. Am. Soc. Civ. Eng.*, *106*, 381–396, 1980.

Takahashi, T., Debris flow, *Annu. Rev. Fluid Mech.*, *13*, 57–77, 1981.

Takahashi, T., *Debris Flow*, 165 pp., A. A. Balkema, Brookfield, Vt., 1991.

Takahashi, T. (Ed.), Japan-China joint research on the prevention from debris flow hazards, *Res. Rep. 03044085*, 195 pp., Grant-in-Aid for Scientific Research, Jpn. Min. of Educ. Sci. and Cult. Int. Sci. Res. Program, Tokyo, 1994.

Terzaghi, K., Stress conditions for the failure of concrete and rock, *Proc. Am. Soc. Test. Mater.*, *45*, 777–801, 1945.

Thomas, D. G., Transport characteristics of suspension, VII, A note on the viscosity of Newtonian suspensions of uniform spherical particles, *J. Colloid Sci.*, *20*, 267–277, 1965.

U.S. Geological Survey (USGS), Debris flow hazards in the San Francisco Bay region, *U.S. Geol. Surv. Fact Sheet*, *112-95*, 4 pp., 1995.

Vaid, Y. P., and J. Thomas, Liquefaction and postliquefaction behavior of sand, *J. Geotech. Eng.*, *121*, 163–173, 1995.

Vallance, J. W., Experimental and field studies related to the behavior of granular mass flows and the characteristics of their deposits, Ph.D. dissertation, 197 pp., Mich. Technol. Univ., Houghton, 1994.

Vallance, J. W., and K. M. Scott, The Osceola mudflow from Mount Rainier: Sedimentology and hazard implications of a huge clay-rich debris flow, *Geol. Soc. Am. Bull.*, *109*(2), 143–163, 1997.

Vanoni, V. A. (Ed.), *Sedimentation Engineering*, 745 pp., Am. Soc. of Civ. Eng., New York, 1975.

Varnes, D. J., Slope movement types and processes, in *Landslides—Analysis and Control*, edited by R. L. Schuster and R. J. Krizek, *Spec. Rep. Natl. Res. Counc. Transp. Res. Board*, *176*, pp. 11–33, Natl. Acad. of Sci., Washington, D. C., 1978.

Vignaux, M., and G. J. Weir, A general model for Mt. Ruapehu lahars, *Bull. Volcanol.*, *52*, 381–390, 1990.

Vreugdenhil, C. B., *Numerical Methods for Shallow-Water Flow*, 261 pp., Kluwer Acad., Norwell, Mass., 1994.

Walton, O., Numerical simulation of inelastic, frictional particle-particle interactions, in *Particulate Two-Phase Flow*, edited by M. C. Roco, pp. 884–911, Butterworth-Heinemann, Newton, Mass., 1993.

Weir, G. J., Kinematic wave theory for Ruapehu lahars, *N. Z. J. Sci.*, *25*, 197–203, 1982.

Whipple, K. X., Debris-flow fans: Process and form, Ph.D. dissertation, 205 pp., Univ. of Washington, Seattle, 1994.

Whipple, K. X., and T. Dunne, The influence of debris-flow rheology on fan morphology, Owens Valley, California, *Geol. Soc. Am. Bull.*, *104*, 887–900, 1992.

Wieczorek, G. F., E. L. Harp, R. K. Mark, and A. K. Bhattacharyya, Debris flows and other landslides in San Mateo, Santa Cruz, Contra Costa, Alameda, Napa, Solano, Sonoma, Lake, and Yolo counties, and factors influencing debris-flow distribution, in *Landslides, Floods and Marine Effects of the Storm of January 3–5, 1982, in the San Francisco Bay Region, California*, edited by S. D. Ellen and G. F. Wieczorek, *U.S. Geol. Surv. Prof. Pap.*, *1434*, 133–162, 1988.

Wierich, F. H., The generation of turbidity currents by subaerial debris flows, *Geol. Soc. Am. Bull.*, *101*, 278–291, 1989.

Yamashita, S., and K. Miyamoto, Numerical simulation method of debris movements with a volcanic eruption, paper presented at Japan-U.S. Workshop on Snow Avalanche, Landslide and Debris Flow Prediction and Control, Jpn. Sci. and Technol. Agency, Tsukuba, 1991.

Yano, K., and A. Daido, Fundamental study on mud-flow, *Bull. Disaster Prev. Res. Inst. Kyoto Univ.*, *14*, 69–83, 1965.

Zhang, Y., and C. S. Campbell, The interface between fluid-like and solid-like behaviour in two-dimensional granular flows, *J. Fluid Mech.*, *237*, 541–568, 1992.

R. M. Iverson, Cascades Volcano Observatory, U.S. Geological Survey, 5400 MacArthur Boulevard, Vancouver, WA 98661. (e-mail: riverson@usgs.gov)